DESIGN ISSUES IN ELECTROMECHANICAL FILTERS WITH PIEZOELECTRIC TRANSDUCERS

by

Michael P. Dmuchoski

B.S. in M.E., University of Pittsburgh, 2000

Submitted to the Graduate Faculty of

School of Engineering in partial fulfillment

of the requirements for the degree of

Master of Science

University of Pittsburgh

2002

UNIVERSITY OF PITTSBURGH

SCHOOL OF ENGINEERING

This thesis was presented

by

Michael P. Dmuchoski

It was defended on

December 11, 2002

and approved by

Dr. Jeffrey S. Vipperman, Professor, Mechanical Engineering Department

Dr. Marlin H. Mickle, Professor, Electrical Engineering Department

Dr. William W. Clark, Professor, Mechanical Engineering Department
Thesis Advisor

ABSTRACT

DESIGN ISSUES IN ELECTROMECHANICAL FILTERS WITH PIEZOELECTRIC TRANSDUCERS

Michael P. Dmuchoski, MS

University of Pittsburgh, 2002

The concept of filtering analog signals was first introduced almost one hundred years ago, and has seen tremendous development since then. The majority of filters consist of electrical circuits, which is practical since the signals themselves are usually electrical, although there has been a great deal of interest in electromechanical filters. Electromechanical filters consist of transducers that convert the electrical signal to mechanical motion, which is then passed through a vibrating mechanical system, and then transduced back into electrical energy at the output. In either type of filter, electrical or electromechanical, the key component is the resonator. This is a two-degree-of-freedom system whose transient response oscillates at its natural frequency. In electrical filters, resonators are typically inductor-capacitor pairs, while in mechanical filters they are spring-mass systems. By coupling the resonators correctly, the desired filter type (such as bandpass, band-reject, etc.) or specific filter characteristics (e.g. center frequency, roll-off, ripple, etc.) can be realized. Even though mechanical filters are in general more complex than electrical filters, given the required transducers and the additional fabrication steps, they are desirable because of the extremely good resonator characteristics of mechanical systems, which can result in superior filter characteristics. Existing mechanical filter technology could be considered to be "macro-scale" (centimeters and up), and the design process has been somewhat of an art. There is interest in developing micro-scale filters that are well-integrated with electronics. This thesis discusses the overall design process of mechanical filters, bringing together information from the filter design literature that is somewhat spread out. An example of the design and analysis of a narrow-band mechanical filter with piezoelectric transducers is offered. This design was constructed and tested, and the results are presented. Finally, the thesis also presents implications for designing mechanical filters at the micro-scale.

ACKNOWLEDGEMENTS

I would like to thank my advisor, Dr. William W. Clark, for his guidance and assistance throughout this tenure, as well as for the opportunity to work for him as a graduate student. I also express my gratitude to the members of the Vibration and Control Laboratory. Your help has been invaluable. Finally, I would like to thank all of my friends and family. I especially want to thank Alexandra Wood for always being there even when you couldn't. And yes Mom, it's really finished this time.

The author also gratefully acknowledges the long time support of Aerotech Inc., dating back to when I was an undergraduate.

TABLE OF CONTENTS

1.0 INTRODUCTION 1

1.1 Outline of Thesis.. 2

2.0 GENERAL FILTER BACKGROUND 4

2.1 Description of What They Are and What They Do 4

2.2 Filter Responses 4

2.2.1 Low-pass Filters... 6

2.2.2 High-pass Filters 7

2.2.3 Bandpass Filters 7

2.2.4 Band-reject Filters.. 9

2.2.5 All-pass Filters 9

3.0 LITERATURE REVIEW 10

3.1 Electrical and Electromechanical Filter Background Information 10

3.2 Electromechanical Filters... 11

3.2.1 Knowledge Involving All Electromechanical Filter Sizes.. 12

3.2.1.1 Types of Electromechanical Filters 12

3.2.1.1.1 Crystal and Ceramic Filters 12

3.2.1.1.2 Surface Acoustic Wave (SAW) Filters 14

3.2.1.1.3 Mechanical Filters.. 15

3.2.1.2 Electromechanical Transducers 16

3.2.1.2.1 Types of Transducers 16
3.2.1.2.1.1 Magnetostrictive Transducers 16
3.2.1.2.1.2 Piezoelectric Transducers 17
3.2.1.3 Resonators 18
3.2.1.3.1 Geometries, Vibrational Modes, and Boundary Conditions 19
3.2.1.3.2 Cantilever Beam Example 20
3.2.2 Macro-scale Mechanical Filters 22
3.2.2.1 Mathematical Models 22
3.2.2.1.1 Pictorial Form 22
3.2.2.1.2 Electromechanical Analogy 23
3.2.2.1.2.1 Conventional Analogy 24
3.2.2.1.2.2 Mobility Analogy 25
3.2.2.1.2.2.1 Schematic Form Using Mobility Analogy 26
3.2.2.1.2.2.1.1 Mechanical Schematic 26
3.2.2.1.2.2.1.2 Electrical Schematic 27
3.2.2.2 Coupling Wires 27
3.2.2.2.1 Effects and Development 28
3.2.2.2.2 Flexural Beam Coupling Example 28
3.2.2.2.3 Bridging 30
3.2.2.3 Fabrication 31
3.2.3 Micro-scale Mechanical Filters 32
3.3 Electrical Bandpass Filter Design 33
3.3.1 Wide-band Bandpass Filter Design 33

3.3.2 Narrow-band Electrical Bandpass Filters 34
3.3.2.1 All-pole Network 34
3.3.2.2 Low-pass Prototype Circuit 36
3.3.2.3 Filter Approximations 36
3.3.2.3.1 Butterworth Approximation 36
3.3.2.3.2 Chebyshev Approximation 37
3.3.2.3.3 Legendre Approximation 38
3.3.2.4 Normalized Filter Elements 38
3.3.2.4.1 Butterworth Approach 38
3.3.2.4.2 Chebyshev Approach 40
3.3.2.5 Dimensionless Ratios 47
3.3.2.5.1 Normalized Quality Factor 47
3.3.2.5.2 Normalized Coupling Coefficient 48
3.3.2.6 Electrical Network 49
3.4 Summary of Important Research 51
4.0 MACRO-SCALE DESIGN PROCEDURE 53
4.1 Filter Specifications 53
4.1.1 Example 54
4.2 Minimum Number of Resonators 55
4.2.1 Example 55
4.3 Interior Resonator Dimensions 57
4.3.1 Example 57
4.4 Transducer and Outer Resonator Dimensions 59

4.4.1 Example ... 59
4.5 Normalized Quality Factors and Coupling Coefficients ... 61
4.5.1 Example ... 62
4.6 Coupling Wire Dimensions ... 63
4.6.1 Example ... 64
4.7 Electrical Model ... 65
4.7.1 Example ... 67
4.8 Summary of Design Procedure ... 67
5.0 EXPERIMENTAL SETUP AND RESULTS ... 69
5.1 Equipment Setup ... 69
5.2 Results ... 71
6.0 DISCUSSION ... 87
7.0 CONCLUSIONS AND FUTURE CONSIDERATIONS ... 93
Appendix A ... 97
Frequency Response Plots of Individual Beams Contained Within Mechanical Filter ... 97
BIBLIOGRAPHY ... 117

LIST OF TABLES

Table 1 Conventional and mobility electromechanical analogies 26

Table 2 Filter specifications 54

Table 3 Material properties of stainless steel 58

Table 4 Interior resonator dimensions 58

Table 5 Material properties of the piezoelectric ceramic 59

Table 6 Dimensions of the outer resonators 60

Table 7 Piezoelectric transducers dimensions 61

Table 8 Dimensionless ratios 63

Table 9 Dimensions of the coupling wire 65

Table 10 Electrical network values 67

Table 11 Dimensions of designed mechanical filter 68

Table 12 Frequency and insertion loss values extracted from filter response plots found in Figure 5.5 78

Table 13 Ripple results from filter response plots found in Figure 5.5 78

Table 14 Data values extracted from filter response plots in Figure 5.5 when compared to designed specification values 79

Table 15 Individual beam resonant frequency values used in each filter 79

Table 16 Modifications created by addition of optimal terminating resistance value 82

LIST OF FIGURES

Figure 1.1 Schematic of mechanical filter 1

Figure 2.1 Principal filter responses 5

Figure 3.1 Schematic of mechanical filter with its various elements [Johnson, 1983] 15

Figure 3.2 Magnetostrictive transducer 17

Figure 3.3 Piezoelectric transducer 18

Figure 3.4 Frequency ranges of various resonators used in mechanical filters [Johnson, 1983] 20

Figure 3.5 Cantilever beam 21

Figure 3.6 Mechanical device (a) and corresponding pictorial diagram (b) 23

Figure 3.7 Mechanical schematic diagram 27

Figure 3.8 Electrical schematic diagram 27

Figure 3.9 Low-pass prototype circuit [Blinchikoff, 1976] 36

Figure 3.10 Butterworth (a) and Chebyshev (b) magnitude response plots 37

Figure 3.11 Chebyshev polynomials from n=1 to n=3 40

Figure 3.12 Butterworth and Chebyshev normalized poles for order n=5 45

Figure 3.13 General electrical network for inductively coupled resonator filter 49

Figure 4.1 Cantilevered beam mechanical filter design 53

Figure 4.2 Frequency response using filter specifications and Chebyshev approximation 54

Figure 4.3 Diagram showing composite beam transformation 60

Figure 4.4 Three node electrical network of an inductively coupled resonator filter 67

Figure 5.1 Schematic of testing apparatus 69

Figure 5.2 Photographs of filter testing setup 70

Figure 5.3 Top and bottom faces of individual resonator beam 72

Figure 5.4 Sample frequency response of individual resonator beam 74

Figure 5.5 Magnitude vs. frequency plots of four fabricated filters 75

Figure 5.6 Photograph of fabricated filter 76

Figure 5.7 Magnitude vs. frequency plots of four fabricated filters with larger frequency range77

Figure 5.8 Schematic showing terminating resistances 80

Figure 5.9 Frequency plot showing insertion loss due to addition of terminating resistances that is not shown in Figure 5.10 80

Figure 5.10 Variation of peak-to-valley ripple upon insertion of terminating resistances 81

Figure 5.11 Measured ripple changes and insertion loss with the addition of terminating resistances 82

Figure 5.12 Analytical model of three DOF vibrational system 83

Figure 5.13 Variation of filter bandwidth over range of coupling wire lengths at center frequency of 1590 Hz 84

Figure 5.14 Analytically predicted frequency values at the modes of a third order filter over range of coupling wire lengths at center frequency of 1590 Hz 85

Figure 5.15 Experimental frequency values at the modes of a third order filter over range of coupling wire lengths at center frequency of 1590 Hz 86

Figure A.1 Frequency response plot of tuned, individual beam 1 of filter 1 98

Figure A.2 Frequency response plot of pre-tuned, individual beam 1 of filter 1 99

Figure A.3 Frequency response plot of tuned, individual beam 2 of filter 1 100

Figure A.4 Frequency response plot of pre-tuned, individual beam 2 of filter 1 101

Figure A.5 Frequency response plot of tuned, individual beam 3 of filter 1 102

Figure A.6 Frequency response plot of pre-tuned, individual beam 3 of filter 1 103

Figure A.7 Frequency response plot of pre-tuned, individual beam 1 of filter 2 104

Figure A.8 Frequency response plot of pre-tuned, individual beam 2 of filter 2 105

Figure A.9 Frequency response plot of pre-tuned, individual beam 3 of filter 2 106

Figure A.10 Frequency response plot of tuned, individual beam 1 of filter 3 107

Figure A.11 Frequency response plot of pre-tuned, individual beam 1 of filter 3 108

Figure A.12 Frequency response plot of pre-tuned, individual beam 2 of filter 3 109

Figure A.13 Frequency response plot of pre-tuned, individual beam 3 of filter 3 110

Figure A.14 Frequency response plot of pre-tuned, individual beam 1 of filter 4 111

Figure A.15 Frequency response plot of tuned, individual beam 2 of filter 4 112

Figure A.16 Frequency response plot of pre-tuned, individual beam 2 of filter 4 113

Figure A.17 Frequency response plot of tuned, individual beam 3 of filter 4 114

Figure A.18 Frequency response plot of pre-tuned, individual beam 3 of filter 4 115

1.0 INTRODUCTION

Filtering analog signals is certainly not a new topic. It is essential in a variety of applications ranging from communication systems, such as radio, telephone and paging devices, to navigation equipment and system control. It is a subject matter that is more familiar when using strictly electrical components. However, it is known that electromechanical systems can also be used to filter signals.

Specifically, mechanical filters are utilized where good stability, low loss and narrowband selectivity are needed [Johnson, 1983]. A general schematic of a mechanical filter is shown in Figure 1.1.

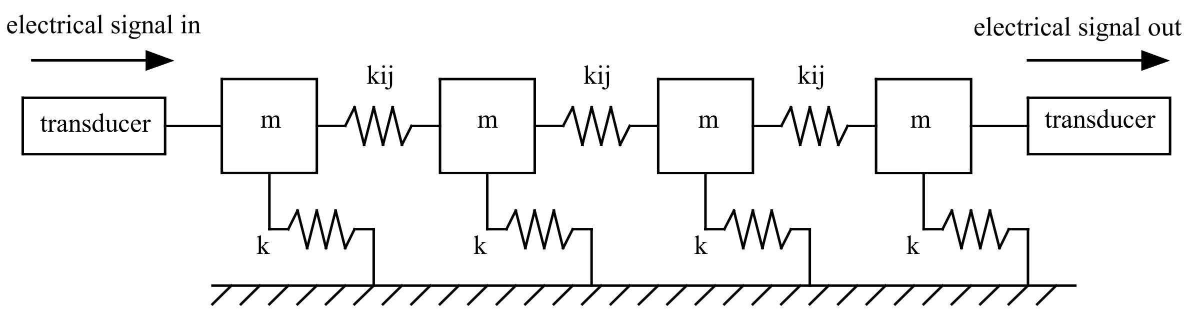

Figure 1.1 Schematic of mechanical filter

In a mechanical filter, an electrical input containing wanted and unwanted signals is used to actuate an electromechanical transducer. This transducer can either be magnetostrictive or piezoelectric. The transducer converts the electrical energy to mechanical energy by exciting a system of mass and spring elements. This system of elements, denoted as *m* and *k*, are spring-mass units that are known as the mechanical resonators. These resonators are connected to each other by spring elements (*kij*), which represent the coupling stiffness. They are designed to oscillate in accordance with a set of desired filter characteristics. A second transducer is excited by the output of the mechanical system and changes the information back to an electrical signal that has been appropriately filtered.

Existing mechanical filter technology could be considered to be macro-scale, which encompasses dimensions of centimeters and larger. There is interest in developing micro-scale filters that are well-integrated with electronics. Filter design literature is also quite diversified, making for a design process that is neither precise, nor easily understood. The objective of this research is to investigate and build a more structured design procedure for developing mechanical filters. This *modus operandi* will be applied and analyzed using a macro-scaled cantilevered beam system with piezoelectric transducers. The desire is to use this general process to design and fabricate a micro-scaled device in the future.

1.1 Outline of Thesis

The study will be completed in the following stages. Initially, a filter background is given explaining general terminology and response characteristics. This is followed by a literature review that elaborates on the necessary filter knowledge and tools. The general procedure to design a mechanical filter, with the assistance of the aforementioned example, is then described. Testing and analysis of the macro-scale filter will then be presented and discussed. Finally, some general conclusions will be brought forth, along with a discussion of future work.

The literature review has two main sections. The first describes the theoretical information that is necessary in the development of any filter, whether it is electrical or electromechanical. The second division covers the knowledge and tools that are essential when dealing with electromechanical filters.

There are three chief subsections within the electromechanical filter division of the literature review. The initial section describes the several forms of electromechanical filters, as well as the items such as the transducers and resonators that are required for every type. In the following section, pertinent information relating to macro-scale mechanical filters is conveyed, with a depiction of such elements as the coupling wires that are specific to the macro-scale mechanical filter. Finally, an overview of a micro-scale mechanical filter is given. A description of existing micro-scale technology is a key component to this final section.

A survey of the information provided in the literature review leads to the formation of a design process. The procedure begins with bandpass filter specifications, such as the center frequency, passband and stopband bandwidths, which must be met. The necessary number of resonators needed to achieve the specifications is then determined. A vibrational analysis of continuous systems ensues to establish the necessary dimensions of each resonator, which includes the resonators that contain the electromechanical transducers. The stiffness of the coupling wires is finally found to determine the dimensions of the wires.

Lastly, a description of the testing procedure on the fabricated mechanical filter is portrayed. The resonance of the individual beams, in addition to the coupled structure will be determined. A magnitude response will show whether the chosen specifications are met. Besides those already mentioned, some of the specifications include the passband ripple and the insertion loss.

2.0 GENERAL FILTER BACKGROUND

The most basic information that pertains to filters will be discussed first. This includes terminology that will be used throughout the text, as well as how to determine and analyze the frequency responses.

2.1 Description of What They Are and What They Do

A filter is used to emphasize, deemphasize, or control the frequency components of either a desired or undesired signal, which would otherwise be present [White Electromagnetics, 1963]. They are used in many devices from wristwatches to telephones and radios to navigation equipment, such as radar and sonar.

The official creation of filter technology occurred in 1915 when K. Wagner of Germany, and G. Campbell of the U.S., working independently, proposed the basic concept of the filter. Their findings came from earlier work based on classical vibrational theory and loaded transmission lines [Ellis, 1994].

2.2 Filter Responses

There are five principal classifications of attenuation versus frequency filter response plots. They are shown in Figure 2.1. The figure however does not represent the ideal responses though. An ideal response would demonstrate a completely vertical rolloff, and therefore would have no transition region to reach the stopband. The stopband is defined as the span of frequencies that will not be allowed to pass through the filter. Some common attenuations defining the beginning of the stopband range from 20 to 60 dB.

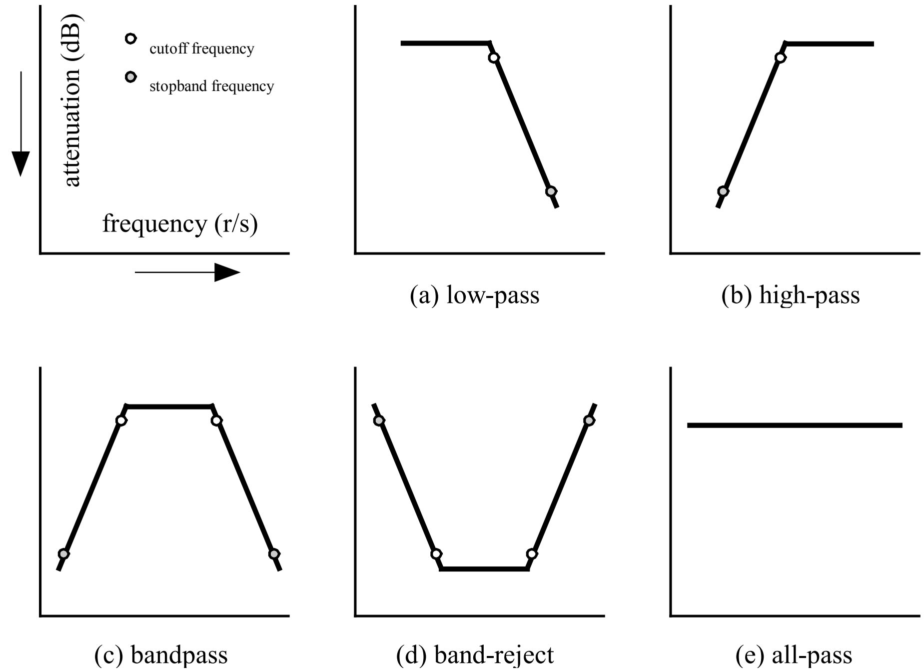

Note: the region between each cutoff frequency and the corresponding stopband frequency is the transition band

Figure 2.1 Principal filter responses

The rolloff is known as the area from the cutoff frequency to the frequency in which the stopband begins. The ratio of these two frequencies, or frequency bandwidths, is a measure of the signal rolloff, and is identified as the shape factor (*SF*). The cutoff frequency is ideally defined as being the point between the signal acceptance and rejection bands [White, 1963]. It generally occurs at an attenuation, or loss of signal, of 3dB below the attenuation of the passband.

The cutoff frequency is said to be the point at which the output contains half of the power of the maximum output, otherwise known as the half power point [Beckwith, 1993]. Often related to power, the squared magnitude at the cutoff frequency, ω_c, becomes

$$\left|H(j\omega_c)\right|^2 = \frac{1}{2}. \tag{2.1}$$

When the magnitude is determined in units of decibels, the loss is

$$A = -20\log(\frac{1}{\sqrt{2}}) \cong 3dB \,. \tag{2.2}$$

The above explains the reasoning behind the use of the 3dB attenuation in filter terminology.

The insertion loss of a filter is the loss of signal caused by the filter being activated. In general, it is the ratio of the amplitude with the insertion of the filter, to the amplitude of a perfect, lossless transformer replacing the filter [Aatre, 1986]. With the difference by way of the insertion loss, there is a greater maximum signal without the filter inserted, than with it inserted. Also, the passband is not measured at zero decibels, but at a reference attenuation that is equal to the insertion loss.

2.2.1 Low-pass Filters

A low-pass filter, shown in Figure 2.1(a), allows low frequencies to pass through the device until the cutoff frequency is reached. After that point, a transition band ensues through which frequencies are attenuated. At a specified value of attenuation the stopband begins. In the stopband, the filter is considered to reject all frequencies. The shape factor of a low-pass filter is the ratio of the frequency when rejection first occurs to the cutoff frequency.

$$SF = \frac{\omega_a}{\omega_c} \tag{2.3}$$

2.2.2 High-pass Filters

Conversely, a high-pass filter will attenuate the low frequencies, while passing the high frequencies until the cutoff point. This can be found in Figure 2.1(b). The transition band slopesin the opposite direction, when compared to a low-pass filter. Its shape factor can be equated as

$$SF = \frac{\omega_c}{\omega_a}. \tag{2.4}$$

2.2.3 Bandpass Filters

Seen in Figure 2.1(c), a bandpass filter is the addition of a high-pass and low-pass filter. There are now two cutoff frequencies, designated as the upper and lower, as well as two transition bands and stopbands. The difference between the two cutoff frequencies is known as the 3dB bandwidth, B, (but will be further referred to as just the bandwidth) while the region between the two is identified as the passband. The difference between the two stopband frequencies is known, for example, as the 40 dB bandwidth (B_{40}) if that is where it occurs.

Another important term, when speaking of bandpass filters, is the center frequency, ω_o. It is defined as the geometric mean of the upper and lower cutoff frequencies, as in Equation (2.5).

$$\omega_o = \sqrt{\omega_1 \omega_2} \tag{2.5}$$

The bandpass quality factor, Q_{bp}, is identified as

$$Q_{bp} = \frac{\omega_o}{B}, \tag{2.6}$$

and is a measure of the frequency selectivity of the bandpass filter. At a particular resonance frequency, if the bandwidth is wide, the quality factor, which is inversely proportional, is a small value and is therefore considered to have poor selectivity. Conversely, the filter is said to be highly selective if the bandwidth is tight, creating a large Q_{bp} value [Aatre, 1986].

For quality factors equaling ten or greater, the center frequency can be characterized as Equation (2.7), known as the arithmetic center frequency.

$$\omega_o = \frac{\omega_1 + \omega_2}{2} \tag{2.7}$$

This is true because as the bandpass quality factor (Q_{bp}) increases, the response shape near the passband approaches the arithmetically symmetrical condition [Williams, 1988]. Therefore, Equations (2.5) and (2.7) are nearly equal in value.

Phrases such as the fractional bandwidth and the shape factor are also significant when speaking of bandpass filters. Fractional bandwidth, B_f, is the ratio of the bandwidth to the center frequency,

$$B_f = \frac{B}{\omega_o}, \tag{2.8}$$

whereas the ratio of the 40 dB bandwidth to the 3dB bandwidth is identified as the shape factor

$$SF = \frac{B_{40}}{B}. \tag{2.9}$$

2.2.4 Band-reject Filters

Filters known as band-reject filters, represented in Figure 2.1(d), are those that attenuate one band of frequencies, while passing both higher and lower bands. They also commonly go by the terms band-stop or notch filter. The shape factor for the band-reject filter is the reciprocal to that of the bandpass.

$$SF = \frac{B}{B_{40}} \tag{2.10}$$

2.2.5 All-pass Filters

An all-pass filter is a proper name for this filter. It is one that passes all frequencies equally well. That is, the magnitude, shown in Figure 2.1(e), is constant for all frequencies it sees. The shape factor will be unity at all points because the all-pass filter experiences no rolloff.

The primary purpose of an all-pass filter is for phase shift. If the amplitude response of a system is adequate but the phase needs correction, a filter can be cascaded with an all-pass section. The desired amplitude response will be retained, but a phase shift from the filter will be added [D. Johnson, 1976].

3.0 LITERATURE REVIEW

The following text provides theoretical information that pertains to mechanical filters and their design and development. The information is broken up into segments. Initially, pertinent general information regarding most bandpass filters is depicted, followed by knowledge specifically concerning electromechanical filters. The divisions become more specialized when speaking directly of mechanical filters. A breakdown of the components of macro-scale mechanical filters, as well as their fabrication, is described. General information pertaining to micro-scale mechanical filters is also touched upon. The final topic includes the initial design process of a mechanical filter that stems from electrical filter network theory. Several design approximations are discussed, along with the procedures used to create the electrical values needed to translate into mechanical filters.

3.1 Electrical and Electromechanical Filter Background Information

After gaining a background of general filter knowledge via Section 2.0, a more specific sector of information is brought forth. The two major fields of filters, electrical and electromechanical, are discussed along with a brief history of the relationship between them.

There are two principal genres of filter technology. They include electrical filters that use strictly electrical components and signals. Electromechanical filters make up the other genre. These filters convert electrical inputs into mechanical energy that is filtered before being converted back to the altered electrical output.

There are several forms of electrical and electromechanical filters, mainly bandpass in nature, which are used in industry. The question becomes which type of filter is most beneficial for different needs. The passive LC filter was the first developed, and is still widely used. It encompasses a collection of elements where electrical resonances are developed by tuning circuits composed of inductors and capacitors.

Items such as cost, size, and performance became negative issues with the LC filters. Among others, the electromechanical filter was studied to help solve some of the concerns. It was discovered that electromechanical filters, specifically mechanical filters, presented favorable results. Mechanical filters are used in systems that demand narrow bandwidths, as well as low loss and good stability. These characteristics are achieved mainly because of the properties of the mechanical resonators. These include large material property values of quality factor (Q) that allow for bandwidths as narrow as 0.05% of the center frequency, without excessive loss. Another property of the resonators is the excellent temperature and aging characteristics. These properties prevent problems such as stability and frequency drifting with time and with temperature change [Johnson, 1983].

The development of mechanical filters can be thought of as an extension of LC filter technology. The mechanical filter devices are developed using existing electrical filter knowledge, as well as information pertaining to mechanical vibrations. The process begins with the theory behind narrow-band electrical bandpass filters.

3.2 Electromechanical Filters

Before any form of electromechanical filter can be created, or even designed, there is a plethora of theoretical information that needs to be brought to the attention of the reader. This includes information that is pertinent to all electromechanical filters, compiled in Section 3.2.1, including the several different types that are used in industry. A breakdown of the components of each filter, such as the electromechanical transducer and the resonator, is also necessary.

Section 3.2.2 explains the topics that are specific to mechanical filters. This includes information regarding issues such as the coupling wires, the fabrication of the filter, and their support systems. The subject of micro-scale mechanical filters will also be touched upon in Section 3.2.3.

3.2.1 Knowledge Involving All Electromechanical Filter Sizes

Although the electrical filter knowledge is essential, this text will focus on electromechanical filters. Therefore, background information including the different types, as well as the differences between them should be clarified. Also, the development process could not take place if the components and their roles are not understood. With that, the following is an overview of electromechanical filters.

3.2.1.1 Types of Electromechanical Filters

There are several categories of electromechanical filters, specifically bandpass filters. Some use different components. Some use different materials. Some use different theory. In the end, they all seek to pass a single band of frequencies, while rejecting those frequencies above and below it. In order to achieve this, each receives electrical energy that is transformed into mechanical vibrations. The unwanted frequencies are next filtered out, before the mechanical energy is converted back into electrical energy at the output.

3.2.1.1.1 Crystal and Ceramic Filters

Crystal and ceramic filters, monolithic filters in particular, are formed by acoustically coupling bulk or lumped resonators on the same substrate. If the adjacent resonators are physically close enough, acoustic coupling will occur through the wafer, also known as a blank [Kinsman, 1987]. The resonator is most often made of crystalline quartz when using the crystal filter, while the ceramic filter consists of a resonator made from a piezoelectric ceramic, usually PZT (Lead Titanate Zirconate). The design of the resonators requires a particular blend of acceptable mechanical dimensions, as well as the optimal electrode location, to excite the proper frequencies. An interesting property of these resonators is that they have their own built-in electromechanical transducer. Therefore, they can take an electrical signal and convert it to mechanical energy, and vice versa. Both ceramic and crystal filters can operate in frequency ranges from several kilohertz up to the megahertz and possibly gigahertz regions.

Whereas the resonators of a mechanical filter (described in Section 3.2.1.3) are depicted as the volume of some metallic geometry, crystal and ceramic resonators are defined differently. These resonators are not portrayed as depending on the actual boundaries of the crystal or ceramic material. Electrodes that are deposited on both sides of the substrate create the boundaries. This allows the mechanical energy to be confined to the area of the crystal or ceramic material where the electrodes overlap, thus leaving room outside of this area for electrical connections and the support structure. Any small amount of energy that leaks into a region of the substrate without any electrode falls off exponentially away from the electrode. This phenomenon is known as energy trapping [Sheahan, 1975].

In terms of frequency stability and quality factor, the ceramic resonator cannot compete with those manufactured from quartz. Ceramics also age more than quartz crystals. Though, if the application calls for a loosely specified, low-cost device, piezoelectric ceramics are the better choice [Fujishima, 2000].

3.2.1.1.2 Surface Acoustic Wave (SAW) Filters

Generally, an SAW filter consists of comb-like, metallic-film electrodes, known as inter-digital-transducers (IDTs), deposited on the flat surface of a piezoelectric crystal. When a voltage is applied, the generating transducer creates an alternating pattern of material deformations just under its finger-like geometry. When a sinusoidal voltage is applied, a standing wave, known as a surface acoustic wave, is formed. A surface acoustic wave is a mode of material deformation that circulates at the surface of a solid, similar to the ones that propagate on a water surface.

When the wavelength of the surface acoustic waves and the period of the electrode fingers are the same, the waves are most strongly excited because they are applied at the same phase. Thus, travel to the receiving transducer at these periods is at the highest sensitivity. This results in a filtered response. Enclosing the transducer pair, diffraction gratings are used to compensate for the traveling wave that occurs at the positions before the generating, and after the receiving, transducers [Mitra, 1989].

By and large, the frequency range for the SAW filter begins at approximately 30 MHz, while the highest acceptable frequency is a few GHz. The dimensions of the device tend to be inconveniently large if the frequency is lower than 30 MHz [Mitra, 1989]. While the opposite is true at large frequencies above a few GHz, ever increasing technology in the micro- and nano-regions can help to raise the higher end frequencies.

3.2.1.1.3 Mechanical Filters

A mechanical filter is a composition of both electrical and mechanical elements to output a response that has been filtered from the input. The schematic for such a filter is given in Figure 3.1. A bandpass filter is the most common form, passing the wanted signals while attenuating the unwanted.

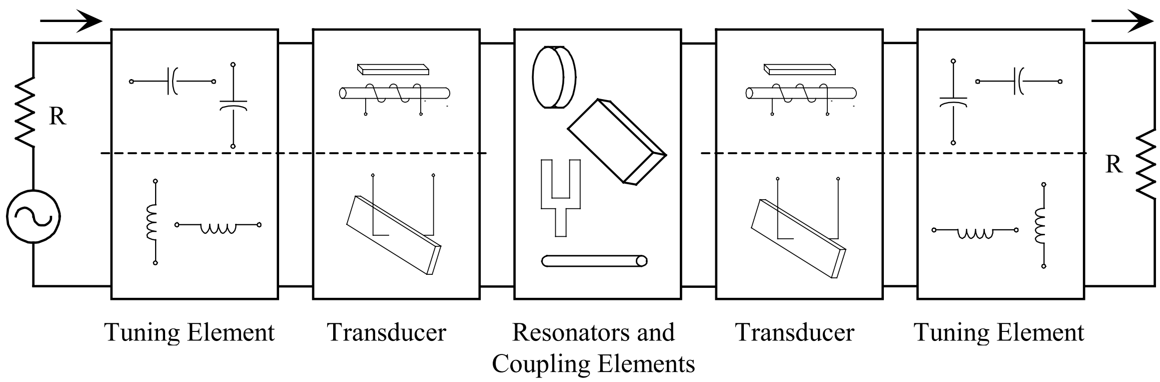

Figure 3.1 Schematic of mechanical filter with its various elements [Johnson, 1983]

There are several components in a mechanical filter. The input voltage and source resistance cause current to flow into the electromechanical transducer. This transducer, either magnetostrictive or piezoelectric, transfers the electrical signal to the mechanical resonators. The resonators vibrate at a specified frequency, while driving a second transducer. This transducer converts the mechanical signals back to electrical, only now they are filtered in a bandpass form. Terminating resistances are needed to ensure a flat or moderate ripple in the passband response [Johnson, 1983]. Electrical tuning elements must also be inserted if the filter is not a narrow-bandwidth design to adjust the response where necessary.

The center frequency of a macro-scale mechanical filter can range from a few hundred Hz using a tuning fork design, up to just below one MHz by utilizing the extensional or torsional modes of a rod, or a disc vibrating in a flexural mode. A discussion will ensue containing information regarding several of the modes and geometries used in the resonator of a mechanical filter. It will also contain an in-depth description of the functions of the transducers and coupling wires.

3.2.1.2 Electromechanical Transducers

The electromechanical transducer performs energy conversion within a filter. This means that it creates mechanical energy from an electrical signal, and converts the mechanically filtered response back into electrical energy. The transducer is either integral to the system, such as in a crystal filter, or is externally coupled, which takes place in a mechanical filter.

3.2.1.2.1 Types of Transducers

For the several forms of electromechanical filters used in industry, there are only two categories of transducers. They are magnetostrictive and piezoelectric. Magnetostrictive transducers were discovered first, and in the past, played a primary role, especially in mechanical filters. However, piezoelectric transducers have gained acclaim for their broad frequency range, as well as their use of many different modes.

3.2.1.2.1.1 Magnetostrictive Transducers

A magnetostrictive transducer, as seen in Figure 3.2, is composed of a coil, a rod made from a metal alloy or a ferromagnetic material, and a biasing magnet. The north and south ends of the magnet are denoted as N and S, respectively. Electrically, V and I respectively represent the voltage of current of the coil, while the mechanical force and velocity are labeled as F and v_p respectively. The material expands or contracts when subjected to a magnetic field, and inversely changes in magnetization when the material is externally stressed. Within the filter, these effects change the electrical and mechanical signals from one form to another.

These materials are crystalline in form. The domains of each crystal have a random alignment while in the demagnetized state. When a magnetic field is applied, the domains rotate into alignment with the field. It is this process that can cause large changes in the physical stature of the material [Johnson, 1983].

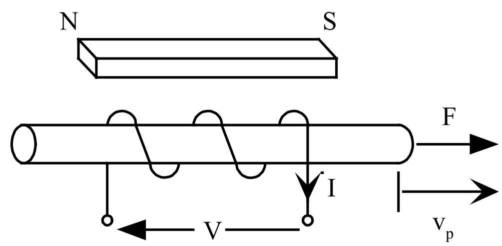

Figure 3.2 Magnetostrictive transducer

3.2.1.2.1.2 Piezoelectric Transducers

As mentioned, the piezoelectric transducer can be utilized for numerous modes of vibration, as well as covering a wide range of frequencies. For these reasons, the piezoelectric transducer is more commonly used. Similarly to the magnetostrictive transducer, the piezoelectric is capable of acting as both a sensing and a transmitting element. When a voltage stresses the piezoelectric element electrically, its dimensions change. Inversely, an electrical charge is generated when the element is stressed by a mechanical force. A piezoelectric transducer is shown in Figure 3.3 with the symbols being defined via Figure 3.2.

There are two main categories of piezoelectric transducers. They include crystals and ceramics. Crystal transducers are used in crystal and SAW filters. In contrast, ceramic filters and mechanical filters use ceramic transducers.

An example of a crystal transducer is quartz. There are a variety of crystalline materials that exhibit piezoelectric properties, but quartz has become the most popular because of its high mechanical quality factor, as well as its exceptional stability with time and temperature. Presently, most crystal quartz is cultured which has also helped make it fairly inexpensive [Kinsman, 1987].

Lead Zirconate Titanate, or PZT, ceramics are the most widely used for both sensing and actuating applications. Domains within the material are randomly oriented in their original, unpoled state. When an electric field is applied, the charge dipoles align with a parallel orientation. As a result, the dimension that is aligned with the field expands, while there is a contraction along the axes normal to the electric field [Physik Instrumente, 1998].

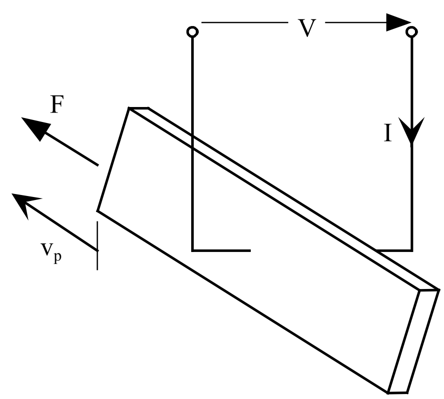

Figure 3.3 Piezoelectric transducer

3.2.1.3 <u>Resonators</u>

The resonators are the heart of the electromechanical filter. An integral or externally coupled transducer excites the resonator within the filter. The output is a filtered response based on the dominant frequency of the oscillations produced by the resonators. This text will focus primarily on resonator information pertinent to mechanical filters.

The parameters of the mechanical resonators play a vital role in producing the characteristics of the filter. The natural frequencies of the resonators establish the center frequency of the filter. Additionally, the number of resonators used in the system determines the shape factor. The shape factor (*SF*) is a measure of the selectivity, or vertical rolloff, of the response. Also, one of the variables that affect the bandwidth is the equivalent mass of each resonator [Mitra, 1989]. The equivalent mass is a measure of the distributed-mass of a resonator, and corresponds to the mass of a comparable spring-mass resonator tuned to the same frequency [Sheahan, 1975].

3.2.1.3.1 Geometries, Vibrational Modes, and Boundary Conditions

A mechanical resonator can oscillate in a number of ways. Continuous vibration theory is used to model mechanical resonators with such geometries as bars, beams, rods, and disks. The governing equations of a system are partial differential equations used to solve for the characteristic function, or mode, of the structure [Rao, 1995]. In mechanical filter design, the end result is to determine the natural frequencies of the resonators.

Certain geometries and mode shapes are chosen to fulfill specific filter specifications. Figure 3.4 shows geometries and modes generally used in typical frequency ranges for macro-scale mechanical filters. The initial and final frequencies of Figure 3.4 can be somewhat extended in either direction, but practical limitations must be accounted for. These include manufacturing tolerances and physical thresholds that ensue due to nonlinear vibrational behavior [Johnson, 1983].

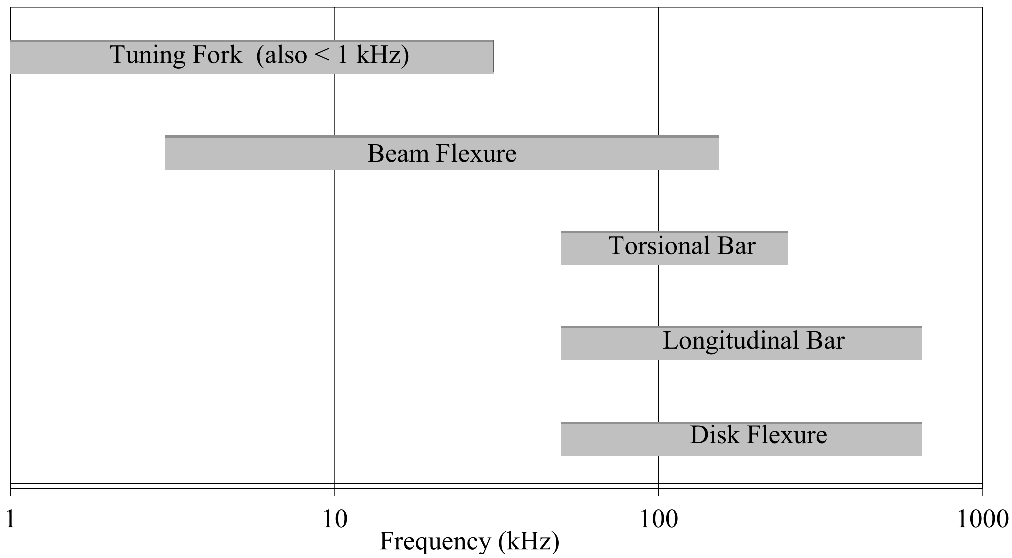

Figure 3.4 Frequency ranges of various resonators used in mechanical filters [Johnson, 1983]

Knowledge of the boundary conditions of the system is also essential to solve for the vibrational outputs. In objects with similar geometries vibrating in the same mode, different boundary conditions create very dissimilar mode shapes and frequencies. Therefore, within each range of Figure 3.4, favorable boundary conditions are chosen based on frequency specifications of the filter.

3.2.1.3.2 Cantilever Beam Example

As an example of the vibrational theory used for resonators, this text will concentrate on the lateral vibration of a beam that is fixed at one end, or cantilevered, revealed in Figure 3.5. The characteristic mode shape for a beam is first developed. From the equation of motion of a beam element based on Euler-Bernoulli theory, the mode shape, a function of horizontal displacement, is found as

$$W(x) = C_1 \cos \beta x + C_2 \sin \beta x + C_3 \cosh \beta x + C_4 \sinh \beta x \,, \qquad (3.1)$$

where $C_{1\text{-}4}$ are constants dependent on the boundary conditions. The natural frequencies can also be expressed as

$$\omega = (\beta l)^2 \sqrt{\frac{EI}{\rho A l^4}}\,, \tag{3.2}$$

where βl is a constant based on the mode number and end conditions of the beam (Inman, 2001). Young's modulus and the moment of inertia of the beam are represented respectively as E and I. The length (l) and area (A) of the beam are also needed, as well as the material property, density (ρ).

Examination of the deflection, slope of the deflection, bending moment, and shear force is required to solve the governing equations. One end of the beam vibrates freely; therefore the bending moment and shear force must vanish. Conversely, the other end is clamped creating no restrictions on the moment or shear force. It does, however, force the deflection and slope of the deflection to be zero. The numerical values of βl are determined by implementing the boundary conditions to help solve for the natural frequencies, as well as the mode shapes for a cantilever beam as

$$W(x) = (\sin\beta x - \sinh\beta x) - \left[\frac{\sin\beta l + \sinh\beta l}{\cos\beta l + \cosh\beta l}\right](\cos\beta x - \cosh\beta x)\,. \tag{3.3}$$

[Rao, 1995]

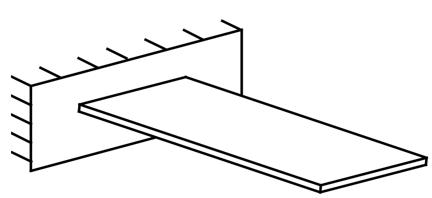

Figure 3.5 Cantilever beam

3.2.2 Macro-scale Mechanical Filters

Whereas Section 3.2.1 dealt with topics that are related to all electromechanical filters, the following section shares information specialized to mechanical filters. Electromechanical filters are those that transform electrical signals to mechanical energy, and then back to electrical signals after filtering takes place. Mechanical filters specifically use mechanically coupled mechanical resonators. They differ from other electromechanical filters such as monolithic crystal and ceramic filters that are mechanically coupled without physical attachment of the resonators.

Specifically, the text addresses larger, or macro-scale mechanical filters. These generally tend to have dimensions within the centimeter range. One of the featured topics regards the coupling wires, which are exclusive to mechanical filters.

3.2.2.1 Mathematical Models

In order to understand mechanical filters one must comprehend the topic of mathematical models. A filter designer must be able to appreciate the analogous nature of dynamics or acoustics with electrical network theory. These similarities produce equivalent circuits that are important because most literature and computer programs used for the design and analysis of filters are written in electrical terms [Temes, 1973]. Therefore, it is desirable to convert the electromechanical model into electrical terms.

3.2.2.1.1 Pictorial Form

The first stage in generating the mathematical model of a mechanical filter is creating the model in pictorial form. The pictorial diagram takes the essentials of the actual mechanical device, and represents it in a spring-mass-damper system [Johnson, 1983]. Figure 3.6 is an example that depicts a pair of mechanically coupled cantilevered beams via a wire, and the corresponding reproduction in pictorial form. The pictorials will be used to determine the mechanical and electrical schematic diagrams, which are clarified in Section 3.2.2.1.2.2.1.

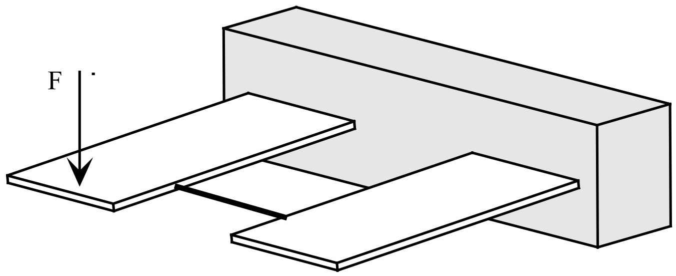

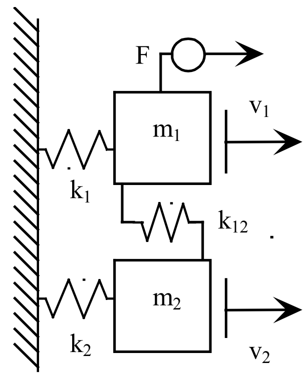

Figure 3.6 Mechanical device (a) and corresponding pictorial diagram (b)

3.2.2.1.2 Electromechanical Analogy

There is no unique analogy for use between mechanical and electrical systems. However, there are two primary forms that can be utilized when electromechanical devices are involved. The conventional analogy was the primary analogy used for many years. It poses some inconsistencies and is sometimes difficult to work with, but many users still prefer it. The second form, known as the mobility analogy, is more recently developed, and attempts to eliminate some of the difficulties created by the prior form with a more common sense approach.

The analogies are based on the assumption that certain mechanical elements have similar characteristics to an electrical counterpart. This theory is used to convert a mechanical system to an equivalent electrical network. A major contributor to the principles of electromechanical analogies is the concept of "through" and "across" variables. An across-variable is one that is measured when an instrument is placed across its ends, or nodes, within a system. A through-variable is a quantity that is measured by inserting an instrument at a single point in a branch of a system [Temes, 1973].

To elaborate on this new terminology, a spring element can be used as an example. A spring has two nodes in which an outside force can be applied. Since the force is equal at every portion of the spring, this quantity is referred to as the force through a spring [Firestone, 1933]. Similarly, the displacement or velocity is measured between the two ends of the spring. Therefore, it is offered as a quantity across the element.

3.2.2.1.2.1 Conventional Analogy

The conventional electromechanical analogy can be derived from the foundation that the differential equations of both types of systems will be of the same form, as expressed in terms of displacement and charge [Firestone, 1933]. Table 1 shows this form of analogy for each element. The differential equations of both the mechanical and electrical systems, respectively, will have the form of

$$\begin{aligned} m\dot{v} + cv + k\int v\,dt &= F \\ L\dot{I} + RI + \frac{1}{C}\int I\,dt &= E. \end{aligned} \tag{3.4}$$

There are a few points of interest to note when this analogy is used. The first point occurs when mechanical elements are placed in parallel form. It is known that the electrical equivalent must be connected in series, and vice versa. This is to employ the fact that the velocity across a mechanical system of elements is analogous to the current through an electrical system. Similarly, the combination of mechanical elements in series is equal to the reciprocal of the sum of the reciprocals of the elements. In electrical terms, series elements are additive [Firestone, 1933].

A final point pits elements that are defined as across, to be analogous to through elements. The variable section of Table 1 shows that the velocity, which is measured across an element, is analogous to the through element, current. This is also true for a mechanical force and an electrical voltage. It respectively compares a through element with one that is measured across. This point, in conjunction with the others mentioned, can cause confusion when dealing with mechanical filters.

3.2.2.1.2.2 Mobility Analogy

The analogy used more commonly by mechanical filter users and designers is known as the mobility analogy. A categorization of this analogy can also be found in Table 1. Its basis is to relate mechanical through-variables with electrical through-variables. A similar argument can be made for across-variables. The mobility analogy also assures that the network topologies are the same [Johnson, 1983]. Therefore, a series connection in a mechanical circuit can be easily converted to an electrical circuit in series. Also, the summation of series components in both mechanical and electrical terms is additive. Parallel connections and components also behave in the same manner in mechanical and electrical terms. The differential equations obtained by using the mobility analogy are

$$\begin{aligned} m\dot{v} + cv + k\int v\,dt &= F \\ C\dot{E} + \frac{1}{R}E + \frac{1}{L}\int E\,dt &= I. \end{aligned} \tag{3.5}$$

Table 1 Conventional and mobility electromechanical analogies

Analogy		*Conventional*	*Mobility*
System	Mechanical	Electrical	Electrical
Variable	Velocity across (v) Force through (F)	Current through (I) Voltage across (E)	Voltage across (E) Current through (I)
Network parameters	Damping (c) Compliance ($1/k$) Stiffness (k) Mass (m)	Resistance (R) Capacitance (C) Reluctance ($1/C$) Inductance (L)	Conductance ($1/R$) Inductance (L) Inductance^{-1} ($1/L$) Capacitance (C)
Network topology	Series connection Parallel connection	Parallel connection Series connection	Series connection Parallel connection

3.2.2.1.2.2.1 Schematic Form Using Mobility Analogy

A schematic diagram is used to convert a pictorial diagram into a network that is easier to analyze, using the electromechanical analogies. Finding the terminals of each mechanical element will help in the creation of the schematics. It is not difficult to determine that both a spring and a damping element have two terminals, but a mass element is not as obvious. A force cannot be applied to a spring or damper without grasping it at two points, but a mass can acquire an applied force from contact at just one point [Firestone, 1933]. The second terminal of a mass element is always connected to a reference ground, which is represented as the earth. All other terminals that are clamped, and do not move, are also connected to the reference ground [Johnson, 1983].

3.2.2.1.2.2.1.1 Mechanical Schematic

The information from Section 3.2.2.1.2.2.1 can be used to convert the example pictorial diagram of Figure 3.6(b) into the mechanical schematic diagram of Figure 3.7. The mechanical schematic looks similar to an electrical circuit using just the mechanical elements.

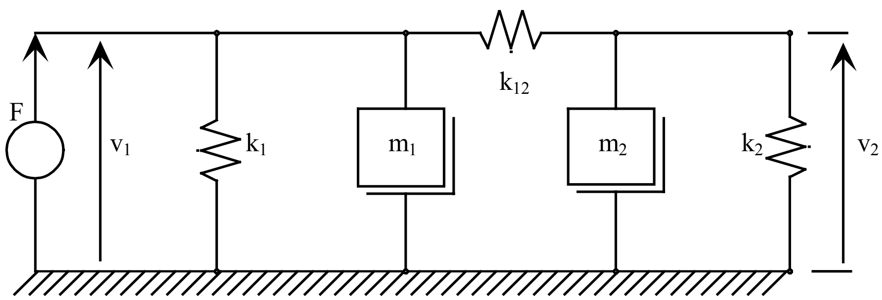

Figure 3.7 Mechanical schematic diagram

3.2.2.1.2.2.1.2 Electrical Schematic

Using the mobility analogy, the mechanical schematic in Figure 3.7 can be converted into the electrical schematic of Figure 3.8. Except for the addition of a source and load resistance, Figure 3.8 is a legitimate electrical representation of a mechanical filter.

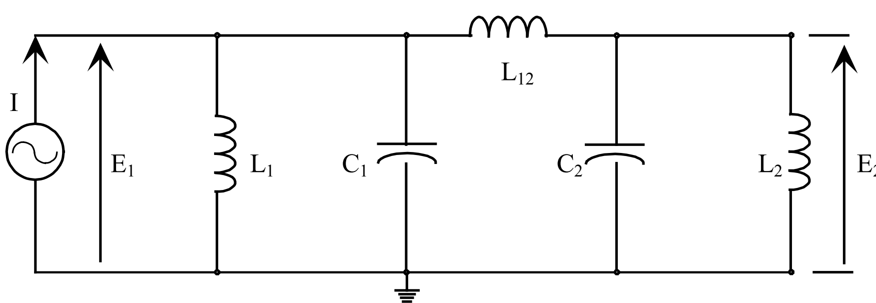

Figure 3.8 Electrical schematic diagram

3.2.2.2 <u>Coupling Wires</u>

Mechanical resonator coupling can be achieved in several ways. These include mass coupling, shunt resonator couplers, and various cross sections that approximate simple wire coupling [Johnson, 1983]. The coupling of one or more small diameter wires though, is the most common.

3.2.2.2.1 Effects and Development

The coupling of a mechanical filter affects several features of the device. The bandwidth of the filter is a direct function of the stiffness of the coupling wires. As the stiffness becomes greater, the bandwidth also becomes larger. Resonator-to-resonator coupling also influences the shape of the attenuation versus frequency curve. A more rounded passband shape, with less ripple, is the result of greater coupling between the outer resonators, relative to the inside resonators [Johnson, 1983].

Similar to the resonator concepts clarified in Section 3.2.1.3, continuous, vibrational theory is used to develop the coupling wires. Therefore, the couplers can oscillate in such modes as torsional, extensional, and flexural. Unlike resonator theory though, the natural frequencies of the coupling wires are not the focal point of ascertaining the physical dimensions. The emphasis is placed on the determination of the coupling stiffness to establish the size of the wires. The stiffness equation can be found by implementing the numerical technique known as the finite element method. This procedure is used to uncover the stiffness matrix of the element, which is a $2n$-by-$2n$ matrix where n represents the number of degrees of freedom necessarily applied to each end of the element. The boundary conditions of the wires are next applied to the matrix to determine the correct equation for the coupling stiffness.

3.2.2.2.2 Flexural Beam Coupling Example

The technique can be further clarified through the use of an example. The use of several cantilevered beams, such as the one found in Figure 3.5, can be coupled to oscillate in a flexural manner, as seen in Figure 3.6(a). This requires the assumption of a sliding support (strictly vertical displacement) at the ends of each flexurally vibrating coupler.

Because the coupling wires vibrate in a transverse direction, the stiffness matrix for a beam element must be determined. The following stiffness matrix derivation can be found in Logan, 2002. The degrees of freedom considered per node, or endpoint, for a beam element are the transverse displacement (d_y) and rotation (θ). The first step to develop the matrix is to assume a transverse velocity function through the element length as

$$v(x) = a_1 x^3 + a_2 x^2 + a_3 x + a_4 . \tag{3.6}$$

This cubic function is appropriate due to there being four total degrees of freedom at the two nodes. Equation (3.6) is then expressed as a function of the nodal degrees of freedom by evaluating each a term at the nodes. The new function is used in conjunction with the bending moment and shear force equations that are related to the transverse displacement function, respectively found as

$$\begin{aligned} M(x) &= EI\frac{d^2 v}{dx^2} \\ \bar{V}(x) &= EI\frac{d^3 v}{dx^3}. \end{aligned} \tag{3.7}$$

In matrix form, the assembly of the shear forces and moments at each node, as functions of displacement and rotation, are

$$\begin{pmatrix} \bar{V}_1 \\ M_1 \\ \bar{V}_2 \\ M_2 \end{pmatrix} = \frac{EI}{l^3}\begin{pmatrix} 12 & 6l & -12 & 6l \\ 6l & 4l^2 & -6l & 2l^2 \\ -12 & -6l & 12 & -6l \\ 6l & 2l^2 & -6l & 4l^2 \end{pmatrix}\begin{pmatrix} d_{1y} \\ \theta_1 \\ d_{2y} \\ \theta_2 \end{pmatrix} \tag{3.8}$$

Because of the assumed sliding supports, there is no rotation at either node. Also, the shear forces are known to be zero, but no information is known regarding the moments at each end. Therefore, Equation (3.8) can be reduced and the stiffness matrix K, can be extracted as

$$K = \frac{EI}{l^3}\begin{pmatrix} 12 & \cancel{6l} & -12 & \cancel{6l} \\ \cancel{6l} & \cancel{4l^2} & \cancel{-6l} & \cancel{2l^2} \\ -12 & \cancel{-6l} & 12 & \cancel{-6l} \\ \cancel{6l} & \cancel{2l^2} & \cancel{-6l} & \cancel{4l^2} \end{pmatrix} \tag{3.9}$$

The flexural coupling stiffness equation between each flexurally vibrating resonator becomes

$$K_{ij} = \frac{12EI}{l^3}. \tag{3.10}$$

The coupling stiffness is determined as a function of filter specifications, as well as the normalized coupling coefficient. Equation (3.10) can then be applied to determine the dimensions of the wires.

3.2.2.2.3 Bridging

In an attempt to create a tighter stopband bandwidth, hence a larger shape factor value, a technique known as bridging across mechanical resonators is used. This is accomplished by coupling non-adjacent resonators, in addition to the already coupled system. The idea is to produce attenuation poles in the filter stopband to improve the frequency response. The poles are the result of the bridging wire signal canceling the signal through the main coupling wires [Mitra, 1989].

Generally speaking, the bridging of an odd number of resonators will produce a pole in either the lower or upper stopband, but not in both. Conversely, when bridging occurs across an even number of resonators, dual poles will result producing a symmetric frequency response [Johnson, 1983].

3.2.2.3 Fabrication

There are various assembly processes needed to complete the construction of a mechanical filter. These include the bonding of the piezoelectric transducers to the outer resonators, the bonding of the coupling wires to each resonator, and also a filter support system.

There are several methods that can be used to attach a piezoelectric (ceramic) transducer to a metal resonator, but most of which involve solders or epoxies. The compositions of the bonding materials are numerous, with solders coming in foils, pastes, or wire form, and the epoxies varying in consistencies, application procedures, cure times, and chemical makeup.

Stages that are of major importance in the bonding process are the preparation of the attached surface and the thickness of the bonding layer. The resonator surface must be thoroughly cleaned before and after the application of a solder or epoxy. When soldering, the surface might need to be primed using tinning, flux, or other necessary treatments [Mitra, 1989]. A more significant step when bonding with an epoxy is the control of the thickness. Typically, pressure is used to promote a uniform attachment using the minimum amount of epoxy. A minimum volume of epoxy also results in a minimum amount of damping or resistance that is the effect of the epoxy bond.

Soldering or welding processes are normally used in the attachment of coupling wires to the resonators. Epoxy does not result in good coupling because of its damping characteristics. Problems that could arise due to soldering or welding include deformation of the wire and/or resonator due to thermal effects, and physical deformation of the wire that can occur from some welding processes.

A filter support system is designed with two principal objectives. The first is to create a structure that will allow the components to vibrate consistently and predictably. The second is to isolate the filter from external shock and vibration that could cause both damage and unwanted responses [Johnson, 1983]. Ideally, attachment of the support occurs at the nodes of the resonators.

3.2.3 Micro-scale Mechanical Filters

Current micro-scale mechanical filter research has proved to show favorable results. Many resonators are developed using polycrystalline silicon, which is a low-loss material, and are driven by interdigitated electrodes that provide a linear excitation [Lin, 1998]. They are mechanically coupled by soft, flexural-mode springs and are equipped with capacitive-comb-transducers [Nguyen, 1998]. These developments can provide an ever-growing demand for higher quality factors, better stability to aging and temperature, and good signal-to-noise ratios.

More recently, studies are being conducted with the interest of using thin film piezoelectric transducers on micro-resonators and filters. This has been a topic that had received limited attention in the past, with the exception of acoustic wave devices. This was primarily due to the relative complexity of integrated circuit integration and overall device fabrication [DeVoe, 2001].

Micro-scale piezoelectric devices do have their advantages. For example, it is known that the theoretical coupling strength of an electrostatic clamped-clamped, beam device is known to rapidly drop off as resonant frequencies are increased [DeVoe, 2001]. This is not the case with piezoelectric transducers. According to Devoe, 2001, the electromechanical coupling strength, η, of a piezoelectric doubly-clamped beam is greater than an electrostatic parallel plate resonator at frequencies greater than approximately 80 kHz. The piezoelectric coupling strength is still increasing after this frequency, while the strength of the electrostatic resonator decays considerably as the frequency grows.

Piezoelectric coupling strength also declines at a slower rate than electrostatic coupling. The regression is slower because capacitive actuation results from a distributed force whereas piezoelectric actuation results from a distributed moment independent of the beam length. This improved coupling can potentially lead to enhanced filter performance and reduced noise [Piekarski, 2001].

3.3 Electrical Bandpass Filter Design

The development of a mechanical filter initially begins with the design of an electrical filter. The process initiates with a normalized, low-pass prototype model and concludes with an electrical bandpass circuit. The two major divisions known as the wide-band and narrow-band filters will be discussed. The focus turns to the narrow-band approach where several approximation methods are brought forth in Section 3.3.2.3 to solve for normalized filter elements, clarified further in Sections 3.3.2.4 and 3.3.2.5. In Section 3.3.2.6, the components can be transformed into denormalized values that create a useful electrical schematic.

3.3.1 Wide-band Bandpass Filter Design

While the primary focus of this thesis is narrowband filter design, a brief discussion of wide-band filters is given to highlight the differences. As mentioned, all filter design begins with a normalized, low-pass model. The wide-band approach is used when the ratio of the upper cutoff frequency to the lower cutoff frequency is greater than an octave. The basis behind the wide-band process is to separate the bandpass specification into individual low-pass and high-pass requirements, and then combine, or cascade, the two filters into one bandpass filter. This is a valid approach based on the assumption that the individual responses of each filter are maintained even though they are cascaded [Williams, 1988].

Once the bandpass specifications are separated, the low-pass and high-pass filters can be designed. The first step is to determine the shape factor, defined in Section 2.0, for each respective filter. This is used to determine the order and the filter approximation necessary to create the design. Specifics regarding the topics of order number and filter approximation will be discussed further in the narrow-band approach, found in Section 3.3.2.

With the order and approximation process known, a normalized lowpass circuit can be found for both the low-pass and high-pass filter. They are denormalized into actual element values with the help of some impedance scaling, and then combined. If the separation of cutoff frequencies is insufficient, an attenuator, in the form of a T- or π-circuit of resistors, is introduced to minimize interaction of impedance variations [Williams, 1988].

3.3.2 Narrow-band Electrical Bandpass Filters

A narrow-band filter is known to have a ratio of upper cutoff frequency to lower cutoff frequency that is less than an octave, while a bandpass quality factor of ten or greater is desirable for this design technique. The design of narrow-band bandpass filters can be realized by using coupling techniques where parallel tuned circuits, known as resonators, are interconnected with coupling elements such as inductors or capacitors. These configurations, because the tuning is simpler since all inductor-capacitor pairs resonate at the same frequency, are desirable for filters that fall into this narrow-band area. The basis behind the design method is the assumption that the coupling elements have a constant impedance with frequency [Williams, 1988].

3.3.2.1 All-pole Network

Every phase that ensues in the development of a filter is dependent upon the choice of low-pass filter approximation. The response approximation approach that could be applied are numerous, including Butterworth, Chebyshev, Cauer, Gaussian, and Legendre, to name a few [Zverev, 1967]. However, several of the common ones stem from the use of a normalized, all-pole, low-pass filter as the basis for obtaining the realizable system responses. The term, all-pole, depicts a transfer function that does not contain zeros in the numerator.

The transfer function that describes a low-pass, all-pole network is found in Equation (3.11).

$$H(s) = \frac{K}{r_0 s^n + r_1 s^{n-1} + \cdots + r_n} \tag{3.11}$$

The term, K, represents the gain of the system, whereas the order of the system is represented by n, which determines the total number of terms in the denominator.

The transfer function of Equation (3.11) is the result of methods used to approximate the ideal, rectangular magnitude response. A general approach used to create this ideal response is found in Equation (3.12). The magnitude can be written as

$$\left|H(j\omega)\right| = \frac{1}{\sqrt{1+\varepsilon^2\left\{\psi_n(\omega)\right\}^2}}. \tag{3.12}$$

where the term, ε, is never greater than unity and represents the height of the change in magnitude of the passband. The function $\psi_n(\omega)$ is an nth-order polynomial containing only even or only odd powers of the frequency, ω. The function $\psi_n(\omega)$ is replaced by a function that is based on the choice of low-pass filter approximation. Predetermined filter specifications are used to determine a satisfactory approximation method. Substitutions for $\psi_n(\omega)$ and ε are developed further in Sections 3.3.2.3 and 3.3.2.4. Equation (3.12) is a good approximation of the rectangular magnitude response if $\psi_n(\omega)$ is large in the stopband, and a small value in the passband [Blinchikoff, 1976].

3.3.2.2 Low-pass Prototype Circuit

The corresponding network that realizes the transfer function in Equation (3.11) is shown in Figure 3.9. The circuit is normalized, therefore the load resistance is always unity, and the circuit elements are dimensionless. The source resistance is denoted as R_S. If the order of the system is even, the final element is a capacitor in parallel. An inductor in series with the load resistance is used when there is an odd order system.

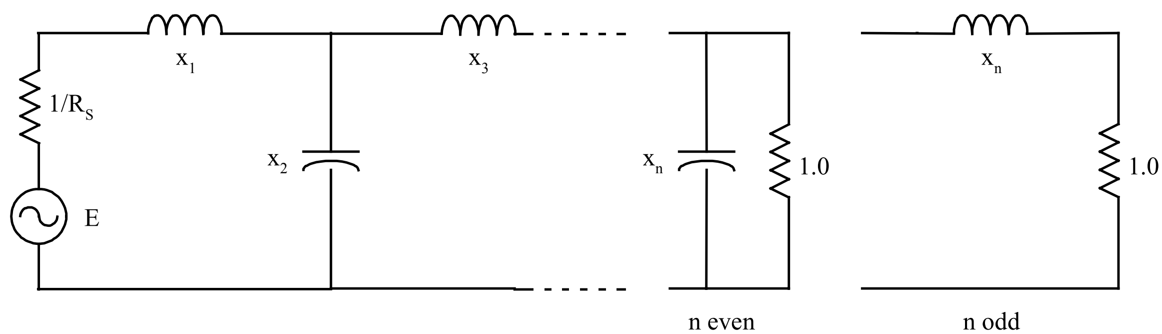

Figure 3.9 Low-pass prototype circuit [Blinchikoff, 1976]

3.3.2.3 Filter Approximations

As mentioned, an integral stage of the design process of a filter is the ideal low-pass approximation. It is a convenient method of obtaining realizable system responses that are useful for finding other filter types (bandpass, high-pass, etc.) by a suitable transformation [Blinchikoff, 1976]. Also, the normalized result does not need to be repeated for each filter type. The following sections review three common low-pass filter approximations, the Butterworth, the Chebyshev, and the Legendre.

3.3.2.3.1 Butterworth Approximation

The Butterworth approximation is a special form of a Taylor series approximation [Aatre, 1986]. It is based on the fact that the passband of the filter response is maximally flat, as shown in Figure 3.10(a). This causes a rolloff that is only moderately steep, as compared to the ideal vertical response. The belief behind this approximation is that a flat response when the frequency is zero is more important than the response at any other frequency [Williams, 1988]. In a normalized Butterworth low-pass filter, when the frequency is at unity, the 3dB attenuation is determined. Also, the poles of the normalized transfer function lie on a unit circle in the Laplace domain.

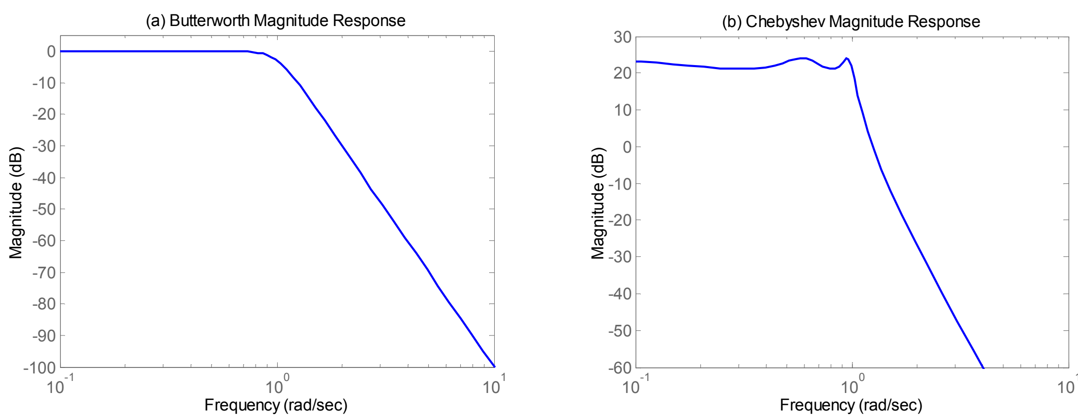

Figure 3.10 Butterworth (a) and Chebyshev (b) magnitude response plots

3.3.2.3.2 Chebyshev Approximation

The basis behind the Chebyshev response is to allow small wavelike variations, known as ripple, in the passband of the frequency response to achieve a steeper rolloff, more like the ideal vertical shape. The variations within the passband appear equally in magnitude, thus the Chebyshev is also known as the equiripple response. Figure 3.10(b) shows this response. The ripple value has units of decibels and denotes the height of the variations [Schaumann, 1990]. The number of half-cycles within the passband represents the order of the Chebyshev system. The minimum order of this system is a smaller value than the Butterworth approximation due to allowance of the ripples. Also, unlike those found by the Butterworth approximation, the normalized Chebyshev poles form the geometry of an ellipse.

3.3.2.3.3 Legendre Approximation

Another approximation method that is based on the all-pole network is known as the Legendre response. Its response falls somewhere between the Butterworth and Chebyshev functions. The steepness rate of the transition between the cutoff and stopband frequencies is more vertical than the Butterworth, but because it lacks passband variations, the Legendre does not compare to the Chebyshev response [Zverev, 1967]. Although somewhat unpopular, the Legendre response can be beneficial when a monotonic, or no passband ripple, requirement is a necessity.

3.3.2.4 Normalized Filter Elements

The end result of the approximation process is to find the normalized filter elements that are used to determine the actual elements of a filter. These normalized elements are the solutions to the values of x found in Figure 3.9. The approach is based on using the minimum order of the system, n, that still satisfies the specified filter characteristics.

3.3.2.4.1 Butterworth Approach

Because the Butterworth approximation is a maximally flat response, the ripple factor, ε, is equal to unity. From Natarajan, 1987, substituting ω^n for $\psi(\omega)$ in Equation (3.12) will produce the Butterworth magnitude response

$$\left|H(j\omega)\right| = \frac{1}{\sqrt{1+\omega^{2n}}}. \tag{3.13}$$

If the minimum stopband attenuation in decibels, A_a, is at and above the stopband frequency, ω_a, then the equation for this attenuation, from Equation (3.13), becomes

$$A_a \le 10\log(1+\omega_a{}^{2n}). \tag{3.14}$$

Equation (3.14) can be solved for the order number of the system. This inequality must be an integer, therefore it should be rounded up.

$$n \geq \frac{\log(10^{A_a*0.1} - 1)}{2\log(\omega_a)} \tag{3.15}$$

The next step is to solve for the poles of the network. Taking the square of both sides of Equation (3.13) is needed because $|H(j\omega)|^2 = H(j\omega)H(-j\omega)$ and all poles can be determined. After substituting s/j for ω, the denominator of Equation (3.13) squared is set equal to zero.

$$s^{2n} + (-1)^n = 0 \tag{3.16}$$

The roots, p_k, of Equation (3.16) can then be solved as

$$p_k = e^{[j(1+\frac{2k-1}{n})\frac{\pi}{2}]} \qquad k = 1, 2, \ldots, n\,. \tag{3.17}$$

The summation extends until $2n$, but because the poles of interest are only those that have negative real values, the value of k extends from one to n [Natarajan, 1987].

The complex Butterworth poles can be restated as

$$p_k = \sigma_k + j\lambda_k\,. \tag{3.18}$$

where the real and imaginary components of each pole are

$$\begin{aligned} \sigma_k &= -\sin[\frac{(2k-1)\pi}{2n}] \qquad k = 1, 2, \ldots n \\ \lambda_k &= \cos[\frac{(2k-1)\pi}{2n}] \qquad k = 1, 2, \ldots n. \end{aligned} \tag{3.19}$$

The normalized filter elements turn out to be equal to twice the negative of the real part of each pole, as shown in Equation (3.20).

$$\begin{aligned} x_i &= -2\sigma_i \qquad i = 1, 2, \ldots n \\ x_i &= 2\sin[\frac{(2i-1)\pi}{2n}] \end{aligned} \tag{3.20}$$

[Blinchikoff, 1976]

3.3.2.4.2 <u>Chebyshev Approach</u>

A Chebyshev polynomial refers to a class of equations that oscillate within the interval $-1 \leq x \leq +1$, while increasing in magnitude outside of this interval. This effect is shown in Figure 3.11.

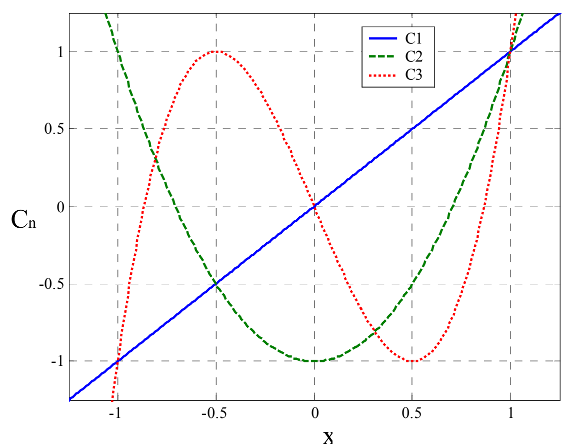

Figure 3.11 Chebyshev polynomials from n=1 to n=3

In terms of the real variable x, these equiripple functions can be defined as

$$C_n(x) = \begin{cases} \cos(n\cos^{-1}x) & |x| \leq 1 \\ \cosh(n\cosh^{-1}x) & |x| \geq 1. \end{cases} \tag{3.21}$$

[Blinchikoff, 1976]

Although it seems unlikely, a recursive formula can be derived to solve for each function. By taking into account only the first equation of Equation (3.21), let

$$\cos\theta = x \quad \& \quad \theta = \cos^{-1}x\,. \tag{3.22}$$

The substitution of Equation (3.22) into Equation (3.21), and the use of a trigonometric identity, gives the solutions to the values that fall one before and one after Equation (3.21).

$$\begin{aligned} C_{n+1}(x) &= \cos[\theta(n+1)] = \cos n\theta\cos\theta - \sin n\theta\sin\theta \\ C_{n-1}(x) &= \cos[\theta(n-1)] = \cos n\theta\cos\theta + \sin n\theta\sin\theta \end{aligned} \tag{3.23}$$

The addition of the two equations of Equation (3.23), and the substitution of Equation (3.22) and Equation (3.21) will result in

$$\begin{aligned} C_{n+1}(x) + C_{n-1}(x) &= 2\cos n\theta \cos\theta \\ C_{n+1}(x) + C_{n-1}(x) &= 2xC_n(x). \end{aligned} \qquad (3.24)$$

To find a Chebyshev polynomial in terms of the two polynomials that are the degrees immediately lower than it

$$C_{n+1}(x) = 2xC_n(x) - C_{n-1}(x)\,. \qquad (3.25)$$

[Su, 1996]

The magnitude response of a Chebyshev approximation can now be formed. The function $\psi(\omega)$ of Equation (3.12) is substituted by the Chebyshev polynomial, $C(\omega)$, determined in Equation (3.21). This allows for small passband deviations. The term, ε, represents the ripple height.

$$\left|H(j\omega)\right| = \frac{1}{\sqrt{1+\varepsilon^2 C_n^{\,2}(\omega)}} \qquad (3.26)$$

When the frequency of the system is at zero,

$$\left|H(j0)\right| = \frac{1}{\sqrt{1+\varepsilon^2 C_n^{\,2}(0)}}\,. \qquad (3.27)$$

In accordance to Equation (3.21), when n is an odd number

$$\begin{aligned} C_n(0) &= 0 \\ \left|H(j0)\right| &= 1, \end{aligned} \qquad (3.28)$$

and when n is even

$$\begin{aligned} C_n(0) &= \pm 1 \\ \left|H(j0)\right| &= \frac{1}{\sqrt{1+\varepsilon^2}}. \end{aligned} \qquad (3.29)$$

[Blinchikoff, 1976]

It is shown by Equation (3.28) that a Chebyshev filter with an odd order has no relative attenuation at DC. However, Equation (3.29) reveals that an even order system has some loss when the frequency is zero. This loss is known as passband ripple. Odd order filters are able to operate with equal source and terminating resistances. Conversely, because of the ripple, even order filters must function with unlike resistances [Williams, 1988].

When the attenuation versus frequency response of a filter is analyzed, the passband ripple in units of decibels from Equation (3.29) is

$$R_p = 10\log(1+\varepsilon^2)\,. \tag{3.30}$$

The ripple factor is defined in terms of the passband ripple

$$\varepsilon = \sqrt{10^{0.1*R_p} - 1}\,. \tag{3.31}$$

Equations (3.21) and (3.26) can be used to determine the minimum order of the network. If the minimum stopband attenuation, A_a, occurs at and above the stopband frequency, ω_a, assuming $\omega_a > 1$

$$A_a \le 10\log[1+\varepsilon^2\cosh^2(n\cosh^{-1}\omega_a)]\,. \tag{3.32}$$

Maneuvering Equation (3.32) to solve for the order number, an inequality is formed such as

$$n \ge \frac{\cosh^{-1}\left[\dfrac{10^{(A_a*0.1)}-1}{10^{(R_p*0.1)}-1}\right]^{0.5}}{\cosh^{-1}(\omega_a)}\,. \tag{3.33}$$

The order of the system must be an integer; therefore the inequality solution must be rounded to the next higher integer.

It is now an appropriate time to solve for the poles of the corresponding network function. The magnitude function, Equation (3.26), is again used in conjunction with Equation (3.21), and after squaring both sides the output becomes

$$\left|H(j\omega)\right|^2 = H(s)H(-s) = \frac{1}{1+\varepsilon^2\cos^2[n\cos^{-1}(\frac{s}{j})]}, \tag{3.34}$$

after the substitution of s/j for ω. The poles of Equation (3.34) can be determined, via Equation (3.35), from the values of s that make the denominator zero, while having negative real parts.

$$\cos[n\cos^{-1}(\frac{s}{j})] = \frac{\pm j}{\varepsilon}. \tag{3.35}$$

To begin, let us define a new complex variable

$$z = u + jv = \cos^{-1}(\frac{s}{j}). \tag{3.36}$$

Substituting Equation (3.36) into Equation (3.35) will produce Equation (3.37), as well as the expanded version after using a trigonometric identity

$$\begin{gathered}\cos(nz) = \cos(nu + jnv) \\ \cos(nu)\cosh(nv) - j\sin(nu)\sinh(nv) = \frac{\pm j}{\varepsilon}.\end{gathered} \tag{3.37}$$

The subsequent step is to equate the real and imaginary sections of the second equation of Equation (3.37). Noting that $\cosh(nv) \geq 1$ for any v, the real portion becomes

$$\begin{gathered}\cos(nu) = 0 \\ u_i = \frac{(2i-1)\pi}{2n} \qquad i = 1, 2, \ldots, 2n.\end{gathered} \tag{3.38}$$

For any solution of Equation (3.38), it is always true that

$$\sin(nu) = \pm 1. \tag{3.39}$$

Therefore, solving the imaginary portion of Equation (3.37) for v equates as

$$v = \frac{1}{n}\sinh^{-1}(\frac{1}{\varepsilon}). \tag{3.40}$$

To avoid confusion, let $s = p_i$. Now, in terms of the poles of the system, Equation (3.36) becomes

$$p_i = j\cos(u_i + jv)\,. \qquad (3.41)$$

Expanding the right-hand side of Equation (3.41) will result in a summation where the number of poles is twice the order of the system. This will account for both the positive and negative real parts of each pole.

$$p_i = \sin(u_i)\sinh(v) + j\cos(u_i)\cosh(v) \qquad i = 1, 2, \ldots, 2n \qquad (3.42)$$

Equation (3.42) can be simplified to

$$p_i = \sigma_i + j\lambda_i\,. \qquad (3.43)$$

The substitution of Equation (3.38), as well as realizing that only the negative real poles are wanted, Equation (3.43) can be broken down into

$$\begin{aligned} \sigma_k &= -\sin\left[\frac{(2k-1)\pi}{2n}\right]\sinh(v) \qquad k = 1, 2, \ldots n \\ \lambda_k &= \cos\left[\frac{(2k-1)\pi}{2n}\right]\cosh(v) \qquad k = 1, 2, \ldots n. \end{aligned} \qquad (3.44)$$

[Natarajan, 1987]

The terms of Equation (3.44) can be combined in such a way to produce the equation of the ellipse that contains the poles of the transfer function.

$$\frac{\sigma_k^{\,2}}{\sinh^2 v} + \frac{\lambda_k^{\,2}}{\cosh^2 v} = 1 \qquad (3.45)$$

In a normalized response, the 3dB frequency is usually specified when the frequency is equal to unity. In the Chebyshev case, the frequency at unity refers to the edge of the passband ripple. This means that the 3dB value must be found to normalize the poles. Because the maximum response of the denominator of Equation (3.26) is equal to the square root of two, the magnitude function becomes

$$\left|H(j\omega_{3dB})\right|^2 = \frac{1}{2}\,. \qquad (3.46)$$

Due to Equation (3.46), the following must also be true of the denominator of Equation (3.26).

$$\varepsilon^2 C_n^{\,2}(\omega_{3dB}) = 1 \qquad (3.47)$$

Knowing that ω_{3dB}>1, and that it is the value of interest, the variable will change its identification to ω', and with the substitution of Equation (3.21) into Equation (3.47) becomes

$$\omega' = \cosh[\frac{1}{n}\cosh^{-1}\frac{1}{\varepsilon}]. \qquad (3.48)$$

The normalized poles of the system can then be determined by dividing the existing poles of Equation (3.44) by the ω'value. These are scaled such that the 3dB attenuation falls at 1 rad/s.

$$\begin{aligned} \sigma_k' &= -\sin\left[\frac{(2k-1)\pi}{2n}\right]\left(\frac{\sinh(v)}{\omega'}\right) \qquad k = 1,2,\ldots n \\ \lambda_k' &= \cos\left[\frac{(2k-1)\pi}{2n}\right]\left(\frac{\cosh(v)}{\omega'}\right) \qquad k = 1,2,\ldots n \end{aligned} \qquad (3.49)$$

[Blinchikoff, 1976]

Figure 3.12 shows an example of a comparison between the normalized poles of both the Butterworth and Chebyshev systems, noting that the Chebyshev shape indicates a steeper rolloff.

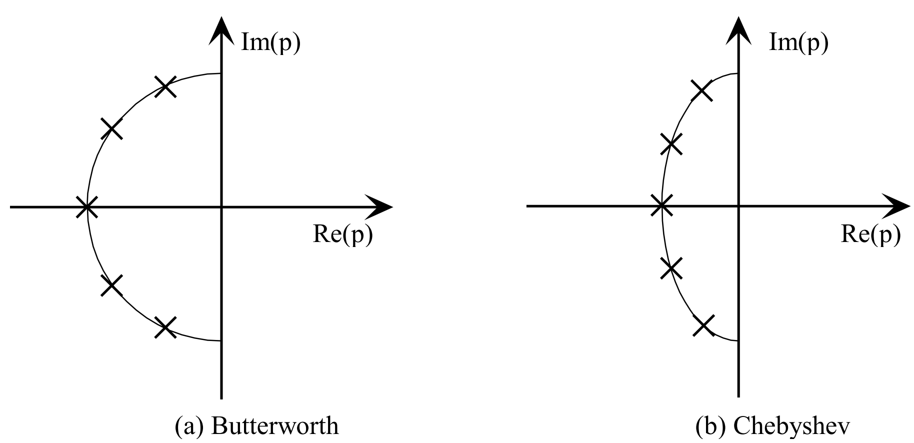

Figure 3.12 Butterworth and Chebyshev normalized poles for order n=5

All of the necessary components are now completed to determine the normalized Chebyshev element values. A few variables must first be equated though.

$$\begin{aligned} \beta &= \ln\left[\coth \frac{R_p}{40 \log e}\right] \\ \eta &= \sinh\left(\frac{\beta}{2n}\right) \\ b_k &= \eta^2 + \sin^2 \frac{k\pi}{n} \qquad k = 1, 2, \ldots, n-1 \\ a_k &= \sin(2k-1)\frac{\pi}{2n} \qquad k = 1, 2, \ldots, n \end{aligned} \tag{3.50}$$

The normalized element values, x, are a function of the ω' value, as well as the values of the variable g. These g values are determined by a backward summation using the a and b values of Equation (3.50).

$$\begin{aligned} g_n &= \frac{2a_n}{\eta} \\ g_{n-k} &= \frac{4a_{k+1}a_k}{b_k g_{n-k+1}} \qquad k = 1, 2, \ldots, n-1 \end{aligned} \tag{3.51}$$

$$x_i = \omega' g_i \qquad i = 1, 2, \ldots, n \tag{3.52}$$

[Cohn, 1957]

To summarize, the normalized elements values, represented by x, are dependent on which approximation method is chosen, as well as on the order of the system. They correspond to the x variables of the low-pass prototype circuit found in Figure 3.9. They will be employed to find the normalized coupling coefficients and quality factors, developed in Section 3.3.2.5.

The values can be found using Equation (3.20) if the Butterworth approach is chosen. Utilizing the Chebyshev approximation results in the use of Equation (3.52) to find the normalized elements.

3.3.2.5 Dimensionless Ratios

The normalized filter elements, such as determined in Equations (3.20) and (3.52), can be used to transform the lowpass prototype circuit, shown in Figure 3.9, into bandpass elements via useful dimensionless ratios. These ratios include the coefficient of coupling between the resonators, and the input and output normalized quality factors. The quality factor ($q_{1\ldots n}$) is defined as the quality of each reactive element influenced by the source and load resistance, if present. The coefficient of coupling (k_{ij}) is the ratio of the series-resonant frequency of the *i*th and *j*th reactive elements to the cutoff frequency [Zverev, 1967]. Explained in Section 3.3.2.6, these dimensionless ratios are used to determine denormalized bandpass elements in an electrical circuit. When developing a mechanical circuit, the normalized coupling coefficient is used to help develop the stiffness of the coupling wires.

3.3.2.5.1 Normalized Quality Factor

The quality factor is used to measure the losses of a reactive component of a filter. For an inductor L in series with a resistor R, and a capacitor C in parallel with a resistor R, as shown in Figure 3.9, the respective quality factors are

$$\begin{aligned} q &= \frac{\omega L}{R} \\ q &= \omega RC. \end{aligned} \tag{3.53}$$

If the capacitive or inductive elements have a finite quality factor when a lossless reactance was intended, setbacks could ensue. A problem that may occur is that the shape at the passband edge could become more rounded, therefore outputting a poor response. Also, if the filter calls for ripple in the design, the ripple within the response might be reduced in size or even fade away possibly causing unwanted increases in insertion loss and stopband magnitude [Williams, 1988].

A lossless network, such as in Figure 3.9, depicts the quality factor being represented at the normalized cutoff frequency, at which this frequency is known to equal unity. The quality factor of every element is equal to infinity, except for the first and the last. These are the only reactive elements that are influenced by the source or load resistance. With a few exceptions, the resistances will also become unity for the low-pass prototype circuit. This will make the normalized quality factors, Equation (3.54), equal to their respected normalized filter elements, equated in either Equation (3.20) or (3.52).

$$q_1 = x_1 R_s \qquad q_2 = q_3 = \cdots = q_{n-1} = \infty \qquad q_n = x_n R_L \tag{3.54}$$

3.3.2.5.2 Normalized Coupling Coefficient

Coupling is a phrase that is used somewhat loosely when spoken in terms of filters. The reference to coupling in modern filters is only with respect to the parasitic effects of one component on another [Zverev, 1967]. However, it is a common approach for normalizing configurations including low-pass, high-pass, bandpass, and band-reject filters.

With reference to Figure 3.9, the coupling coefficient is defined as

$$k_{ij} = \frac{\omega_{ij}}{\omega_{3dB}}, \tag{3.55}$$

with ω_{ij} representing the resonant frequency of two adjacent elements. The term $i=1 \ldots n-1$, while the value for $j=i+1$. From basic circuit knowledge, this resonant frequency term is identified as

$$\omega_{ij} = \frac{1}{\sqrt{x_i x_j}}. \tag{3.56}$$

Together, the two frequencies represent the normalized coupling coefficient as

$$k_{ij} = \frac{1}{\omega_{3dB}\sqrt{x_i x_j}}. \tag{3.57}$$

For lossless networks though, the cutoff frequency is known to be a value of unity. Therefore, Equation (3.57) becomes

$$k_{ij} = \frac{1}{\sqrt{x_i x_j}} \quad . \tag{3.58}$$

3.3.2.6 Electrical Network

The information throughout Section 3.3.2.5 is used to determine the electrical network of the filter. The schematic, shown in Figure 3.13, represents an n-order, passive, LC circuit, where actual element values can be equated. The resultant network grows from the roots of Figure 3.9, but is transformed from low-pass into bandpass form. The normalized electrical elements are also denormalized into useful inductance and capacitance values.

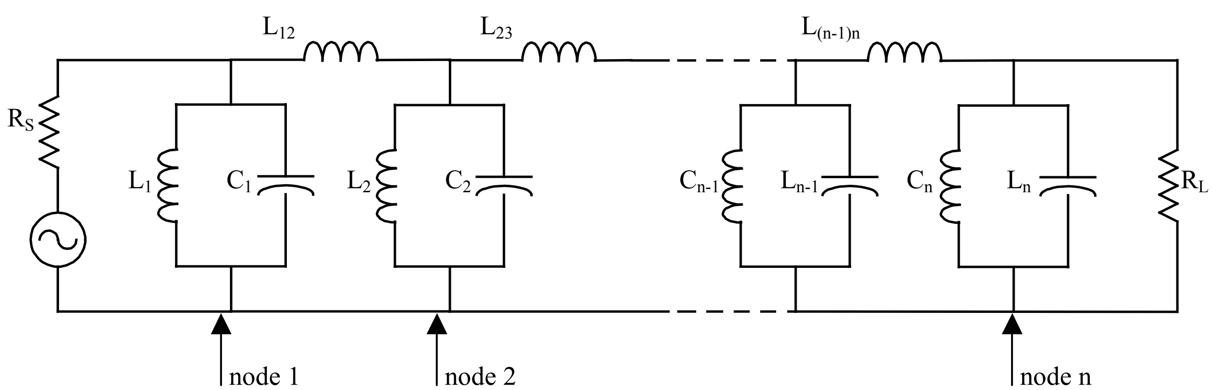

Figure 3.13 General electrical network for inductively coupled resonator filter

Section 3.3.2.5.1 states that the only reactive elements that are influenced by the source or load resistance are the initial and the final. Therefore, the denormalized quality factors ($Q_{1,n}$) can be determined, with the assistance of the bandpass quality formula, Equation (2.6), and the normalized quality factors, as

$$\begin{aligned} Q_1 &= Q_{bp} q_1 \\ Q_n &= Q_{bp} q_n . \end{aligned} \tag{3.59}$$

The normalized coupling coefficients, as well as the bandpass quality factor, are used to determine the denormalized values as

$$\hat{K}_{ij} = \frac{k_{ij}}{Q_{bp}}. \tag{3.60}$$

To determine the source (R_S) and load (R_L) resistances necessary to activate and terminate the circuit, the quality factor for a capacitor can be reworked to solve for the resistances as

$$\begin{aligned} R_S &= \frac{Q_1}{\omega_o C} \\ R_L &= \frac{Q_n}{\omega_o C}. \end{aligned} \tag{3.61}$$

The capacitance, C, is necessarily chosen as an arbitrary value, but the value is based on convenience. Each capacitor value will be identical throughout each parallel-tuned section from unity to n.

$$C_i = C \qquad i = 1, 2, \ldots n \tag{3.62}$$

It is known that each parallel circuit, or node, within the network of Figure 3.13, vibrates at a tuned resonant frequency. Therefore, the total nodal inductance (L_{node}) can be found by using basic electrical frequency knowledge, and is determined as

$$L_{node} = \frac{1}{\omega_o^2 C} \qquad i = 1, 2, \ldots n. \tag{3.63}$$

In order for all nodes to oscillate at the resonant frequency, a network will include n nodes containing the same values of L_{node} and C in each.

The coupling inductors can also be realized, with the help of the denormalized values of Equation (3.60), as well as Equation (3.63), by

$$L_{ij} = \frac{L_{node}}{\hat{K}_{ij}}. \tag{3.64}$$

Each node is also tuned to a resonant frequency with the coupling inductors (L_{ij}) that are adjacent to the ith inductor, shorted to ground. This occurs so that the coupling inductors connected to that node are placed in parallel across the tuned circuit [Williams, 1988]. In addition, the inductor of each node (L_i) can be manipulated from the equation of the total nodal inductance, which is

$$L_{node} = \frac{1}{\dfrac{1}{L_{i-1,i}} + \dfrac{1}{L_i} + \dfrac{1}{L_{i,i+1}}} \qquad i = 1, 2, \ldots n. \tag{3.65}$$

The network of Figure 3.13 is the electrical basis for the mechanical filter. Section 3.2.2.1 explained how mathematical models are used to create mechanical schematics of Figure 3.13. In a mechanical filter that utilizes the mobility analogy, explained in Section 3.2.2.1.2.2, the parallel-tuned, LC circuits are the electrical components that are represented in a mechanical network by the vibrating resonators, while the coupling inductors are analogous to the coupling wires in a mechanical system.

3.4 Summary of Important Research

To review, with the information described in Section 3.0, a design process can be created for mechanical bandpass filters. Facts pertaining to filters, whether purely electrical or electromechanical, were presented initially. All designs begin with a choice of filter approximation. This was explained while specifically describing the basis behind the Butterworth and Chebyshev approximations.

Other topics discussed included those that pertained to the electromechanical family of filters. An explanation of the different forms of electromechanical filters was first presented. The specific subject matters that are unique to electromechanical filters followed. These included passages regarding the electromechanical transducers and resonators.

The strictly mechanical filter was the topic of several subsections. Within these subsections, the subject of mathematical models that are used to describe the filter was included. There are two analogies that can be applied to the models when converting from mechanical-to-electrical terms, and vice versa. The mobility analogy was explained in detail because that is the form that will be exercised in the design example.

Also specific to mechanical filters, the topic of using wires to couple the resonators to create the filter structure was focused on. The idea behind this technique and the necessary derivations were included. Lastly, a clarification of the types of microstructure electromechanical filters was presented.

4.0 MACRO-SCALE DESIGN PROCEDURE

This section presents the theoretical design procedure used to create a mechanical bandpass filter from known filter specifications. General overviews of each phase will be followed by an example that will be designed, fabricated, and tested. In order to be consistent with an approach that a micro-scale filter might use, it was the decision of the author to create a filter using a collection of cantilevered beams that vibrate in a bending mode. The final design can be found in Figure 4.1.

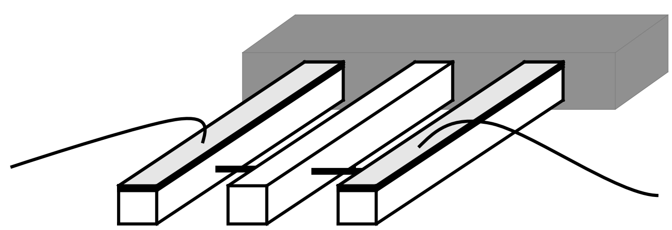

Figure 4.1 Cantilevered beam mechanical filter design

4.1 Filter Specifications

The mechanical bandpass filter design process is somewhat open-ended, with a mastering of this skill coming only through experience. The initial inputs come from filter requirements specified by the user. These include the center frequency (ω_o), as well as the cutoff and stopband bandwidths. Depending on the requirements, a maximum number of resonators can also be specified. In addition, based on the choice of filter approximation, as seen in Section 3.3.2.3, an amount of ripple can be selected. The attenuation at which the cutoff bandwidth (B) is normally found is the 3dB point, while the stopband bandwidth is chosen to occur at 40 dB (B_{40}).

4.1.1 Example

The Chebyshev, or equiripple, approximation (Sections 3.3.2.3.2 and 3.3.2.4.2) will be used to analytically design the amplitude versus frequency response. The specifications that characterize this response include the center frequency, cutoff bandwidth, and stopband bandwidth. A ripple (R_p) of one decibel (1dB) is also considered acceptable within the passband. The specifications are shown in Table 2 and a frequency response using the specifications is shown in Figure 4.2.

Table 2 Filter specifications

Center frequency (ω_o)	10 krad/s	1590 Hz
Passband bandwidth (B)	0.5 krad/s	80 Hz
Stopband bandwidth (B_{40})	2.77 krad/s	440 Hz
Passband ripple (R_p)	1 dB	

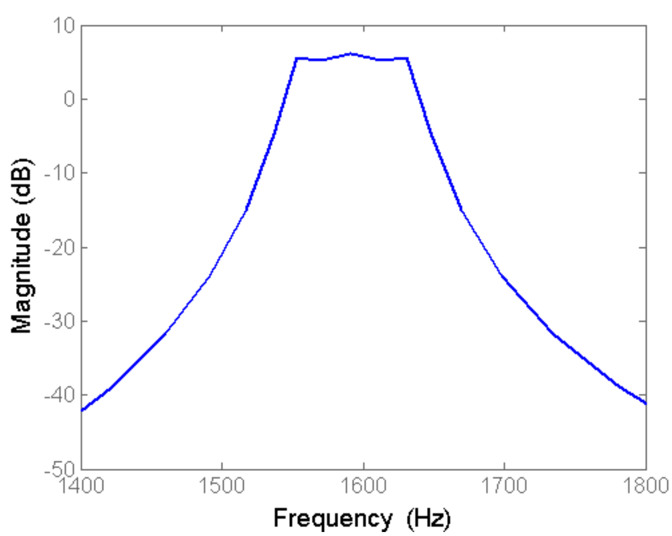

Figure 4.2 Frequency response using filter specifications and Chebyshev approximation

4.2 Minimum Number of Resonators

The minimum number of resonators needed to arrive at the chosen filter specifications can subsequently be found. This inequality is solved based on the filter approximation chosen. Commonly, the equation is a function of the passband and stopband attenuations, as well as the shape factor (B_{40}/B). The solution is rounded up to the next integer. The number of resonators can also be found using the response curves for attenuation characteristics created in such texts as Williams, 1988.

4.2.1 Example

The order number, or the number of resonators, for a normalized lowpass Chebyshev response is derived as

$$n \geq \frac{\cosh^{-1}\left[\frac{10^{(A_a*0.1)}-1}{10^{(R_p*0.1)}-1}\right]^{0.5}}{\cosh^{-1}(\omega_a)}. \tag{3.33}$$

To avoid confusion, let the arbitrary normalized frequency value of $\omega = \Omega$. Once the lowpass-bandpass transformation is applied, two new frequencies are outputted as

$$\begin{aligned} \omega_1 &= -\frac{B\Omega}{2}+\sqrt{\omega_o^2+\left(\frac{B\Omega}{2}\right)^2} \\ \omega_2 &= \frac{B\Omega}{2}+\sqrt{\omega_o^2+\left(\frac{B\Omega}{2}\right)^2}. \end{aligned} \tag{4.1}$$

The two values of Equation (4.1) are related by

$$\omega_1\omega_2 = \omega_o^2 \tag{4.2}$$

and

$$\omega_2 - \omega_1 = B\Omega. \tag{4.3}$$

The bandpass response now has two frequencies in the passband and in the stopband. Knowing that the normalized lowpass cutoff frequency, Ω_c, will occur at 1 and –1 rad/sec, the passband frequencies can be found using Equations (4.2) and (4.3) as

$$\omega_{p1}\omega_{p2} = \omega_o^{\,2} \tag{4.4}$$

and

$$\omega_{p2} - \omega_{p1} = B\,. \tag{4.5}$$

Similarly, the normalized lowpass rejection band has two frequencies occurring at $\Omega = \Omega_a$ and $\Omega = -\Omega_a$. These are now transformed into bandpass form as

$$\omega_{a1}\omega_{a2} = \omega_o^{\,2} \tag{4.6}$$

and

$$\omega_{a2} - \omega_{a1} = B\Omega_a\,. \tag{4.7}$$

Equation (4.5) can be substituted into Equation (4.7) to produce Ω_a. This value is also known as the shape factor (*SF*) of a bandpass response.

$$\Omega_a = SF = \frac{\omega_{a2} - \omega_{a1}}{\omega_{p2} - \omega_{p1}} \tag{4.8}$$

[Natarajan, 1987]

As a design choice, it is known that the minimum stopband attenuation, A_a, occurs at 40dB. Equation (4.8) can be substituted into Equation (3.33) to create a new inequality for the order of a bandpass Chebyshev response as

$$n \geq \frac{\cosh^{-1}\left[\frac{10^{(40*0.1)} - 1}{10^{(R_p*0.1)} - 1}\right]^{0.5}}{\cosh^{-1}(SF)}\,. \tag{4.9}$$

Knowing the shape factor due to the specifications in Table 2, the minimum number of resonators (n) can be found. The result, after rounding to the next highest integer, is three (3).

4.3 Interior Resonator Dimensions

The next step in the design process is to produce the dimensions of the interior resonators. Once a material is chosen, the geometry and vibrational mode is decided upon. Commonly, lower frequency applications (1-100 kHz) use a beam geometry vibrating in the flexural mode, while a disk vibrating in flexure or a longitudinally vibrating bar is used for applications where higher center frequencies (50-500 kHz) are desired. Using vibrational theory of continuous systems, the length, width, and thickness, or length and diameter, can be modified. Boundary conditions, as well as the excited mode number, are chosen and used in conjunction with the center frequency and material properties to solve for the appropriate resonator dimensions.

4.3.1 Example

The designed mechanical filter uses flexurally vibrating cantilevered beams, coupled with wires, to produce the filter specifications. The material chosen for both is stainless steel. Stainless steel has favorable properties such as excellent temperature stability and high mechanical quality factor.

The dimensions of the interior Type 316 stainless steel beam will be calculated using continuous vibrational beam theory, revealed in Section 3.2.1.3.2. It is sufficient to excite the resonators in the fundamental mode to produce the sought after results. The equation for the resonant frequency of a vibrating beam is

$$\omega_o = \beta l_r^2 \sqrt{\frac{E_r I_r}{\rho_r A_r l_r^4}} \,. \tag{3.2}$$

The material properties of the resonators are seen in Table 3. The subscript, r, represents a resonator property. The area and the moment of inertia of each beam can be determined respectively as

$$A_r = w_r t_r \tag{4.10}$$

$$I_r = \frac{w_r t_r^3}{12}. \tag{4.11}$$

Table 3 Material properties of stainless steel

Modulus of elasticity (E_r)	190e9 Pa
Density (ρ_r)	7920 kg/m^3

Equation (3.2) can be altered, in conjunction with Equations (4.10), (4.11), and Table 3, to find a ratio of the resonator thickness to its squared length, Equation (4.12). It can be shown that the final dimensions are independent of the width of the resonator.

$$\frac{t_r}{l_r^2} = \frac{\dfrac{\omega_o}{\beta l_r^2}}{\sqrt{\dfrac{E_r}{12\rho_r}}} \tag{4.12}$$

This beam theory is used under the assumption that the beams are slender, that is, the length is at least ten times the scale of both the width and the thickness. Therefore, the final dimensions are determined in Table 4.

Table 4 Interior resonator dimensions

Length (l_r)	3.893 cm	1.533”
Width (w_r)	0.318 cm	0.125”
Thickness (t_r)	0.305 cm	0.120”

4.4 Transducer and Outer Resonator Dimensions

The next stage is to develop the dimensions that pertain to the electromechanical transducer. A decision must be made regarding the material, followed by an examination into which mode the transducer is to excite within the resonator. Typically, the transducer is attached to the outer resonators, but this is not always the case. An assessment of the transducer properties will also help to discover the dimensions of the outer resonators.

4.4.1 Example

Piezoceramic transducers will be used as the actuator and sensor for the system. The choice of material is PZT-5H manufactured from Piezo Systems Inc. The material properties can be found in Table 5.

Table 5 Material properties of the piezoelectric ceramic

Modulus of elasticity (E_p)	50e9 Pa
Density (ρ_p)	7700 kg/m^3

Total coverage of the resonator is used to excite the fundamental mode, and the PZT thickness of 0.0075" is fixed by the manufacturer. Therefore, most of the dimensions of the transducer are identified. Because there are two different materials combining to form one beam, the length of the outside resonators will be different from the interior in order to resonate at the specified center frequency.

Composite beam theory (Inman, 2001) is used to determine the new moment of inertia, Equation (4.15), with Equation (4.14) establishing the position of the centroidal axis. Figure 4.3 displays a diagram of the composite beam transformation.

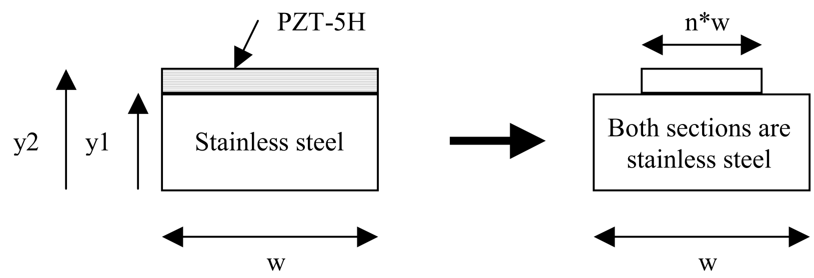

Figure 4.3 Diagram showing composite beam transformation

$$n = \frac{E_p}{E_r} \tag{4.13}$$

$$\bar{y} = \frac{y_1^2 w(1-n) + y_2^2 nw}{2[y_1 w(1-n) + y_2 wn]} \tag{4.14}$$

$$I_x = \frac{w[y_1^3 + n(y_2 - y_1)^3]}{12} + y_1 w(\frac{y_1}{2} - \bar{y})^2 + nw(y_2 - y_1)[\frac{(y_1 + y_2)}{2} - \bar{y}]^2 \tag{4.15}$$

The same lateral vibration frequency equation, seen in Equation (3.2), is used to determine the necessary length of the outside resonators, with the mass per unit length equaling the summation of the density multiplied by the cross-sectional area of each material.

$$l_{ro} = \left[\frac{E_r I_x (\beta l)^4}{(\rho_p A_p + \rho_r A_r)\omega_o^2} \right]^{1/4} \tag{4.16}$$

Using Equation (4.16), the final dimensions of the outer resonators are shown in Table 6.

Table 6 Dimensions of the outer resonators

Length (l_{ro})	3.887 cm	1.530”
Width (w_{ro})	0.318 cm	0.125”
Thickness (t_{ro})	0.305 cm	0.120”

The dimensions of the transducers can also be found using the above information. The thickness of the transducers is a known value. The other dimensions come from Table 6 because full coverage of the resonators is desired. Therefore, the length, width, and thickness of the outer resonators are given in Table 7.

Table 7 Piezoelectric transducers dimensions

Length (l_p)	3.887 cm	1.530”
Width (w_p)	0.318 cm	0.125”
Thickness (t_p)	0.019 cm	0.0075”

The effect of the piezoelectric transducer on the dynamics of the outer resonators is minimal. In this case, when comparing the length of the outer resonators to that of the inner resonator, found in Table 4, there was a change of only a few thousandths of an inch.

4.5 Normalized Quality Factors and Coupling Coefficients

In order to determine the values of the final two constituents related to the mechanical filter, the elements known as the normalized quality factors and coupling coefficients need to be uncovered. Section 3.3.2.5 explains the purpose of these dimensionless ratios that originate from the lowpass prototype circuit, found in Figure 3.9.

The electrical circuit model, discussed in Section 4.7, is determined with the help of both the normalized quality factors ($q_{1 \ldots n}$) and the normalized coupling coefficients (k_{ij}). The coupling coefficients also play an important role in finding the dimensions of the coupling wires, found in Section 4.6. As in Section 3.3.2.5, the equations for the quality factors and the coupling coefficients are respectively derived as

$$q_1 = x_1 R_S \qquad q_2 = q_3 = \cdots = q_{n-1} = \infty \qquad q_n = x_n R_L \tag{3.54}$$

$$k_{ij} = \frac{1}{\sqrt{x_i x_j}} \quad , \tag{3.58}$$

where $i=1...n-1$, $j=i+1$, and x represents each normalized filter element value. The variables R_S and R_L respectively stand for the source and load resistances of the lowpass prototype circuit. The solution for the normalized filter elements is representative of the choice of filter approximation.

The quality value of every element is theoretically equal to infinity, except for the first and the last. These are the only reactive elements that are influenced by the source or load resistance. The values of $q_{1...n}$ and k_{ij} can also be found in table form in such texts as Williams, 1988.

4.5.1 Example

Using the established information regarding the choice of filter approximation, allowable ripple, and the number of resonators, the normalized quality factors ($q_{1...n}$) and coupling coefficients (k_{ij}) can be found by using Equations (3.54) and (3.58). In accordance to Section 3.3.2.4.2, the cutoff frequency for the Chebyshev approach does not occur at unity, but at the edge of the ripple band. Therefore, the 3dB frequency is derived as

$$\omega' = \cosh[\frac{1}{n}\cosh^{-1}\frac{1}{\varepsilon}], \tag{3.48}$$

where the ripple factor, ε, is defined as

$$\varepsilon = \sqrt{10^{0.1*R_p} - 1}\,. \tag{3.31}$$

The normalized element values for the Chebyshev response are determined by

$$x_i = \omega' g_i \qquad i = 1, 2, \ldots, n\,, \tag{3.52}$$

where the values of g_i can be found by the algorithm

$$g_n = \frac{2a_n}{\eta}$$
$$g_{n-k} = \frac{4a_{k+1}a_k}{b_k g_{n-k+1}} \qquad k = 1,2,\ldots,n-1, \tag{3.51}$$

along with the assistance of

$$\beta = \ln\left[\coth\frac{R_p}{40\log e}\right]$$
$$\eta = \sinh\left(\frac{\beta}{2n}\right)$$
$$b_k = \eta^2 + \sin^2\frac{k\pi}{n} \qquad k = 1,2,\ldots,n-1 \tag{3.50}$$
$$a_k = \sin(2k-1)\frac{\pi}{2n} \qquad k = 1,2,\ldots,n.$$

It is understood that the source and load resistances are unity when the order of the system is an odd number. Therefore, all of the segments can be accounted for and the solutions to Equations (3.54) and (3.58), found in Sections 3.3.2.5 and 4.5, are shown in Table 8.

Table 8 Dimensionless ratios

Normalized quality factors (q_1=q_3)	2.210
Normalized coupling coefficients (k_{12}=k_{23})	0.645

4.6 Coupling Wire Dimensions

The design of the coupling wire found between each resonator is the next step in the creation of a theoretical mechanical filter. This design is introduced by the choice of material that suits the needs of the filter, followed by the decision of the vibrational mode in which the wires will oscillate. The geometry of the resonators, as well as the boundary conditions, will be used to determine their equivalent mass (M_{eq}) values. The mass at the coupling position is a point of interest to eventually help determine the stiffnesses of the coupling wires. The importance of this is that the compliances of the coupling wires help determine the bandwidth of the filter. These stiffnesses, known as the required coupling wire stiffnesses, are found by

$$K_{ij} = k_{ij}\frac{B}{\omega_o}\sqrt{\underline{K}_i\underline{K}_j}\ , \tag{4.17}$$

where the stiffness of each resonator is found commonly as

$$\underline{K}_i = \omega_o^{\,2} M_{eq}\ . \tag{4.18}$$

Incorporation of the end conditions for the coupling wire system is used to help develop a finite element stiffness matrix. The elements within this matrix contain the variables needed to complete the design. Sufficient diameters and lengths for each prospective wire can be extracted from the stiffness equation.

4.6.1 Example

The wires, akin to the resonators, vibrate in a flexural mode and are made from a similar stainless steel material (Type 302). The coupling point is at sixty percent (60%) of the length of each resonator from the fixed end. This was a design decision based on the value of the equivalent mass at that position. At this location, the equivalent mass of a cantilevered beam is

$$\begin{aligned} M_{eq_{normalized}} &= 1.176 \\ M_{eq_{60\%}} &= 1.176\rho_r A_r l_r. \end{aligned} \tag{4.19}$$

Equation (4.19) leads to the stiffness solutions for each resonator, which can be found by using Equation (4.18). With that, there is sufficient information, using Equation (4.17), to solve for the required coupling stiffnesses of each wire.

It is assumed that sliding joints, which constrain the movement to a vertical plane, bound the nodes of the wire. Using this boundary condition information, a stiffness matrix is next found using finite element methods. The method for creating the stiffness matrix is explained comprehensively in Section 3.2.2.2.2. After the reduction of the matrix, the coupling wire stiffness equation becomes

$$K_{ij} = \frac{12 E_w I_w}{l_{wij}^{\ 3}}, \tag{3.10}$$

with the subscript w representing the wire. The modulus of elasticity is equal to that of the resonators (Table 3), and the moment of inertia of a circular cross-section beam is

$$I_w = \frac{\pi d_{wij}^{\ 4}}{64}. \tag{4.20}$$

Therefore, suitable dimensions for the coupling wire are given in Table 9.

Table 9 Dimensions of the coupling wire

Wire length ($l_{w12}=l_{w23}$)	1.415 cm	0.557"
Wire diameter ($d_{w12}=d_{w12}$)	0.074 cm	0.029"

4.7 Electrical Model

Although not directly associated with the mechanical design process, the creation of an electrical network is beneficial. The model is a passive LC circuit using inductive coupling. Section 3.3.2.6 explains this topic thoroughly, and a general circuit schematic can be found in Figure 3.13.

The initial stage is to denormalize the previously solved normalized values of $q_{1 \ldots n}$ and k_{ij}. The bandpass quality factor is used in both equations and is repeated here as Equation (2.6) from Section 2.2.3.

$$Q_{bp} = \frac{\omega_o}{B} \tag{2.6}$$

while the denormalized quality factors and coupling coefficients are respectively found as

$$
\begin{aligned}
Q_1 &= Q_{bp} q_1 \\
Q_n &= Q_{bp} q_n
\end{aligned}
\tag{3.59}
$$

$$
\hat{K}_{ij} = \frac{k_{ij}}{Q_{bp}}. \tag{3.60}
$$

The network contains both series-arm inductors, as well as parallel circuits. These circuits, or nodes, are tuned to the same frequency. Therefore, a nominal capacitance value (C) can be chosen, and the corresponding nodal inductance (L_{node}) can be equated. The source and load resistances, as well as the coupling inductances are respectively shown as

$$
\begin{aligned}
R_S &= \frac{Q_1}{\omega_o C} \\
R_L &= \frac{Q_n}{\omega_o C}
\end{aligned}
\tag{3.61}
$$

$$
L_{node} = \frac{1}{\omega_o{}^2 C} \qquad i = 1, 2, \ldots n\,. \tag{3.63}
$$

The coupling inductor values are next found with the assistance of Equations (3.60) and (3.63) as

$$
L_{ij} = \frac{L_{node}}{\hat{K}_{ij}}. \tag{3.64}
$$

Lastly, maneuvering the formula for the total nodal inductance, found in Equation (3.65), can help uncover each nodal inductor, L_i.

$$
L_{node} = \frac{1}{\dfrac{1}{L_{i-1,i}} + \dfrac{1}{L_i} + \dfrac{1}{L_{i,i+1}}} \qquad i = 1, 2, \ldots n \tag{3.65}
$$

4.7.1 Example

The necessary tools are now given to produce an electrical model for the passive LC circuit. The system is third order; therefore it will contain three nodes. Following the steps generated in Section 4.7, Table 10 contains the circuit element values, while the network layout can be seen in Figure 4.4.

Table 10 Electrical network values

Nodal capacitance (C_1=C_2=C_3)	0.295 μF
Nodal inductance (L_1=L_2=L_3)	33.9 mH
Coupling inductance (L_{12}=L_{23})	1.05 H
Source/load resistance (R_S=R_L)	15 kΩ

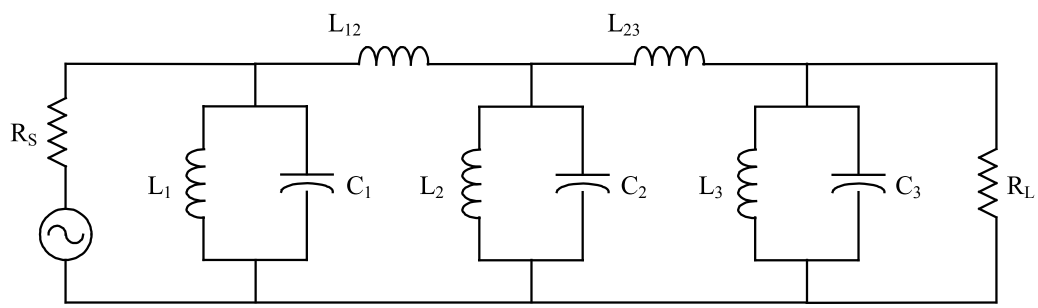

Figure 4.4 Three node electrical network of an inductively coupled resonator filter

4.8 Summary of Design Procedure

The design procedure begins with the selection of filter specifications that are important to the application. These can include such properties as center frequency, bandwidth, and insertion loss. A method of approximating the filter (such as the Butterworth or Chebyshev approach) has to be chosen next. This affects what the frequency response will look like. The order of the filter is then found. This value is equal to the number of resonators needed to output the desired response. The interior resonator dimensions are then determined through vibrational theory. The establishment of the outer resonator and electromechanical transducer dimensions follows this. Composite beam theory is used to assist in finding the dimensions. The normalized coupling coefficients and quality factors are found next and help create the final steps of the design. The normalized coupling coefficients, as well as the center frequency and bandwidth, are used to determine the dimensions of the coupling wires found between each pair of resonators. Although not necessary, the electrical model is lastly determined with the assistance of the normalized quality factors and coupling coefficients. Table 11 shows all dimensions used in the creation of the mechanical filter.

Table 11 Dimensions of designed mechanical filter

Interior resonator dimensions		
Length (l_r)	3.893 cm	1.533”
Width (w_r)	0.318 cm	0.125”
Thickness (t_r)	0.305 cm	0.120”
Outer resonator dimensions		
Length (l_{ro})	3.887 cm	1.530”
Width (w_{ro})	0.318 cm	0.125”
Thickness (t_{ro})	0.305 cm	0.120”
Piezoelectric transducer dimensions		
Length (l_p)	3.887 cm	1.530”
Width (w_p)	0.318 cm	0.125”
Thickness (t_p)	0.019 cm	0.0075”
Coupling wire dimensions		
Wire length (l_{w12}=l_{w23})	1.415 cm	0.557”
Wire diameter (d_{w12}=d_{w12})	0.074 cm	0.029”

5.0 EXPERIMENTAL SETUP AND RESULTS

Section 5.1 will include a description of the necessary equipment needed for the testing of narrowband mechanical filters. Various tests were run to determine if the assorted parameters have been met. These tests will be described, and a listing of the corresponding data and plots will be illustrated throughout Section 5.2.

5.1 Equipment Setup

For the example of the mechanical filter made up of the trio of coupled cantilevered beams, the primary tests that were run involved obtaining a magnitude vs. frequency plot. To obtain the necessary data points, a frequency sweep in the region of the center frequency of the filter was created. This was achieved by following the schematic shown in Figure 5.1. A photograph of the actual setup follows in Figure 5.2.

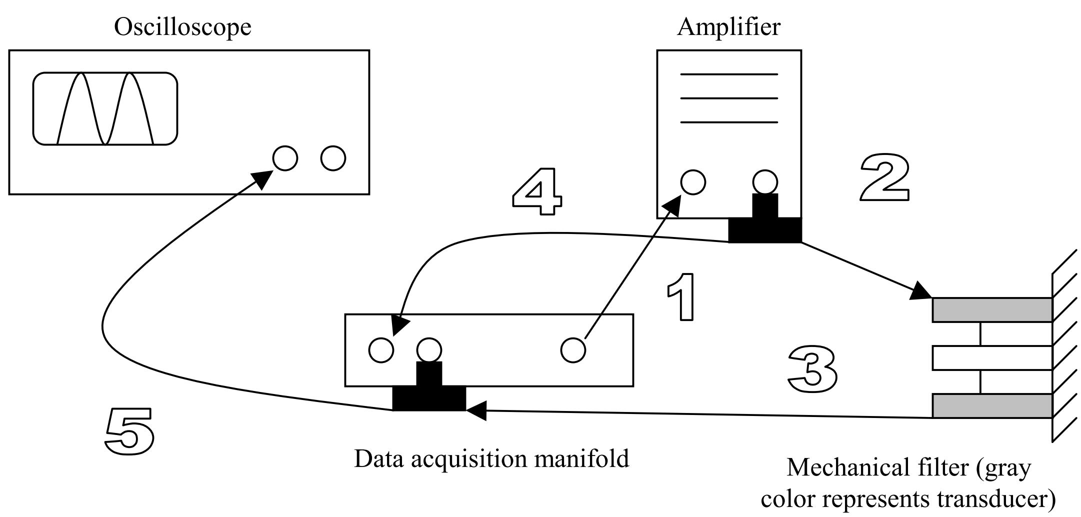

Figure 5.1 Schematic of testing apparatus

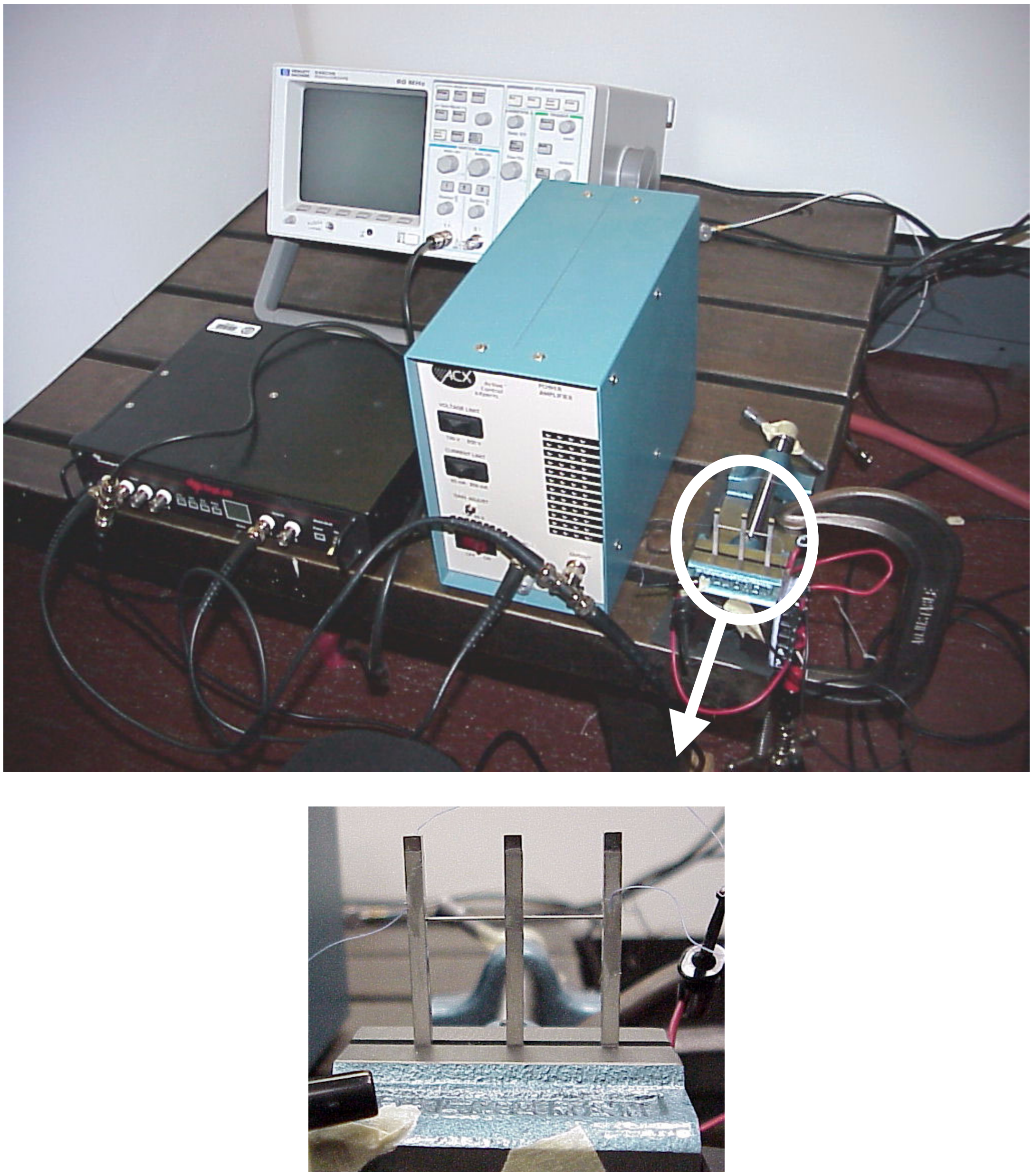

Figure 5.2 Photographs of filter testing setup

SigLab, a data acquisition hardware and software package developed to interface with MATLAB software, was used to carry out the testing. A voltage was created by the SigLab manifold into the ACX power amplifier (1). From the amplifier, the signal was sent to the actuating resonator where the filtering took place (2). Simultaneously, the signal coming directly from the ACX amplifier was sent to channel 1 of the manifold (4). The output resonator of the filter structure acted as a sensor where the signal was sent back to channel 2 of the SigLab manifold (3). The two inputs were used as a comparator in order for the actual voltage signal to be presented. Another cable was connected from the manifold, at channel 2, to an oscilloscope (5) to track the sensed voltage levels during the frequency sweep. The end product was the representative Bode plot with the abscissa and ordinate in terms of hertz and decibels, respectively.

5.2 Results

Several tests were run on the fabricated filter structure to determine whether the design is legitimate. As mentioned, a frequency sweep was used to create a number of magnitude vs. frequency plots. Plots were generated for every beam of each filter, as well as on the completed structure itself. The target of the testing was to output values that fall within the predetermined design specifications.

Also, a range of terminating resistances was inserted into the filter circuit to determine the benefits and setbacks. Finally, the coupling wire length of one of the fabricated filters was varied to determine the effects and how they relate to analytically modeled values.

Each filter contains three beams that vibrate individually, but are coupled to create a bandpass response. Naturally, each individual beam was tested first. A completed beam, such as shown in Figure 5.3, contains a patch of Piezo Systems Inc. PZT-5H on the top face that performs the actuation. A second, smaller patch is placed on the bottom face of the beam to sense the movement.

The stainless steel beams were initially cut to size and then ground and polished, using a Buehler ECOMET 6 variable speed grinder-polisher, to obtain a better surface finish. The PZT was then cut to size using a Buehler ISOMET 1000 precision saw. The attachment of the PZT to both the top and bottom face of each resonator was achieved by bonding the PZT to the beam with Loctite Quick Set epoxy. Once cured, the coupling wires were attached to complete the construction of the filter. Each coupling wire was cut to size and soldered to the beam at the specified coupling point, which is dependent on the position of the equivalent mass. The solder is a 96% tin, 4% silver composite measuring 0.020” in diameter and is manufactured by SRA Inc.

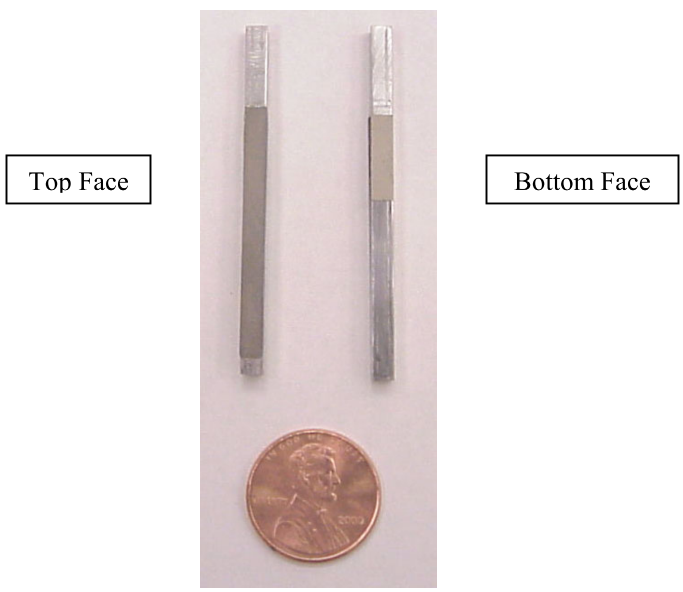

Figure 5.3 Top and bottom faces of individual resonator beam

Using the setup described in Section 5.1 and shown in Figures 5.1 and 5.2, a frequency sweep was conducted to determine the characteristics of the beam. Properties such as the resonant frequency, 3dB bandwidth (*B3*), and peak magnitude were determined. Such an example is given in Figure 5.4. All of the individual beam response plots, as well as their relevant characteristics, can be found in Appendix A. The primary result extracted from these plots was the fundamental resonant frequency of the beam. The center frequency (ω_o) of the mechanical filter stems from the natural frequencies of each beam contained within it. Therefore on occasion, a few of the beams have to be tuned for all to vibrate at the same natural frequency. For these samples, the beam with the highest natural frequency value was used as the set point, while the others were tuned to that frequency. Shortening from the length dimension of the beam, by grinding, constitutes the tuning step.

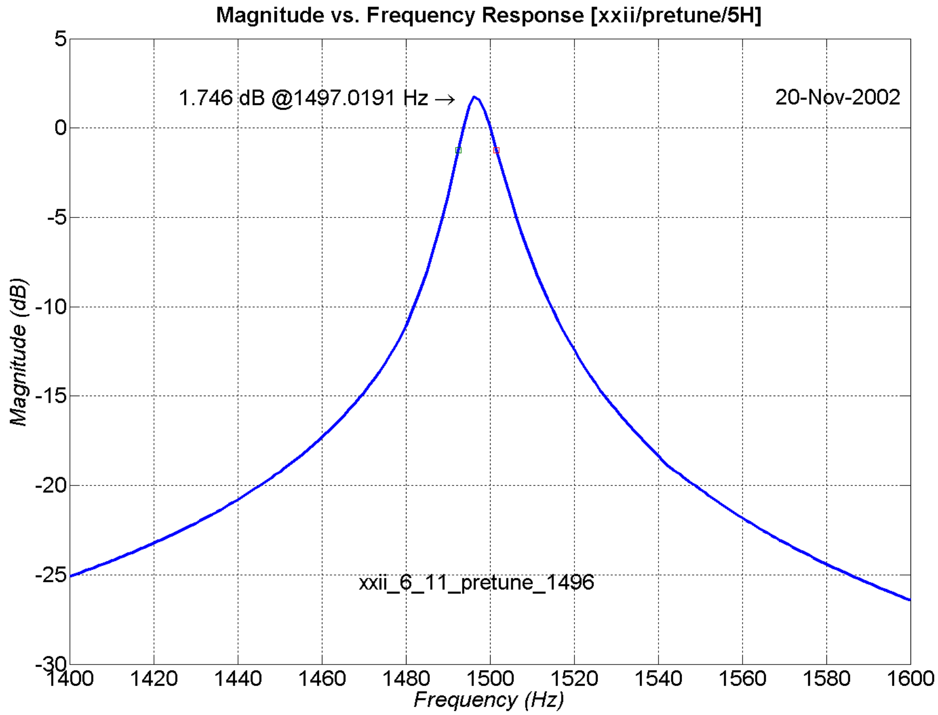

Figure 5.4 Sample frequency response of individual resonator beam

Subsequently, three tuned beams were coupled by a stainless steel wire and were then tested as a complete unit. A frequency sweep was again conducted to determine how closely the output appears similar to the theoretical response shown in Figure 4.2. This plot is used to determine whether the filter specifications were met.

A total of four (4) sets of mechanical filters were constructed and tested. Their frequency plots can be seen in Figure 5.5 and a photograph of a fabricated filter is shown in Figure 5.6. Found in brackets, each response of Figure 5.5 contains the individual sample numbers that were used in creating the filter.

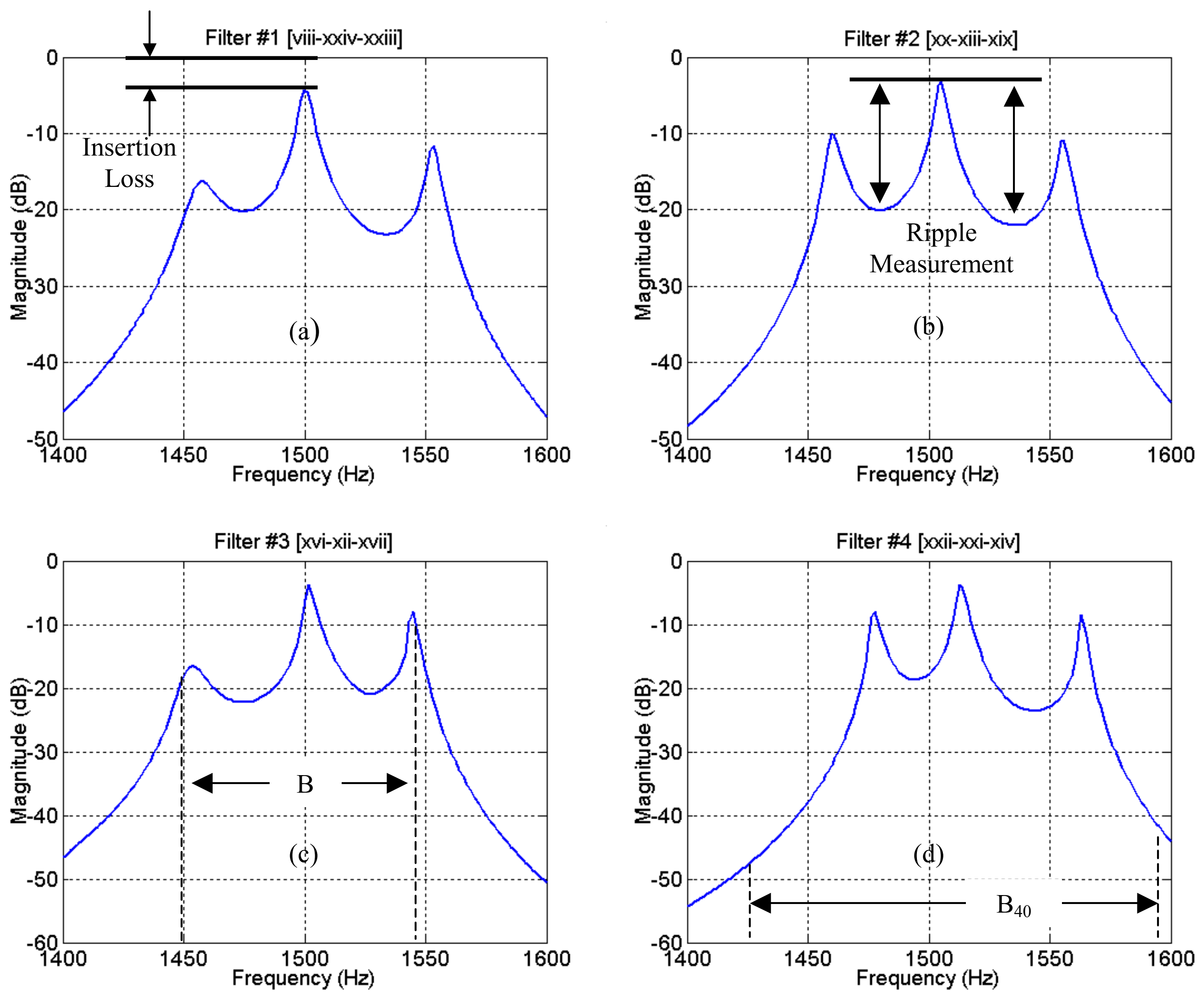

Figure 5.5 Magnitude vs. frequency plots of four fabricated filters

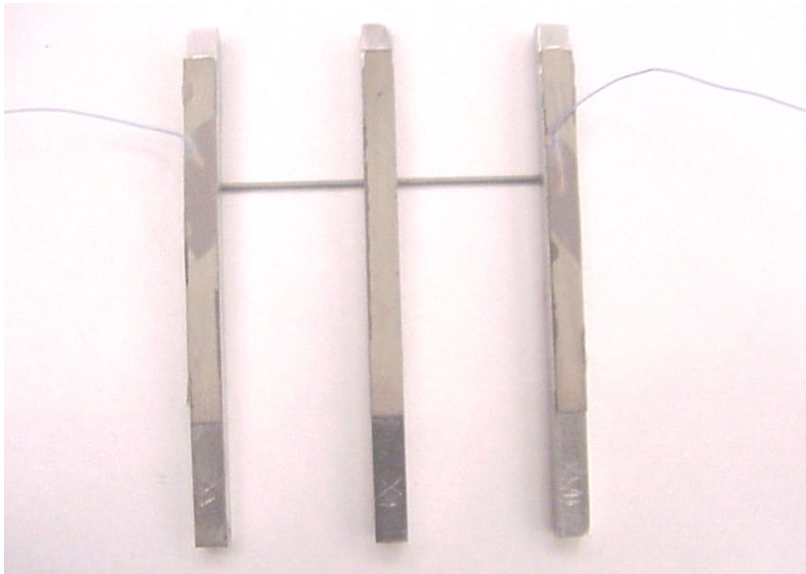

Figure 5.6 Photograph of fabricated filter

Figure 5.7 contains the frequency plots for each filter taken over a larger frequency range. The range is expanded to show from 1200 to 1800 Hz, where Figure 5.5 shows a tighter range from 1400 to 1600 Hz. Figure 5.7 was created to show the effects of the response in the rejection band.

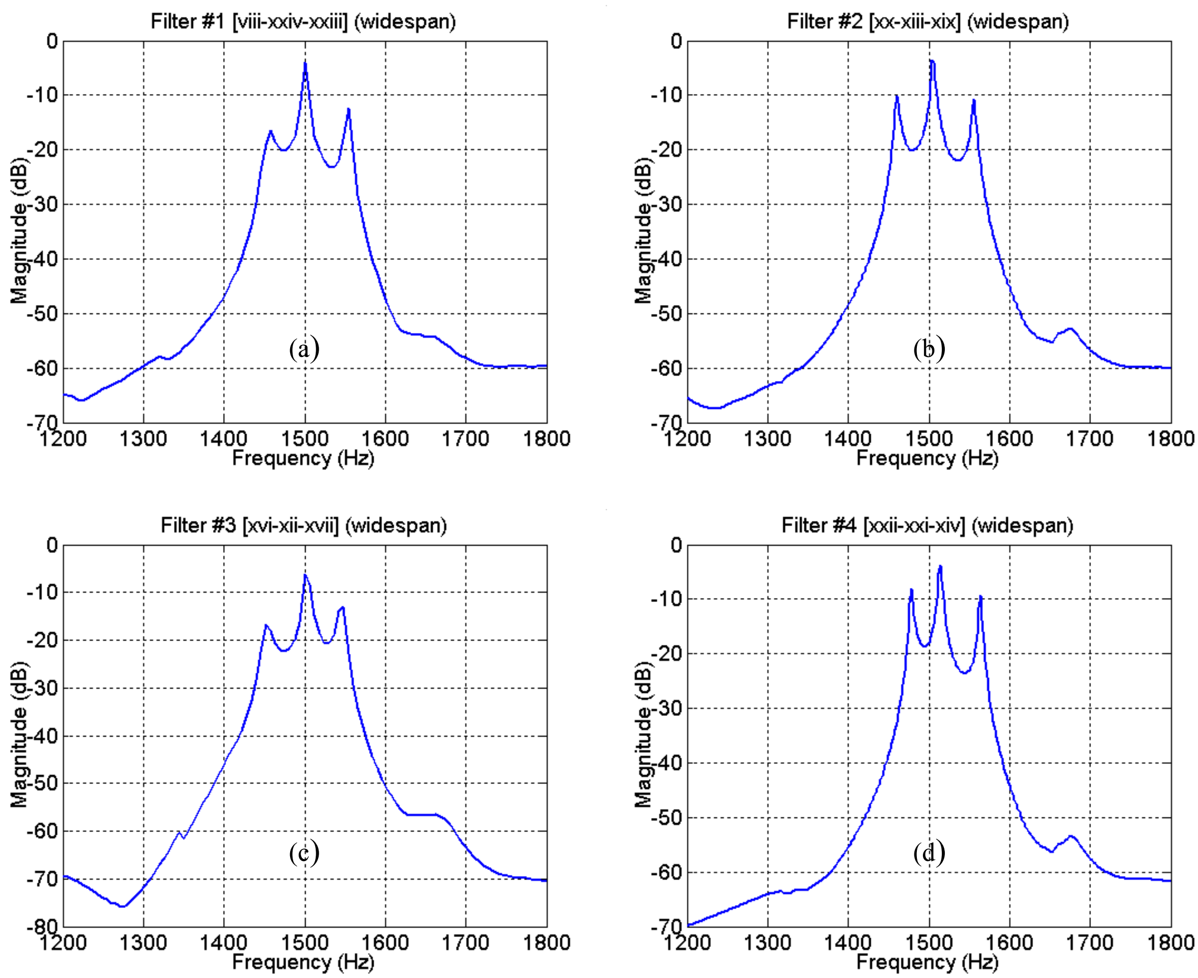

Figure 5.7 Magnitude vs. frequency plots of four fabricated filters with larger frequency range

A set of properties was extracted from Figure 5.5 and the results are shown in Tables 12 through 15. Table 12 depicts the frequency peaks and insertion losses in the response plots of each filter. The insertion loss is defined as the loss in magnitude, shown in decibels, that occurs when inserting the mechanical filter. A value of zero decibels is the reference value, and the insertion loss is measured at the decibel point where the peak magnitude occurs. An example of the measurement can be seen in Figure 5.5(a). Tables 13 and 14 compare experimental results to those that were called upon in the design specifications. Shown in Figure 5.5(b), the ripple is measured from the "peak" magnitude to each "valley" in the response. The center frequency is defined again and was measured as

$$\omega_o = \sqrt{\omega_1 \omega_2} \tag{2.5}$$

with ω_1 and ω_2 representing the cutoff frequencies found at 3dB. The bandwidth (B) is again expressed, as seen in Figure 5.5(c), as the difference between the two cutoff frequencies, while the rejection bandwidth (B_{40}) is the difference in the upper and lower rejection band frequencies, denoted in Figure 5.5(d). Table 15 conveys the resonance frequency values for each individual beam that was used in the filter structures.

Table 12 Frequency and insertion loss values extracted from filter response plots found in Figure 5.5

Filter #	*Frequency peak 1 (Hz)*	*Frequency peak 2 (Hz)*	*Frequency peak 3 (Hz)*	*Insertion Loss (dB)*
1	1456	1500	1552	4.3
2	1460	1505	1556	3.2
3	1452	1500	1544	3.8
4	1477	1512	1563	3.7
Average	1461.3	1504.3	1553.8	3.8
Standard deviation	11.0	5.7	7.9	

Table 13 Ripple results from filter response plots found in Figure 5.5

Filter #	*Peak-to-valley #1 ripple (dB)*	*Peak-to-valley #2 ripple (dB)*	*Average ripple value (dB)*
1	15.7	18.7	17.2
2	16.8	18.8	17.8
3	19.2	17.2	18.2
4	14.3	19.3	16.8
Average value	16.7	18.5	17.6
Specification value	1	1	1

Table 14 Data values extracted from filter response plots in Figure 5.5 when compared to designed specification values

Filter #	*Bandwidth [B] (Hz)*	*40dB Bandwidth [B_{40}] (Hz)*	*Center frequency [ω_o] (Hz)*
1	103	250	1502.6
2	100	220	1507.2
3	98	230	1496.2
4	92	190	1519.3
Average value	98.3	222.5	1506.3
Specification value	80	440	1590
Percent difference	22.8%	49.4%	5.3%

Table 15 Individual beam resonant frequency values used in each filter

	Individually tuned beam frequencies								
Filter #	*Beam 1 (Hz)*		*Beam 2 (Hz)*		*Beam 3 (Hz)*		*Average tuned frequency (Hz)*	*Center frequency [ω_o] (Hz)*	*Percent difference*
	Pre-tuned	*Tuned*	*Pre-tuned*	*Tuned*	*Pre-tuned*	*Tuned*			
1	1477	1495	1444	1500	1504	1504	1499.7	1502.6	0.2%
2	1488	1488	1474	1474	1488	1488	1483.3	1507.2	1.6%
3	1467	1473	1474	1474	1476	1476	1474.3	1496.2	1.5%
4	1516	1516	1451	1511	1497	1507	1511.3	1519.3	0.5%
			Average value				1492.2	1506.3	0.9%

A mechanical filter calls for terminating resistances within the confines of its circuit. These resistances can improve the ripple measurements within the passband of the response. The first resistor is placed in series with the input voltage and the actuating resonator, while the second is placed in parallel with the outputting resonator and ground, as shown in Figure 5.8. Because the order (n) of the system is odd, it is known from the theory that these resistances should be equal, but the value is unknown [Williams, 1988]. Therefore, a range of resistances was inserted into the circuit of mechanical filter sample #1 in an attempt to improve the ripple values.

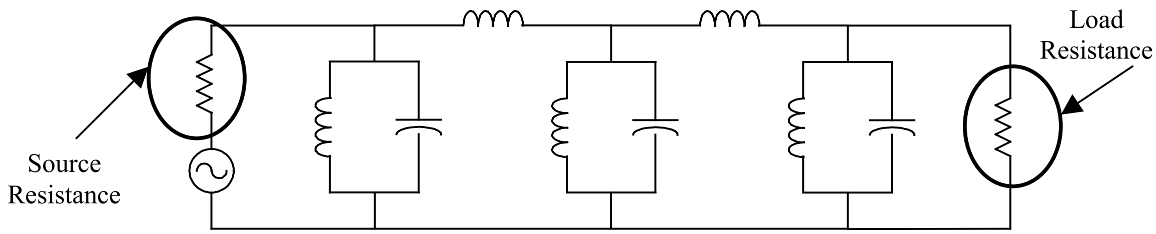

Figure 5.8 Schematic showing terminating resistances

Upon the completion of this test, Figure 5.9 was developed to show the insertion loss that occurs because of the addition of the resistances. Figure 5.10 is a plot that illustrates the differences in peak-to-valley ripple that occur throughout the range of inserted resistances. It is important to note that the insertion losses found in Figure 5.9 were negated in Figure 5.10. In Figure 5.10 the magnitudes of each test case were normalized to the original case, where no resistance was added, to show the plots on a similar scale. The two sets of arrows found in Figure 5.10 represent the difference in ripple for the original case versus the optimal case.

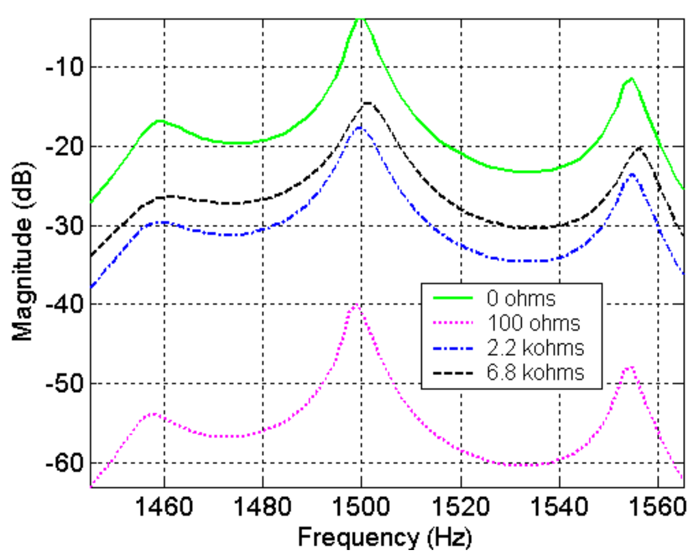

Figure 5.9 Frequency plot showing insertion loss due to addition of terminating resistances that is not shown in Figure 5.10

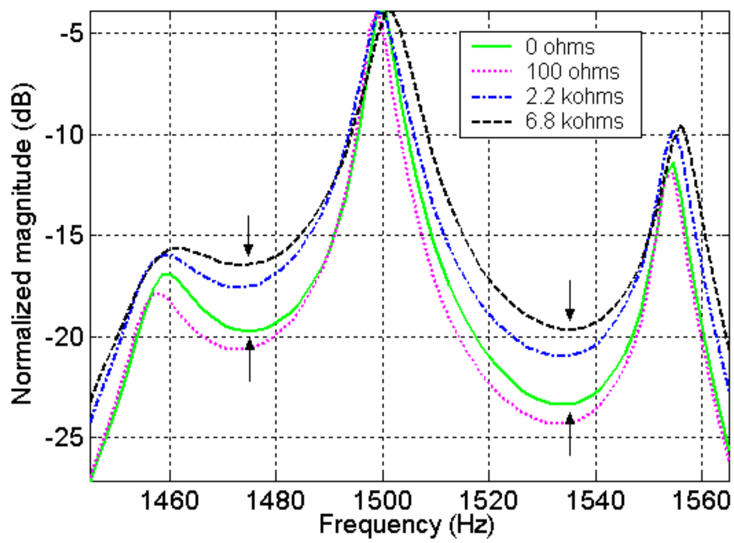

Figure 5.10 Variation of peak-to-valley ripple upon insertion of terminating resistances

Figure 5.11 simplifies the results found in Figures 5.9 and 5.10. It depicts the insertion loss that occurs for each case of added resistance, when compared to the original. Also represented in Figure 5.11 is the change in the ripple value when the responses with the inserted resistances are compared to the original circuit. Table 16 outlines the results of this test.

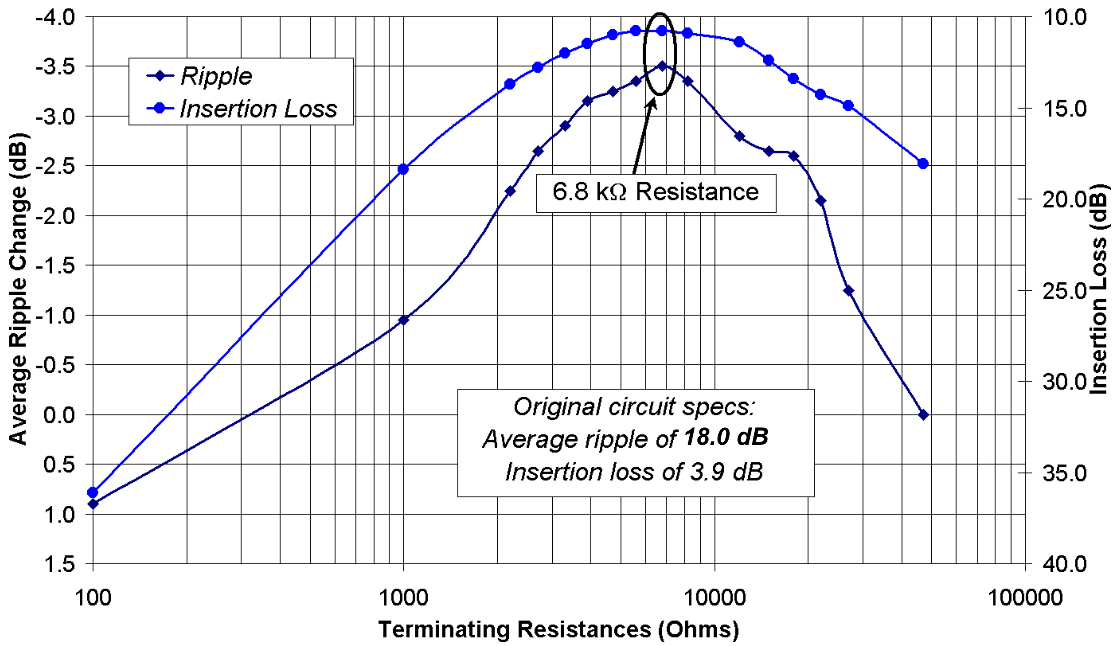

Figure 5.11 Measured ripple changes and insertion loss with the addition of terminating resistances

Table 16 Modifications created by addition of optimal terminating resistance value

Resistance value (ohms)	*Average Ripple (dB)*	*Insertion Loss (dB)*
0	18.0	3.9
6.8 k	14.3	14.7
Change due to addition of resistances (dB)	-3.7	10.8

Figures 5.13 and 5.14 show results that were extracted from an analytical model. This model can be seen in Figure 5.12 where the designed mechanical filter was simplified into a set of mass and spring elements. The values obtained from the filter design were inputted into the necessary parameters of the model to create results that can be compared to experimental results.

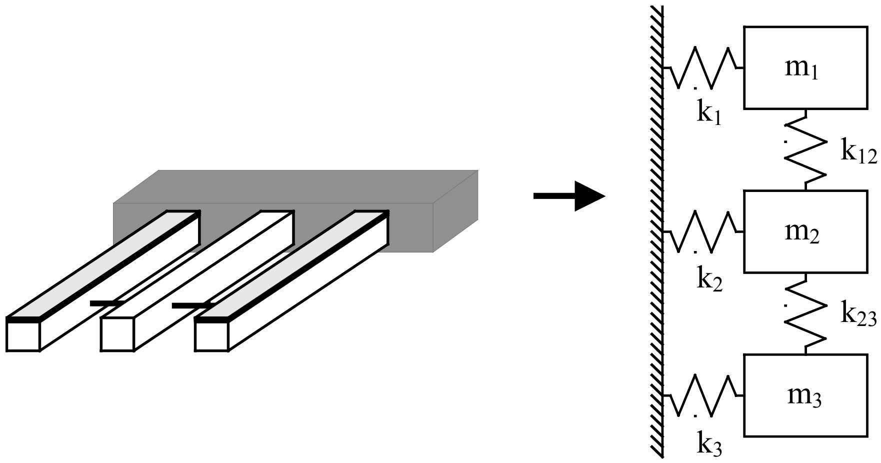

Figure 5.12 Analytical model of three DOF vibrational system

Tests were also run to determine the effects of varying the length of the coupling wire between the resonators. A graph of the analytically predicted and experimentally measured changes in 3dB bandwidth over a range of coupling wire lengths can be seen in Figure 5.13.

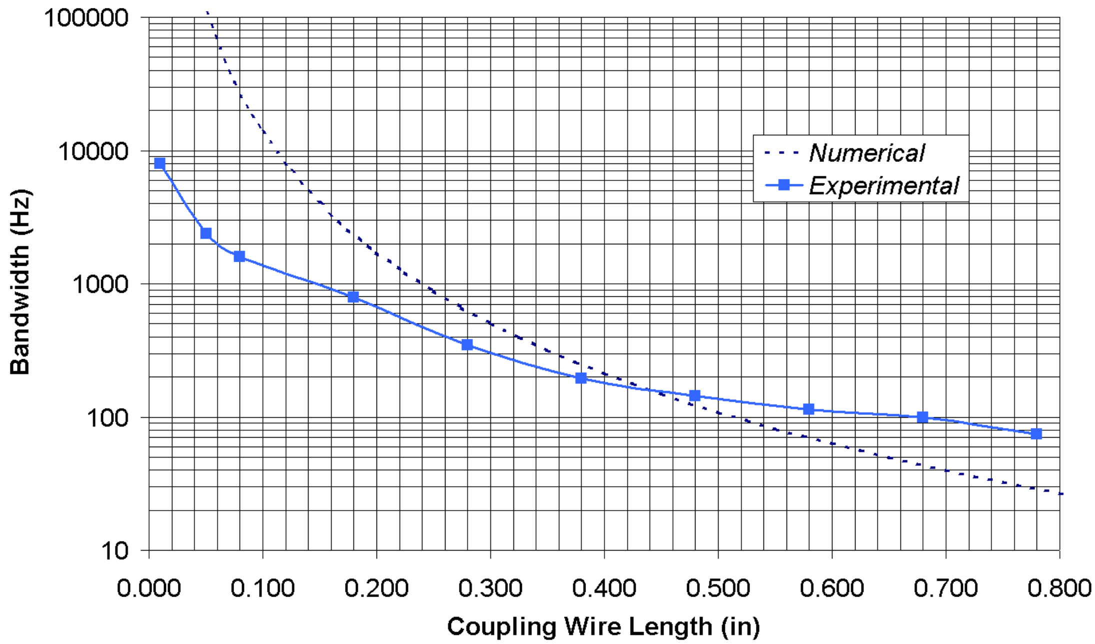

Figure 5.13 Variation of filter bandwidth over range of coupling wire lengths at center frequency of 1590 Hz

The following plots, Figures 5.14 and 5.15, through experimentally and analytically predicted results, demonstrate the variations of each vibrational mode of the third order filter over a scale of different coupling wire lengths.

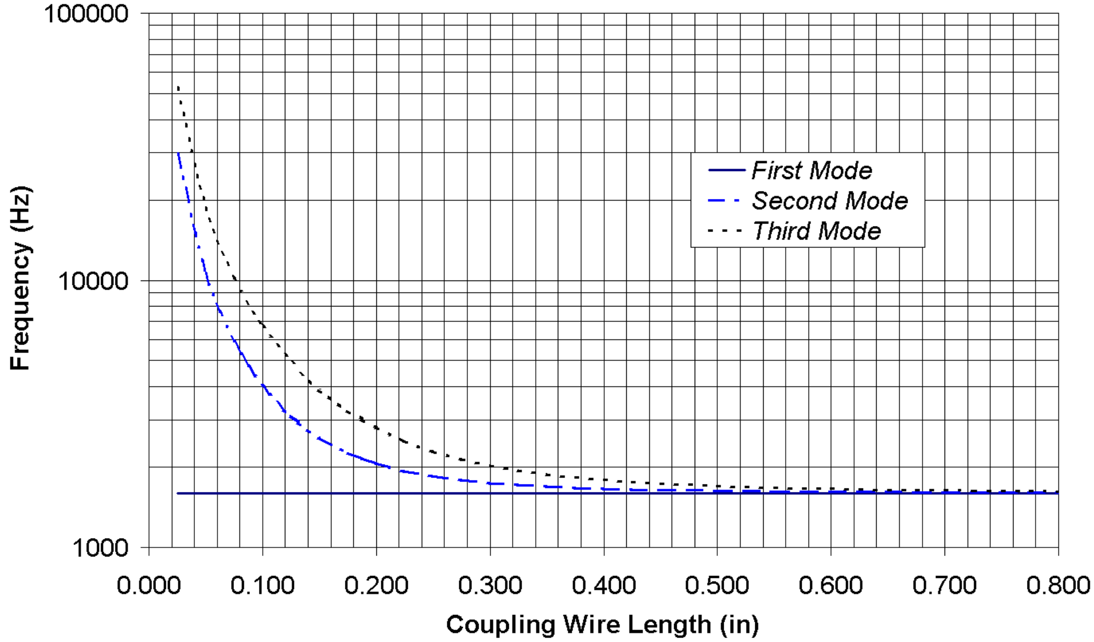

Figure 5.14 Analytically predicted frequency values at the modes of a third order filter over range of coupling wire lengths at center frequency of 1590 Hz

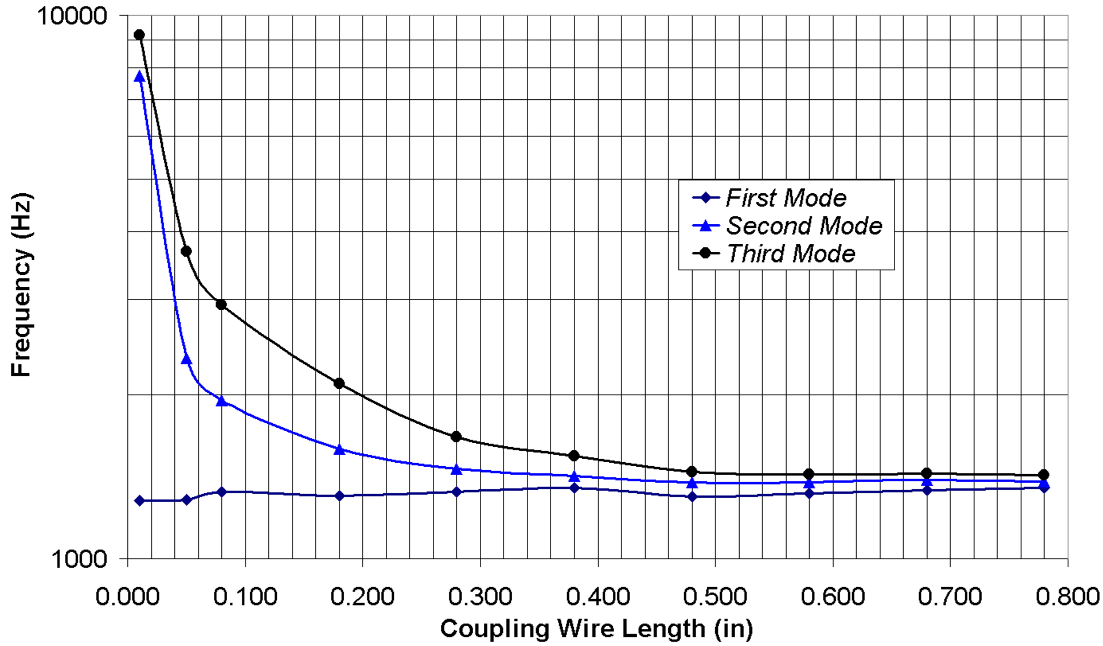

Figure 5.15 Experimental frequency values at the modes of a third order filter over range of coupling wire lengths at center frequency of 1590 Hz

6.0 DISCUSSION

The results taken from the tests conducted on the mechanical filters bring about many interesting and useful observations. Each set of results was analyzed and an interpretation of the analysis ensues.

The initial testing was conducted to find the frequency responses of each individual beam of a filter set. The natural frequencies affect the center frequency of the completed filter. Therefore, each must be tuned to a similar resonance. As mentioned, of the trio of beams, the one with the highest natural frequency became the set point for the others to be tuned toward. A subtraction of the length of a clamped beam increases its natural frequency. Although not through an exact scientific procedure, the trio of resonators was tuned to within 10-15 Hz. This range was considered satisfactory due to the variability of the clamp and the placement of the beam within it. All filters are within this range, with some even tighter. All individual beam plots, containing the resonance frequency, peak magnitude, quality factor, bandwidth, and fractional bandwidth (B/ω_o), can be found in Appendix A.

The plots of Figure 5.5 show the frequency responses of each of the four tested filters. Tables 12-15 outline the results extracted from these plots. The first, Table 12, shows the frequency values found at each peak of the filter response. The main goal behind these results is to show how repeatable the response can be. Table 12 shows that indeed the frequencies are repeatable with standard deviations that range from 5.7 to 11.0 Hz. Also within this table are the values of insertion loss that occur due to the addition of the filters. The insertion loss is measured at the decibel value where the peak magnitude occurs, while being referenced from zero decibels. The average value of 3.8 dB is quite minimal.

Table 13 shows results that are far from the design specification. The amount of ripple can be located in this table. There are two experimental ripple values taken from the highest "peak" to each of the two "valleys" of the response plots. These values were averaged and compared to the value that was designed for. These quantities do not match very well. The results show that the average experimental ripple value is 17.6 dB, while the designed value was 1 dB.

The exact cause of this excessive ripple value is unsure, but it is believed that the coupling between each outer and inner resonator pair plays a role. Approaches to remedy the situation include tuning techniques. An analytical model of the mass and stiffness matrices was formed; pointing out that the design did not include any form of damping. When damping values were added to the resonators and to the coupled areas of the matrix, the peaks of the frequency response were lowered and widened. This means that both the magnitudes of each peak in the frequency response and the quality factors were both lowered. In future work, a possible way of incorporating the damping into the filter is to add PZT shunts to the resonators to tune them effectively. The addition of the damping did not affect the valleys of the frequency response.

Adding terminating resistances into the mechanical filter circuit affects the valleys of the frequency response. This is discussed further later in the section when referring to Figures 5.8-5.11 and Table 16. The correct values of resonator damping and terminating resistances should create an acceptable ripple value, but further research is needed.

The next table describes the other experimental values that were compared to the original design specifications. The first set of data in Table 14 describes the 3dB bandwidth of each filter. The specification called for 80 Hz of bandwidth, while the average tested bandwidth measured 98.3 Hz, a 22.8% difference. The difference is due to losses when coupling the resonators. Discrepancies in the dimensions of the coupling wires, as well as inconsistencies in the equivalent mass of the resonators can be reasons for the dissimilarity. Variations when clamping the filter and inconsistent solders can also account for the loss in coupling. However, the bandwidth of the filter can be modified simply. Shown in Figure 5.13 and explained later in the section, increasing the length of the coupling wires slightly will produce a tighter bandwidth value.

The rejection bandwidth results are also portrayed in Table 14. The average experimental value of 222.5 Hz is almost 50% lower than what the specification calls for at 440 Hz. This is a beneficial difference. Regardless of what a filter specification calls for, a tighter rejection band results in a more vertical, and therefore more ideal, transition band within the response.

Also depicted in Table 14 are the measured center frequency values and the comparison to the values designed for. The average experimental center frequency of 1506.3 Hz is a mere 5.3% different from the specification value of 1590 Hz. The experimental center frequency comes from the solution of Equation (2.5), found in Sections 5.2 and 2.2.3, which uses the 3dB cutoff frequencies determined from the frequency response plots of Figure 5.5. Inconsistencies in the resonator material and dimensions, as well as the level of damping that occurs from the epoxy that holds the transducer to the resonator are the causes for why the experimental center frequency value is lower than expected. It is also important to keep in mind that the individual resonators were tuned to the highest resonant value of the three, not to the specified center frequency.

Table 15 was constructed to determine the effectiveness of tuning the individual beams when their values were compared to the center frequency of the fabricated filter. It must be noted that the individual beams should have been tuned to the designed center frequency of 1590 Hz. The three resonant frequencies of the single beams for each filter were averaged and compared to the value of center frequency that was determined from the frequency plots of Figure 5.5. The results show that the average tuned frequency of 1492.2 Hz is only 0.9% from the average measured center frequency value of 1506.3 Hz. This confirms, with confidence, that tuning the beams of each filter is a successful way to accomplish a specified center frequency. Also, to show the consistency of the beam fabrication, all of the individual beams were tuned with a difference of less than 60 Hz from their original "pre-tuned" values.

The next set of figures show the effects of adding terminating resistances to the mechanical filter circuit. Figure 5.9 shows, in decibels, the amount of loss that takes place with the addition of the resistances. Analytically, it is obvious that this result will take place. Resistances are electrically analogous to a damping mechanism in mechanical terminology. Therefore, the more resistance that is added, the effect will be a greater loss in magnitude. Also, as mentioned earlier in the section, the terminating resistances are used as a tuning device to raise the valleys of the frequency responses of Figure 5.5.

The actual purpose of Figure 5.9 is to set up Figure 5.10. Figure 5.10 shows the variation in the peak-to-valley ripple values when the resistances are incorporated. The magnitudes though have been normalized to have a maximum value that matches the original circuit peak value, where no resistance has been added. Therefore, Figure 5.9 shows the effects of insertion loss that cannot be observed in Figure 5.10.

Figure 5.10 shows the effects on ripple when using several terminating resistance values. It should be noted that the low values of resistance, i.e. 100 Ohms, actually worsen the ripple value by making it greater. Eventually though, the ripple improves with larger resistance values until an optimal value is found. After this value, the ripple will begin to become greater again. Figure 5.11 shows this trend. The same trend also occurs with the insertion loss. This plot shows how the ripple and insertion loss are affected by the addition of a wide range of resistances. The left ordinate represents the change in average ripple when compared to the original circuit, while the ordinate on the right portrays the same comparison for insertion loss. The plot shows that 6.8 kOhms is the optimal resistance value. It decreases the ripple the most, while adding the least amount of insertion loss. Table 16 represents this with a comparison to the original values.

If the ripple values were initially lower, the optimal resistance would have a more positive effect on the end result. In the future, when improvements are made to the filter creating a reduction in ripple, this tuning step should move the ripple into within the design specifications.

Analytically predicted and experimentally measured results were measured from tests that were run to show the effects on bandwidth when the lengths of the coupling wires are altered. The results are shown in Figure 5.13. A few points of interest can be discussed involving this plot. In both cases, the bandwidth rises sharply as the length gets smaller, while the bandwidth gets tighter with longer wire values. Experimentally though, the bandwidth actually crosses the path of the analytical model meaning that the bandwidth does not drop as sharply after the length of 0.440 in (1.12 cm). As the lengths increase, the stiffness of the coupling wires becomes quite low and the beams tend to behave more as if they are separate entities. At the other end of the plot, the trend of the experimental results is similar to the analytical prediction, but does not rise as abruptly with lower coupling wire values. For shorter coupling wires, the trio of beams is coupled closer together, which causes them to behave much like a wider, single beam with a single frequency.

The final two plots, Figures 5.14 and 5.15, illustrate the effects of coupling wire variance on the modes of the third order filter, analytically and experimentally. The results from the two plots follow a similar trend. The first mode stays fairly stationary throughout the range of the different lengths. The second mode begins at a high frequency, and as the length increases, asymptotically declines toward the frequency of the first mode, the center frequency. The third mode acts likewise to the second, but begins at an even larger frequency value, and declines at a slower rate toward the center frequency. The experimental frequency value settled upon as the coupling wires became longer is slightly lower than the analytically predicted value. This is expected, as mentioned earlier, due to the constructed filters producing an average center frequency value 5.3% lower than the designed value.

7.0 CONCLUSIONS AND FUTURE CONSIDERATIONS

This work shows the design process and fabrication of a mechanical filter with piezoelectric transducers. The design began with a set of desired filter specifications including a center frequency of 1590 Hz, a 3dB bandwidth of 80 Hz, a rejection band bandwidth of 440 Hz, and a passband ripple of 1 dB.

The filter was created using a Chebyshev filter approximation. The order of the system needed to create a filter within the specifications was three (3). Stainless steel resonators and coupling wires were the materials used for the fabrication of the filter. The transducers were PZT-5H manufactured from Piezo Systems Inc. Table 11, found in Section 4.8, shows all dimensions used to create the mechanical filter.

The filter was then fabricated and tested. Frequency responses were created for the four fabricated filter samples. The filters were created by successfully tuning each individual resonator to the frequency that was the highest of the three. The measured center frequency value was 0.9% different from the average tuned frequency. Also, the measured center frequency and the designed center frequency were only different by 5.3%.

The average bandwidth of the filter was measured as 98.3 Hz, which is 22.8% greater than the designed value. Simply increasing the coupling wire length can improve this value. The experimental rejection bandwidth is tighter than the 440 Hz specification value by 49.4%. The measured value of 222.5 Hz is quite beneficial. The average insertion loss of the filter was measured as 3.8 dB. A designed ripple value of 1 dB was experimentally measured as an average value of 17.6 dB. This was addressed with recommendations to improve the value.

Terminating resistances were added to the mechanical filter circuit as one approach to improve the ripple value. A range of resistances was inserted with the 6.8 kOhm value improving the ripple by 3.7 dB, while adding 10.8 dB of insertion loss. It was also shown that larger resistance values improve the rejection band by creating a flatter response, while not changing the shape factor.

The coupling wire lengths were altered to see the effects on bandwidth and the modal frequencies of the filter. Experimental results were matched against an analytical prediction for this set of tests. The experimental bandwidth matched up relatively well, but did not rise as sharply for small coupling wire lengths, and leveled off more than the analytical model when the lengths increased. The experimental frequencies of the three vibrational modes followed the same trend as the analytical model. The first mode stayed fairly level, while the second and third modes started at larger frequency values, and asymptotically fell toward the center frequency value as the coupling wire length increased.

Most of the suggestions that can be denoted as future work have to do with two major topics. The first includes improving the frequency response, while the second entails decreasing the dimensions of the filter. The subject of filtering higher frequencies, such as in the megahertz and gigahertz frequency ranges, falls into both categories. Higher center frequencies are typical of improvements made in the frequency response, but a realizable physical size must be determined.

Improvements in the frequency response can come in several ways. Obvious improvements need to be made in the ripple value of the mechanical filter constructed in this thesis. Since adding terminating resistances to the circuit was insufficient, the addition of a PZT shunt to one or more of the resonators, to lower the peaks of the frequency response, should be investigated to achieve a ripple value within the design limits. Also, adjustments in the passband and stopband bandwidths can be made to account for tighter specifications. Moving the position on the resonator where coupling takes place or modifying the length of the coupling wires can create passband bandwidth improvements. The addition of bridging wires to non-adjacent resonators, as well as the addition of more resonators, can improve the rejection band shape and selectivity.

The second significant point involves decreasing the size of the mechanical resonators, and therefore the whole filter system. The cantilevered beam example was chosen because it was known to be deemed as a design possibility when creating smaller scale structures. Other resonator geometries, vibrational modes, and coupling techniques can also be considered. In the macro-scale, flexural disks and longitudinal bars are used for higher center frequencies due to their vibrational properties.

APPENDIX

Appendix A

Frequency Response Plots of Individual Beams Contained Within Mechanical Filter

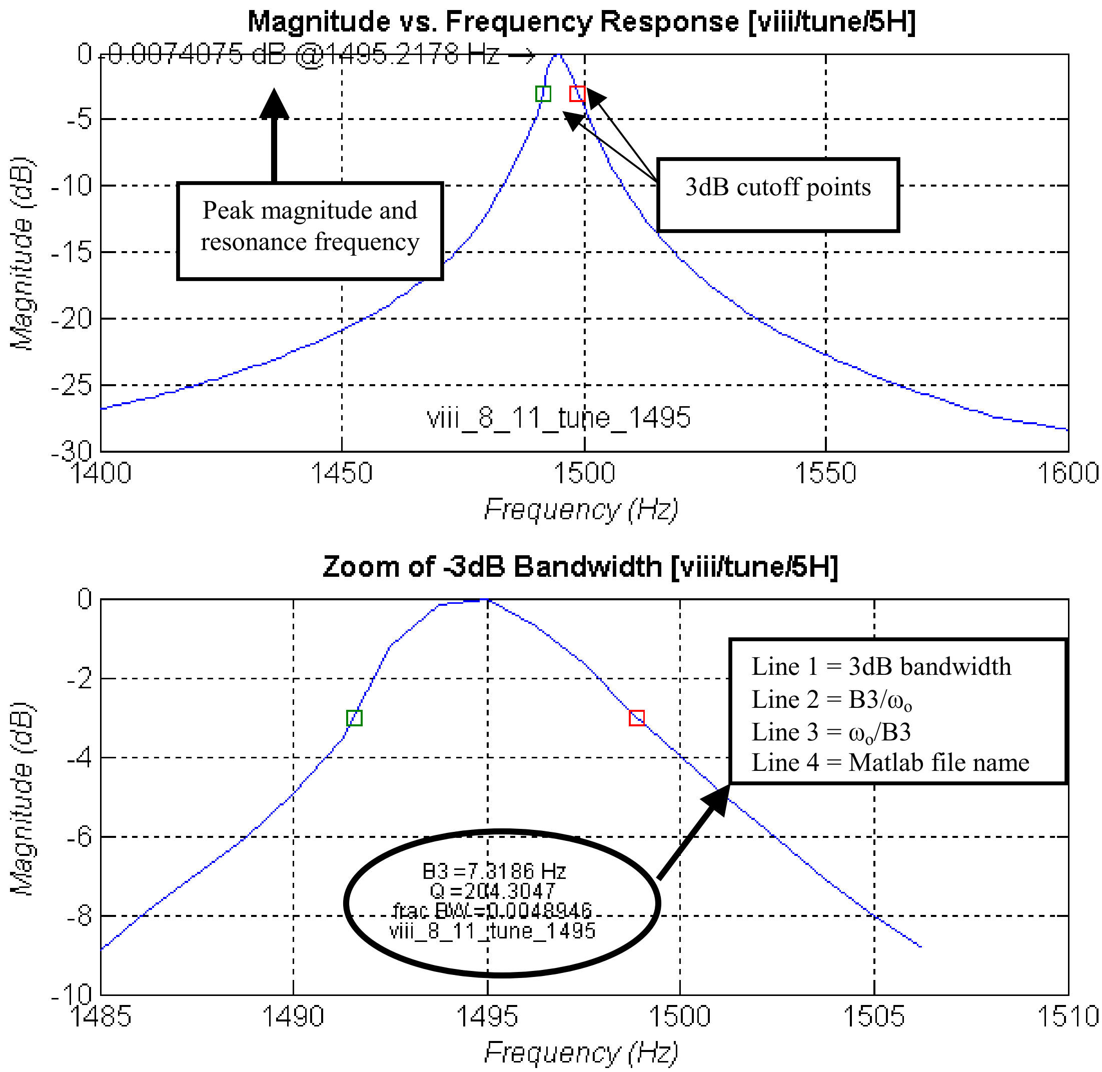

Figure A.1 Frequency response plot of tuned, individual beam 1 of filter 1

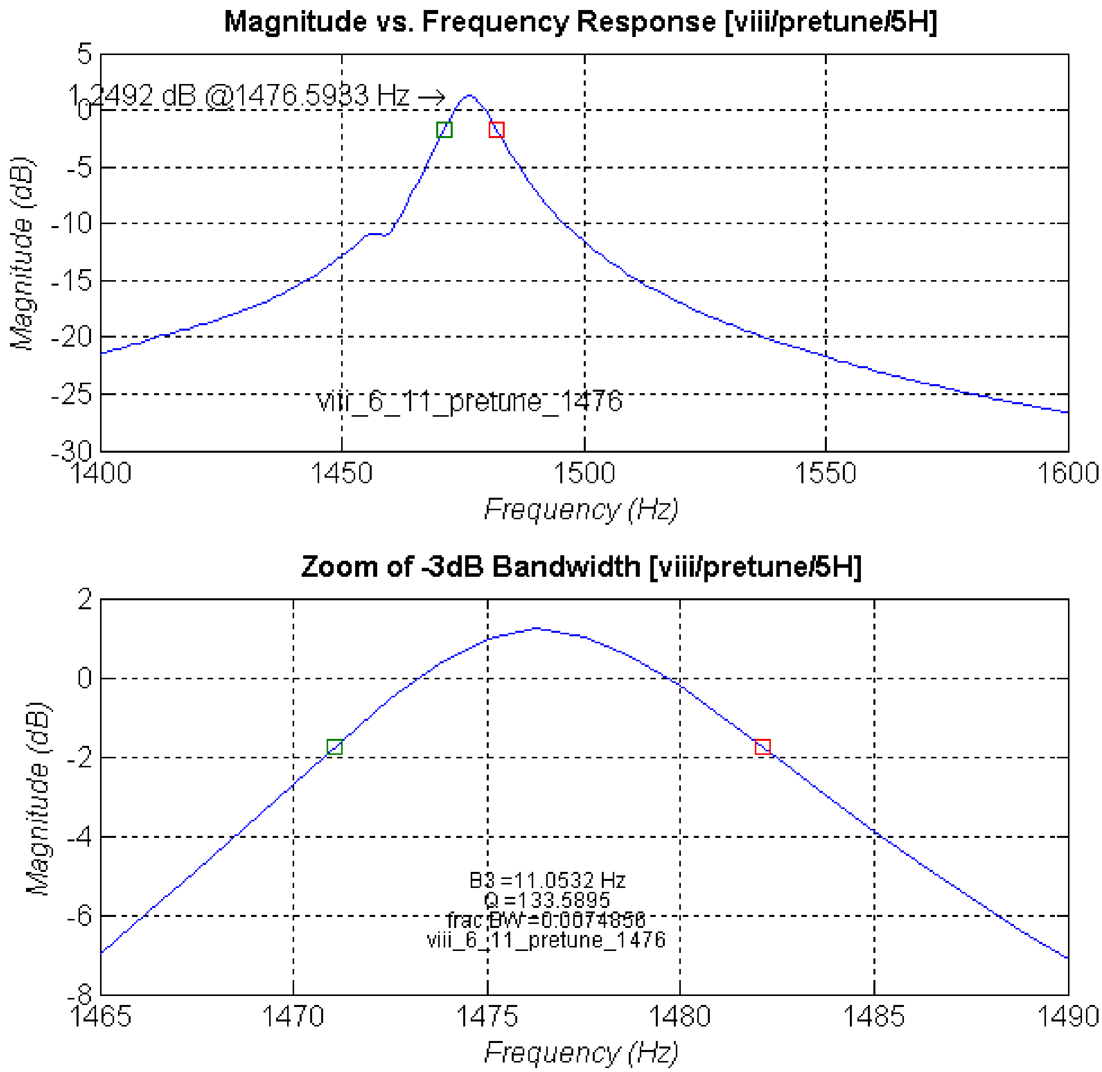

Figure A.2 Frequency response plot of pre-tuned, individual beam 1 of filter 1

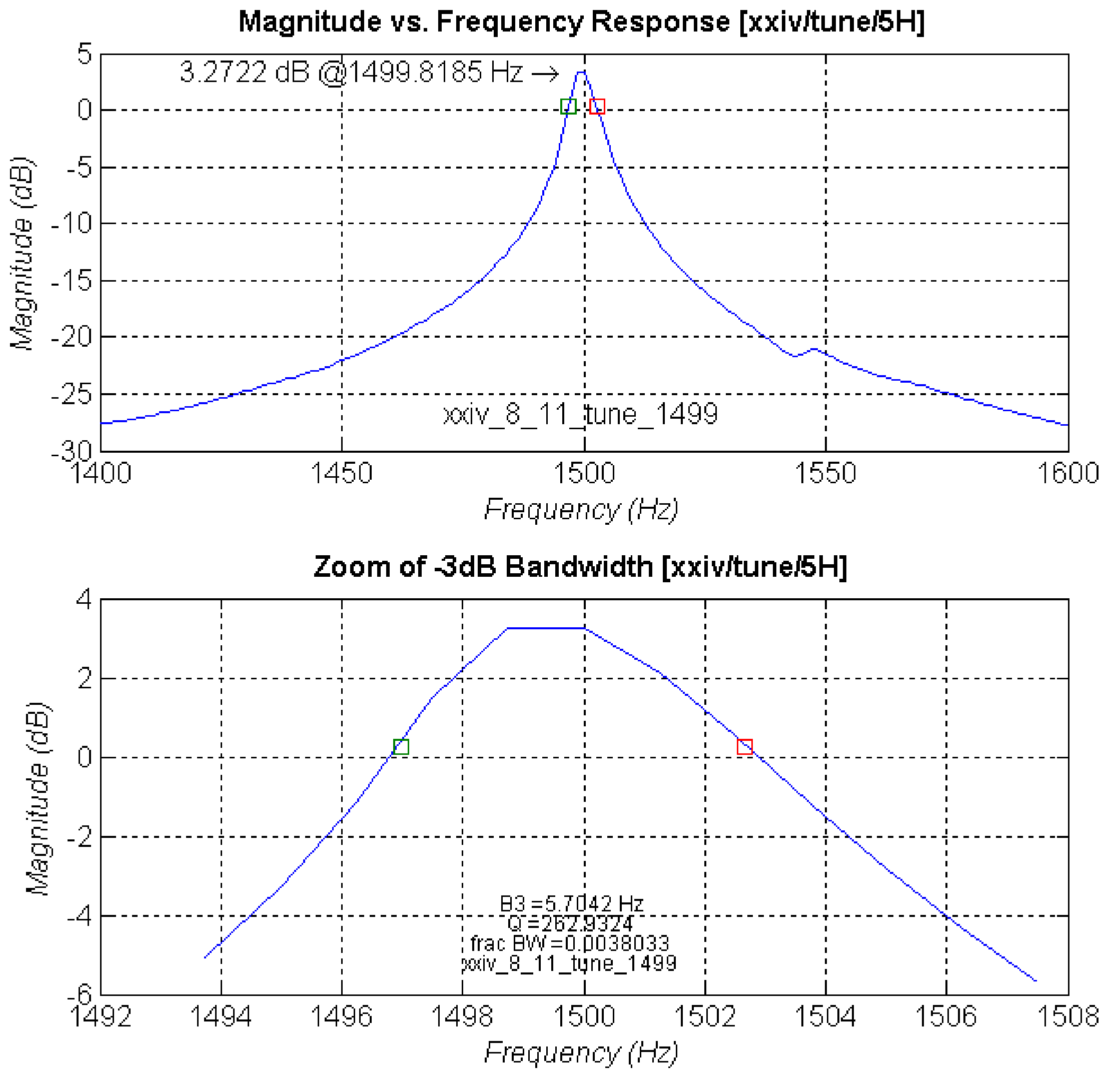

Figure A.3 Frequency response plot of tuned, individual beam 2 of filter 1

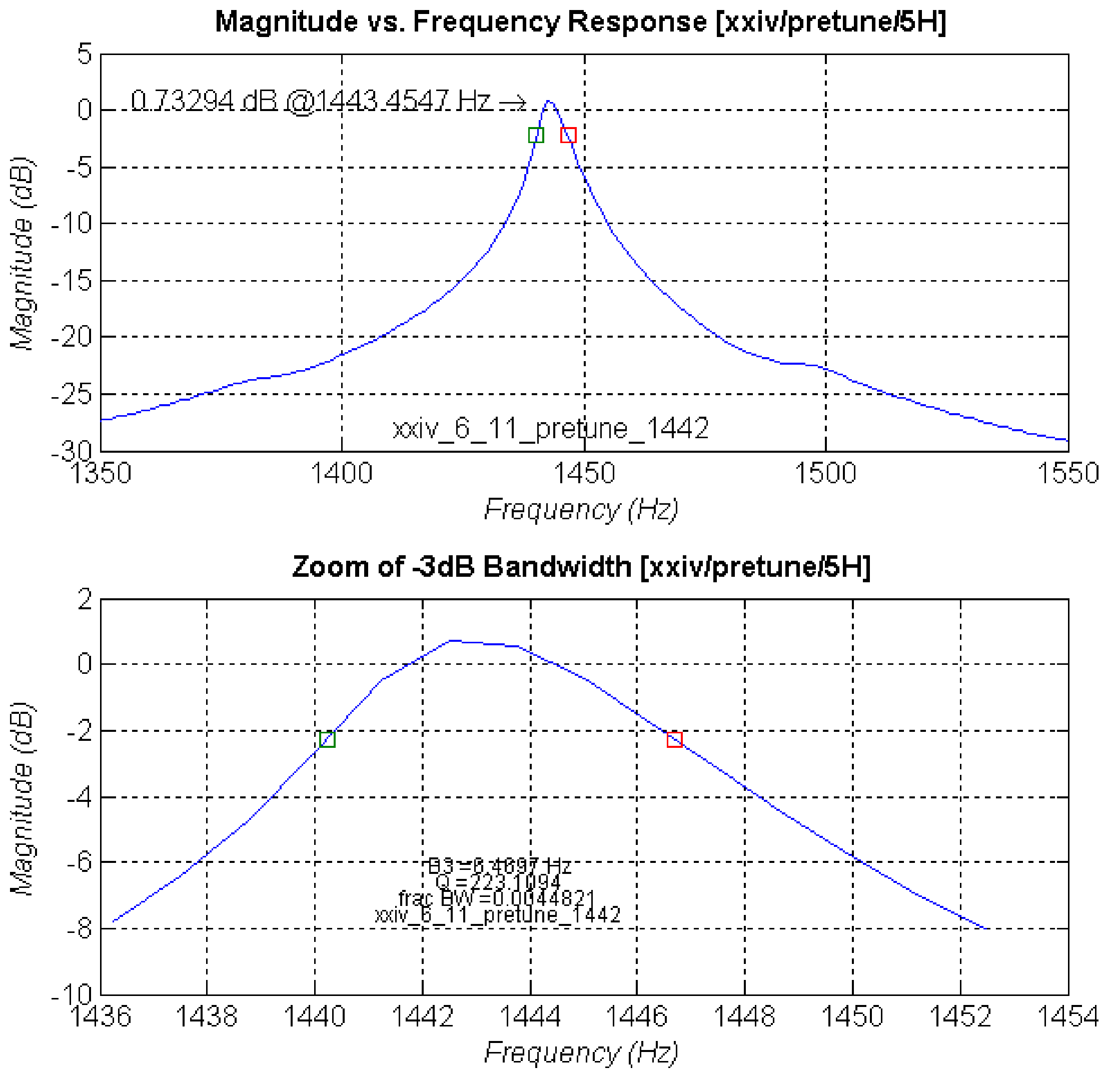

Figure A.4 Frequency response plot of pre-tuned, individual beam 2 of filter 1

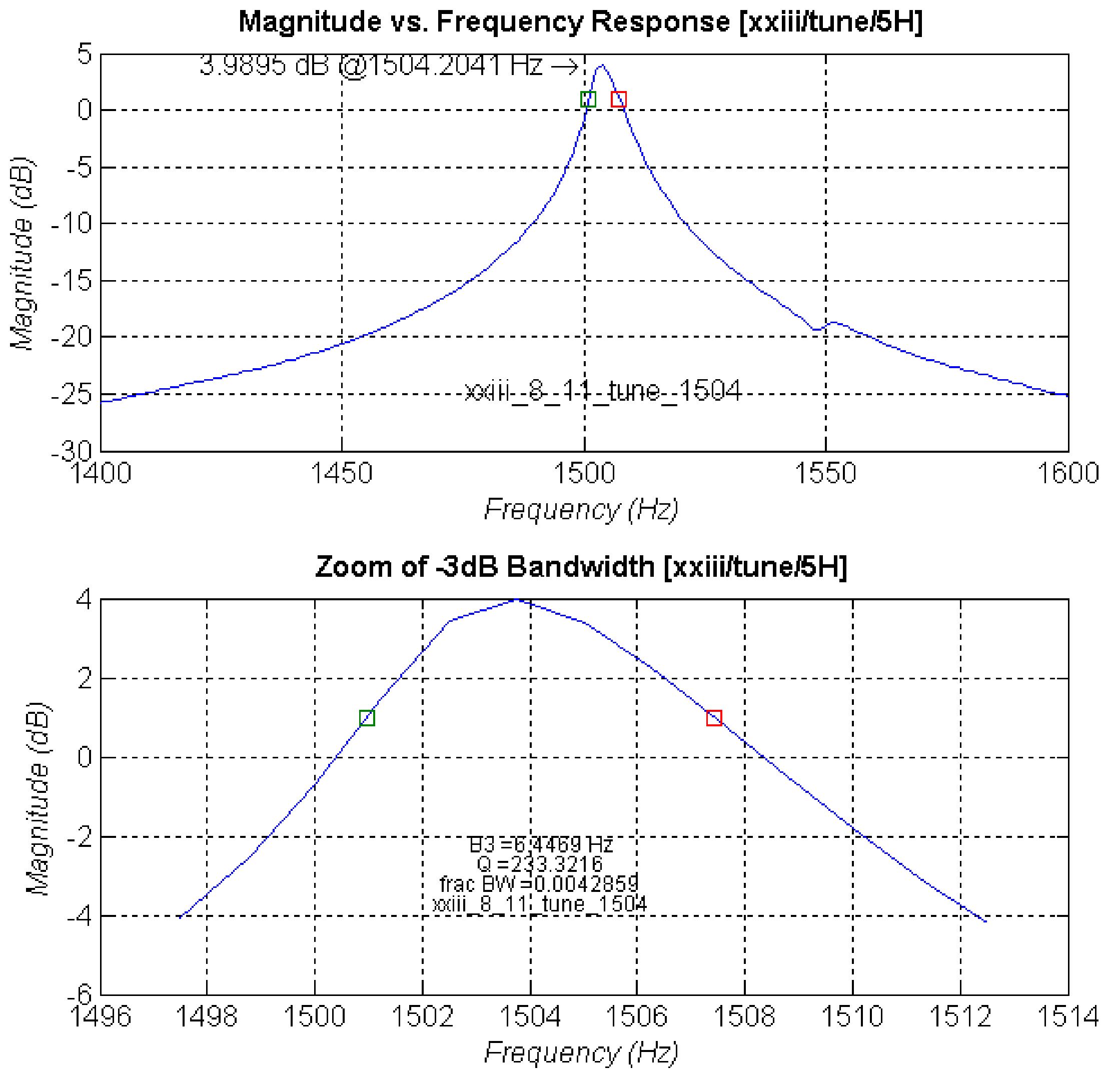

Figure A.5 Frequency response plot of tuned, individual beam 3 of filter 1

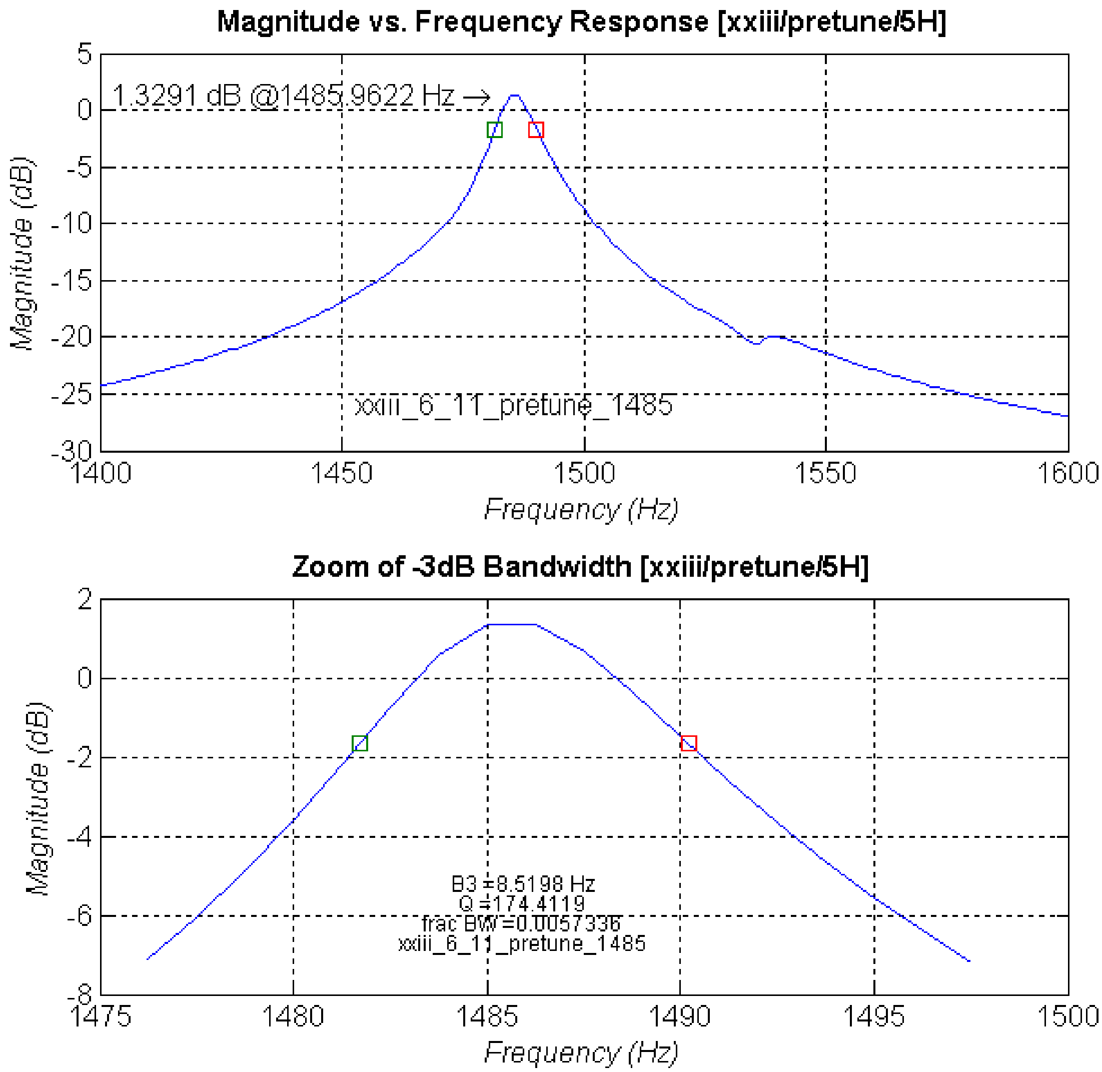

Figure A.6 Frequency response plot of pre-tuned, individual beam 3 of filter 1

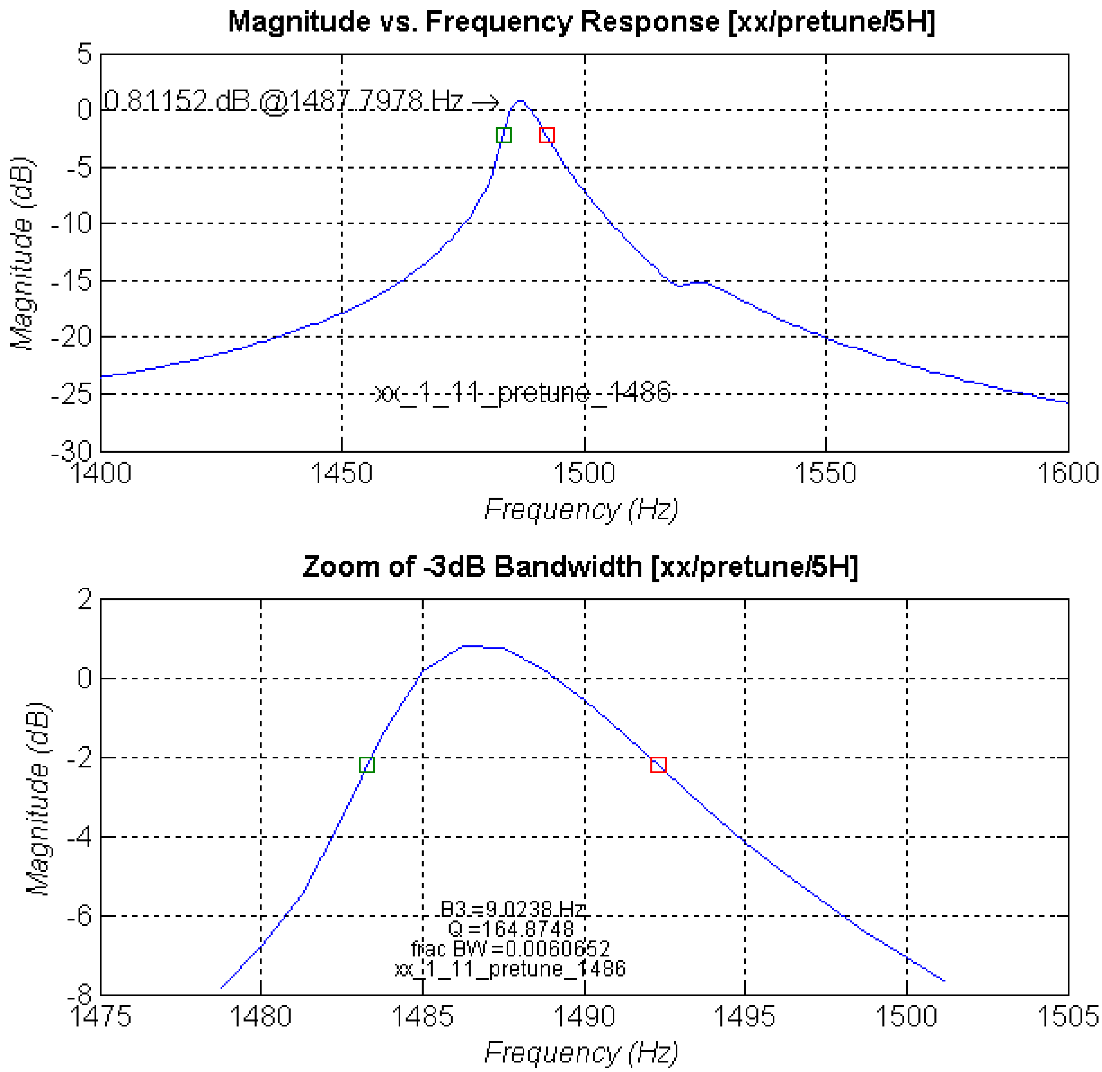

Figure A.7 Frequency response plot of pre-tuned, individual beam 1 of filter 2

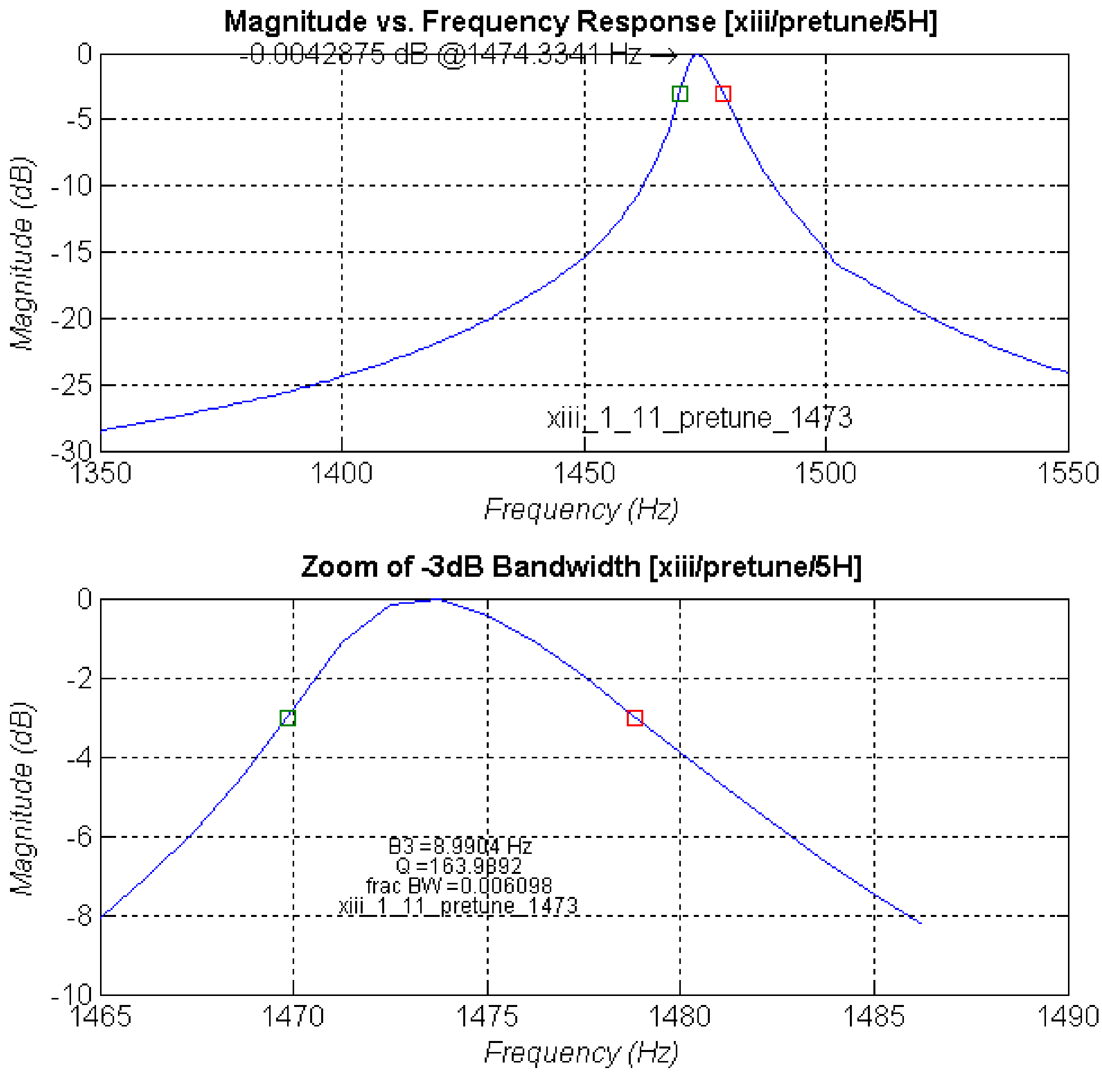

Figure A.8 Frequency response plot of pre-tuned, individual beam 2 of filter 2

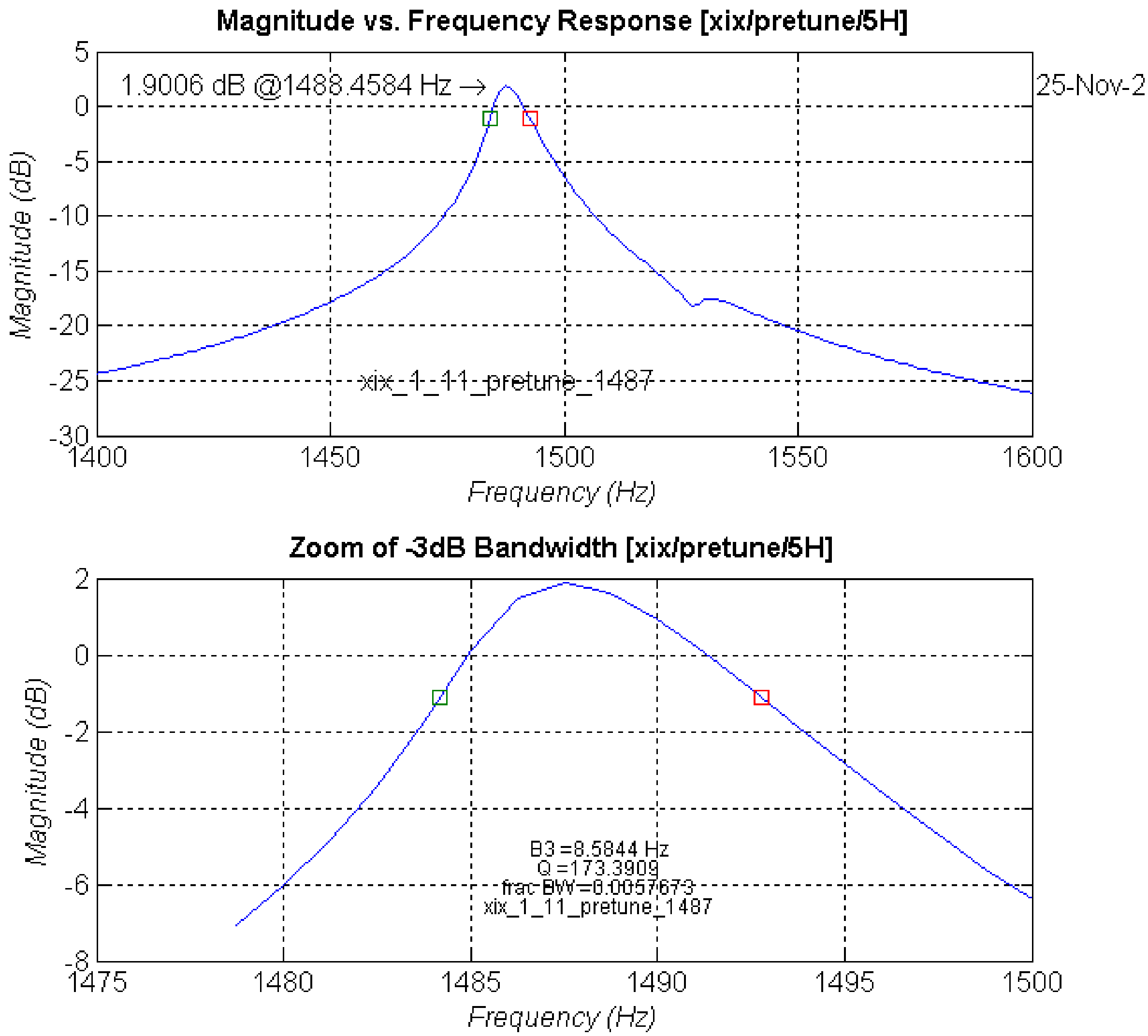

Figure A.9 Frequency response plot of pre-tuned, individual beam 3 of filter 2

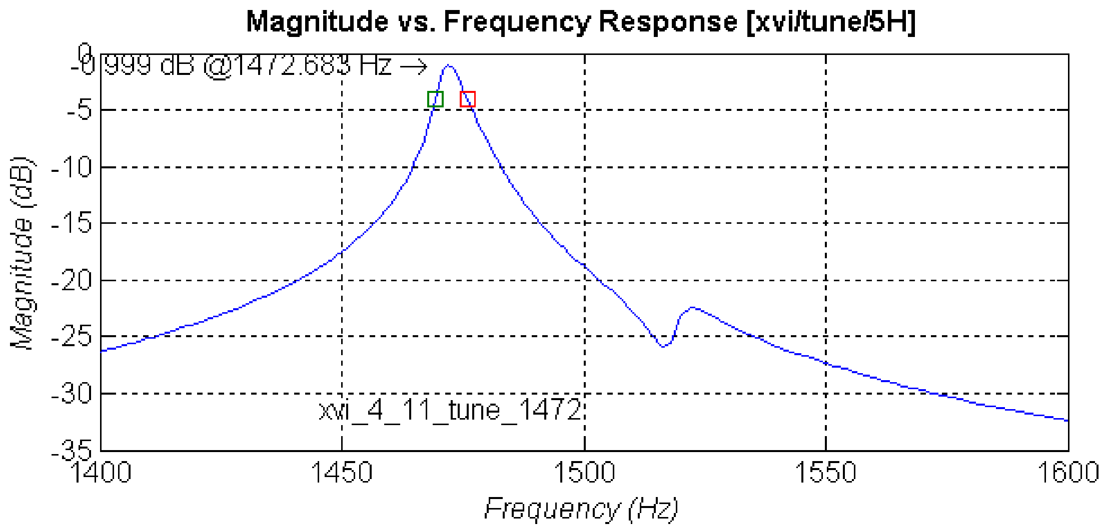

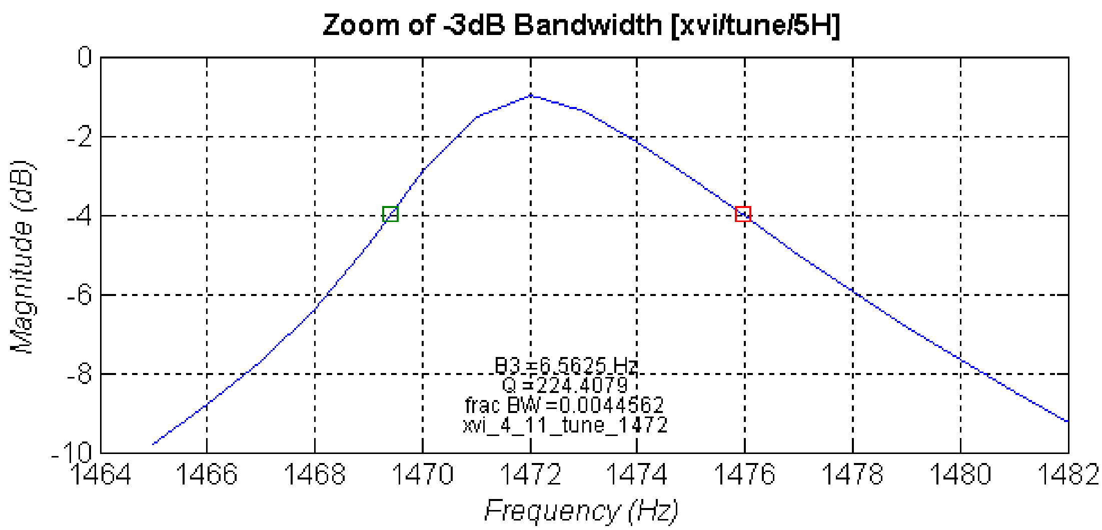

Figure A.10 Frequency response plot of tuned, individual beam 1 of filter 3

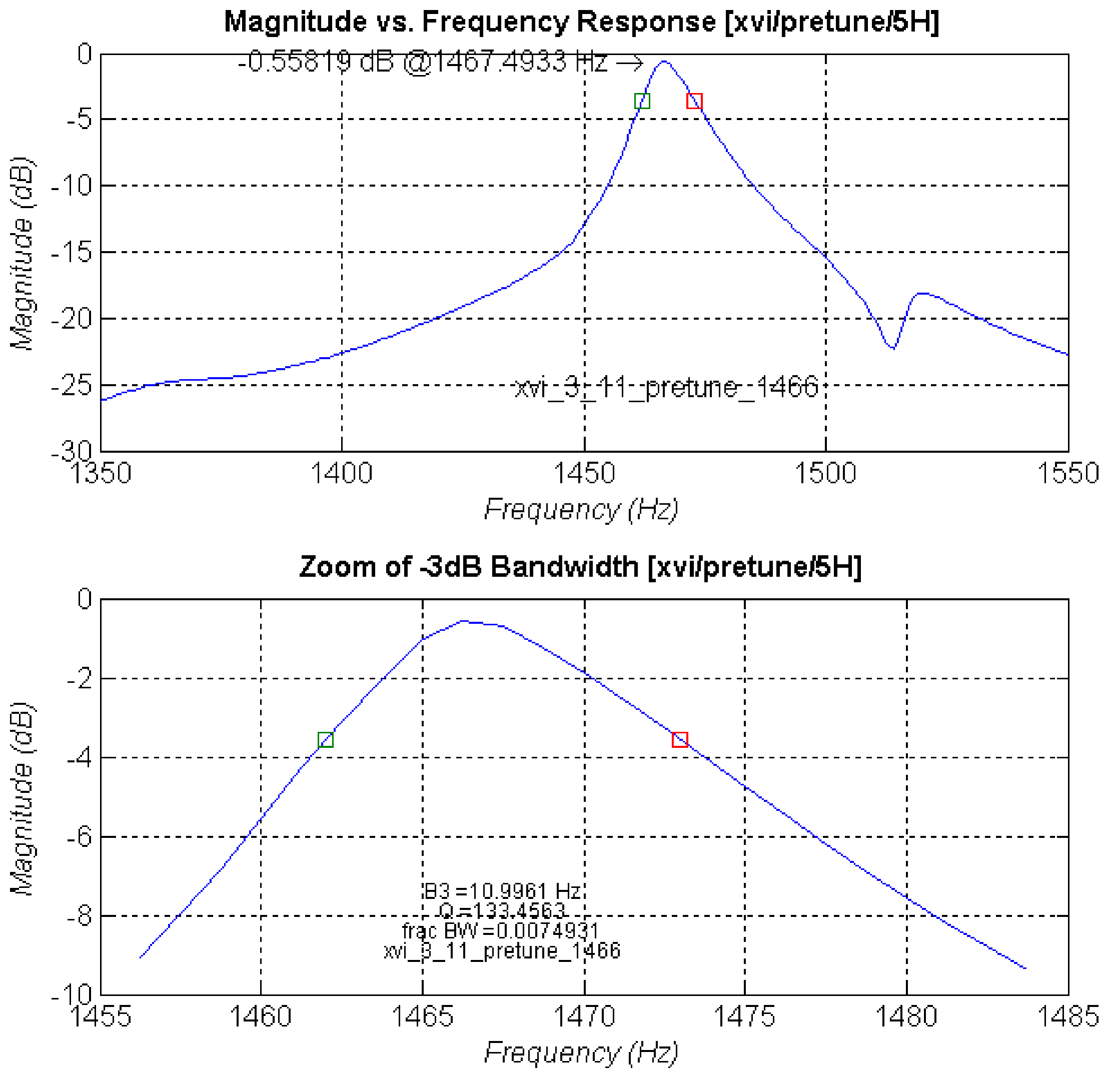

Figure A.11 Frequency response plot of pre-tuned, individual beam 1 of filter 3

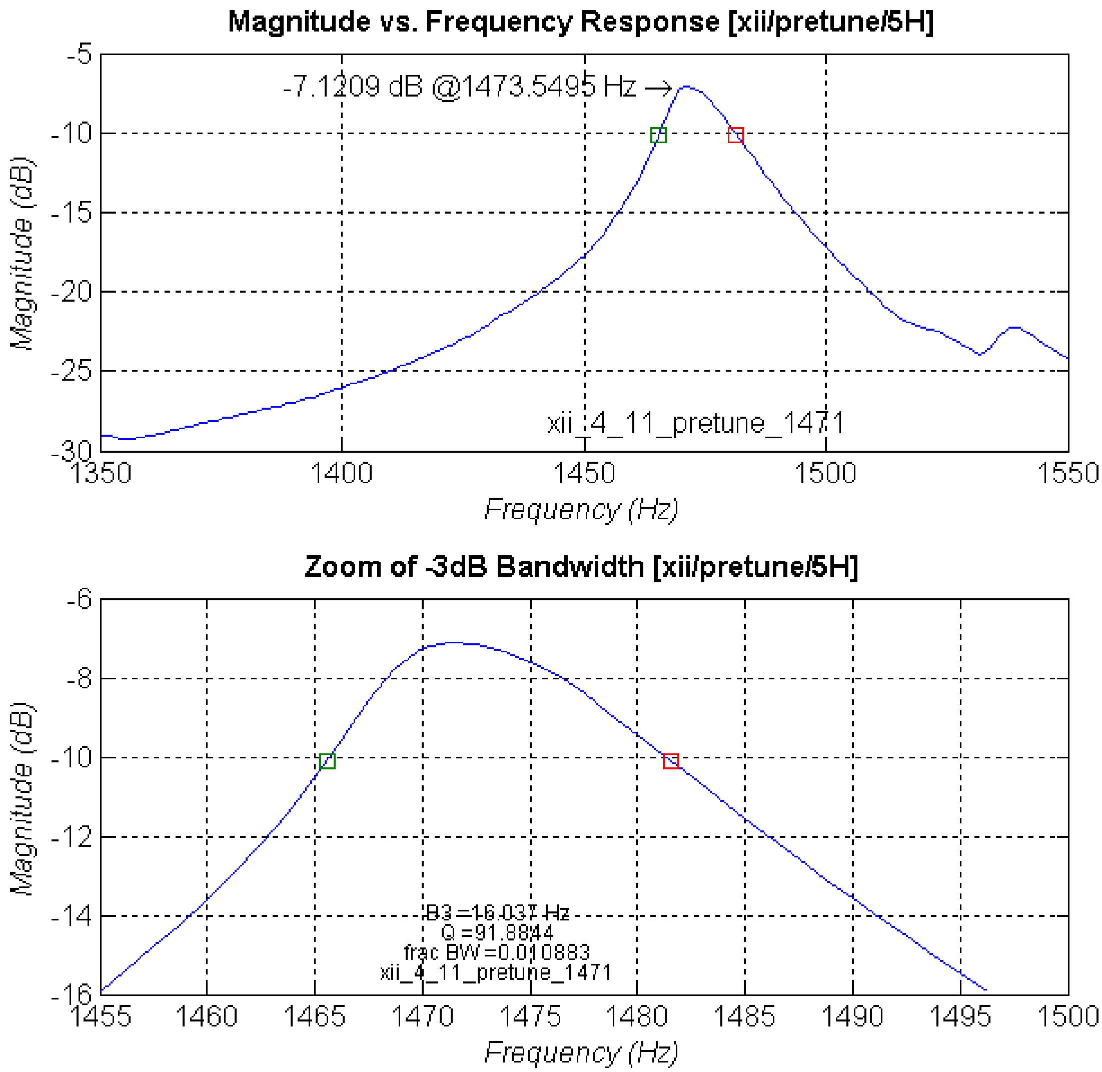

Figure A.12 Frequency response plot of pre-tuned, individual beam 2 of filter 3

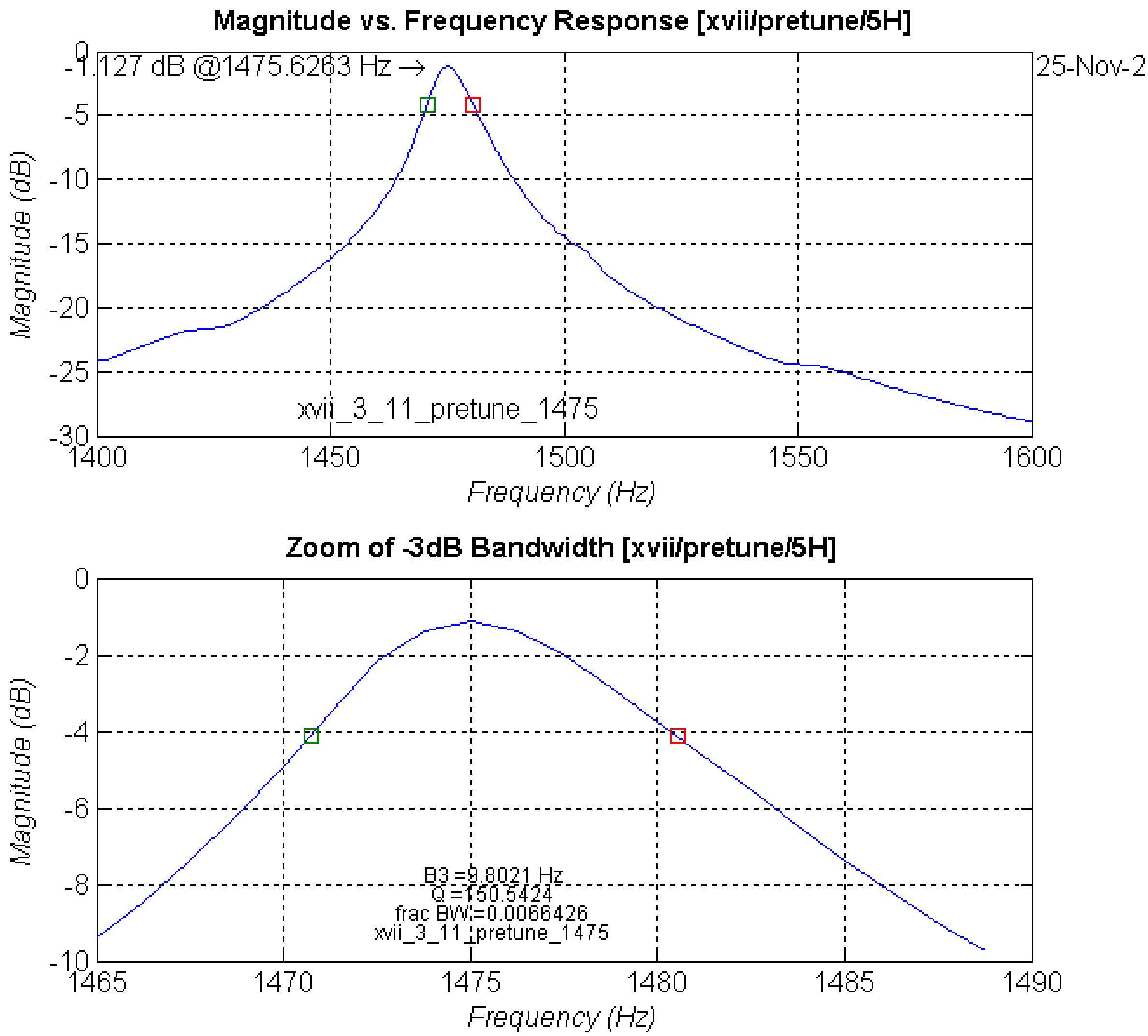

Figure A.13 Frequency response plot of pre-tuned, individual beam 3 of filter 3

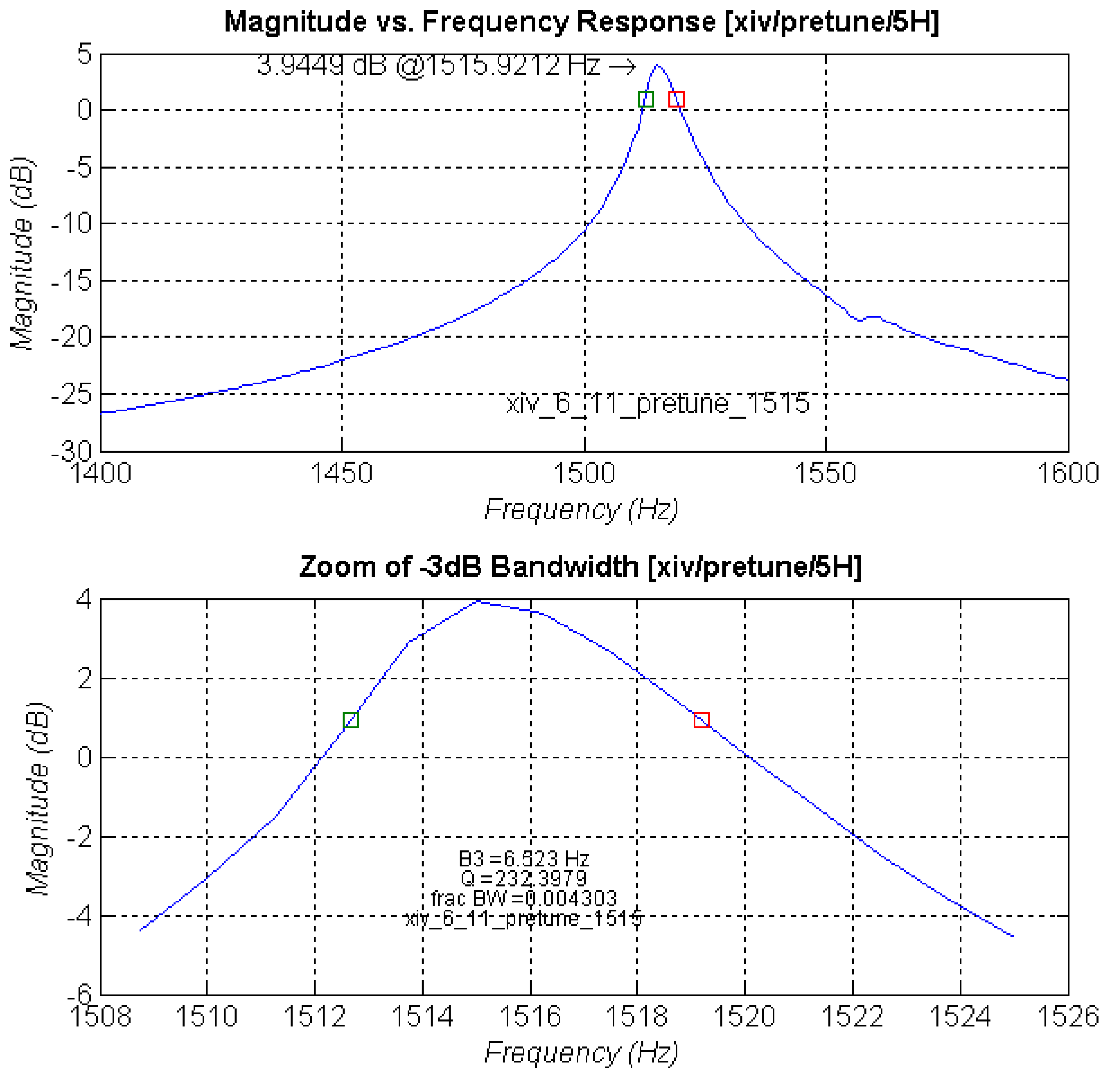

Figure A.14 Frequency response plot of pre-tuned, individual beam 1 of filter 4

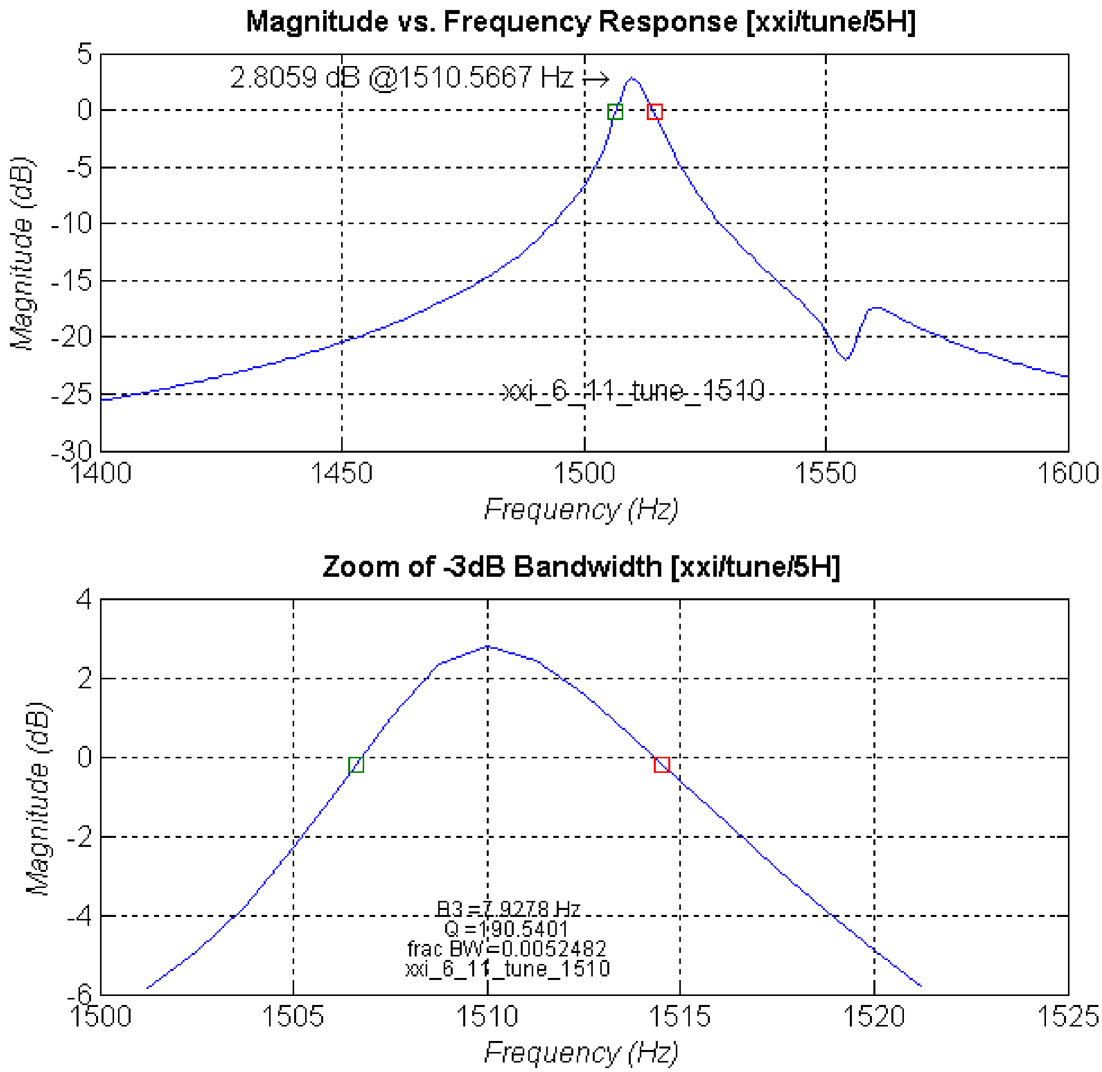

Figure A.15 Frequency response plot of tuned, individual beam 2 of filter 4

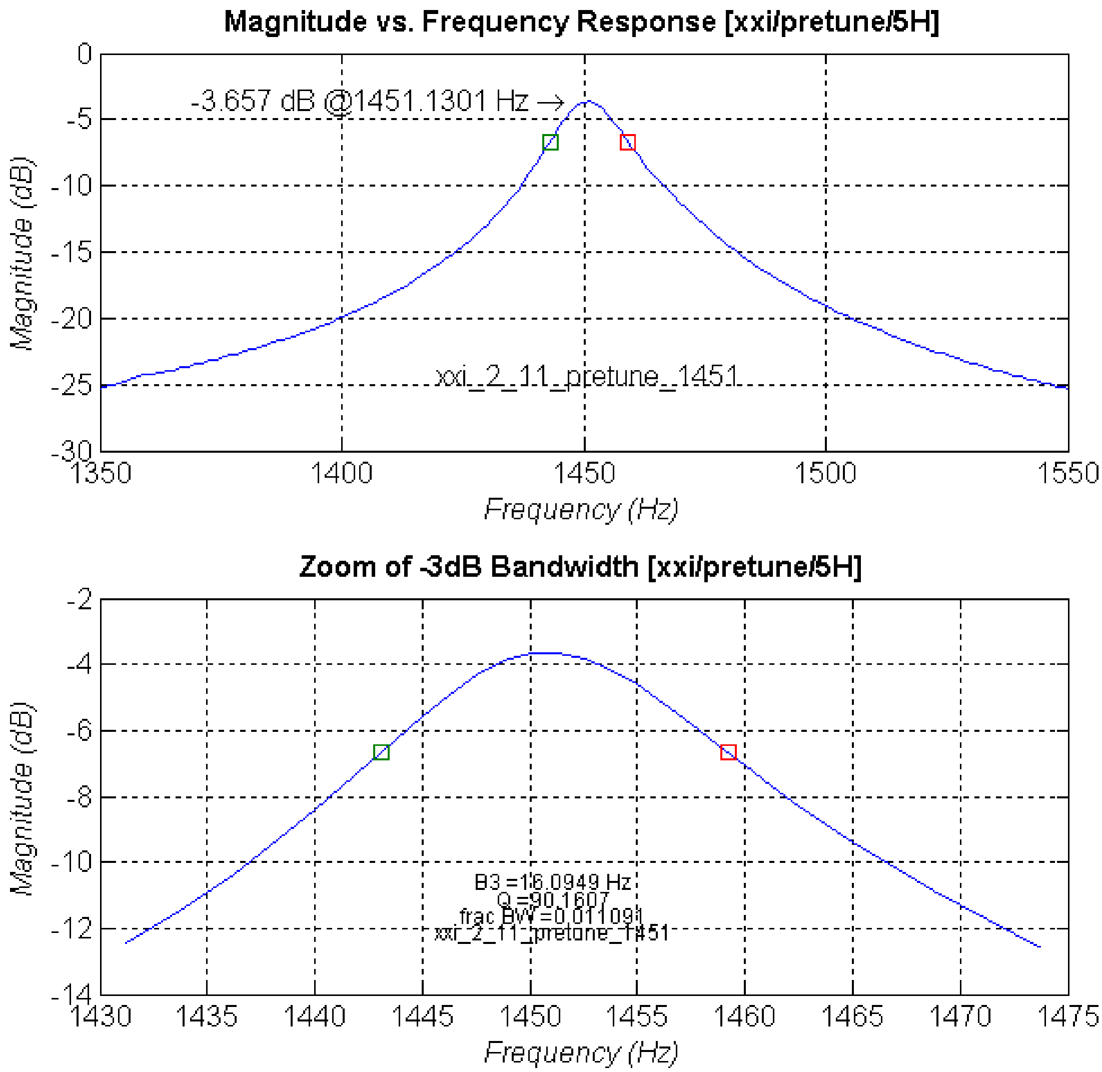

Figure A.16 Frequency response plot of pre-tuned, individual beam 2 of filter 4

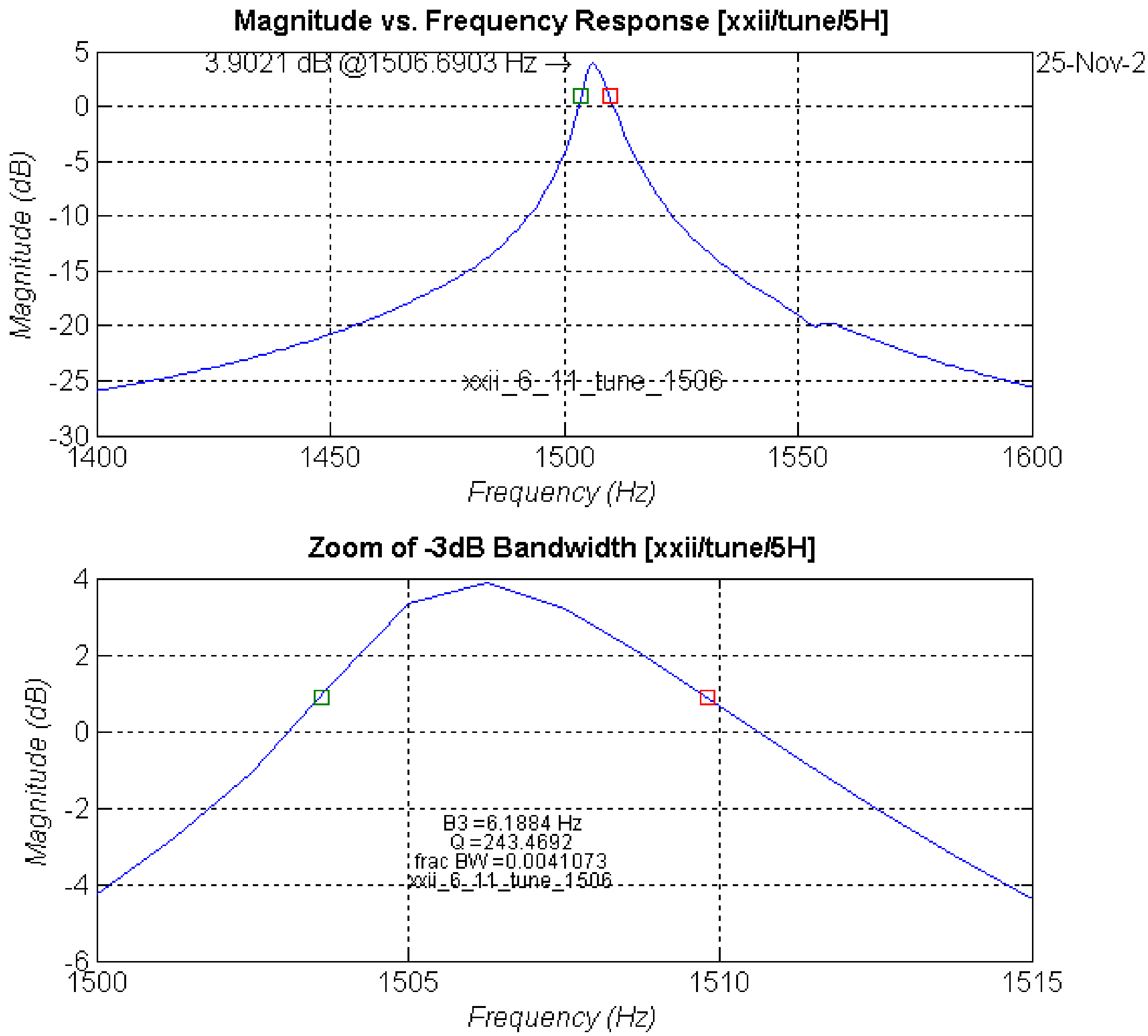

Figure A.17 Frequency response plot of tuned, individual beam 3 of filter 4

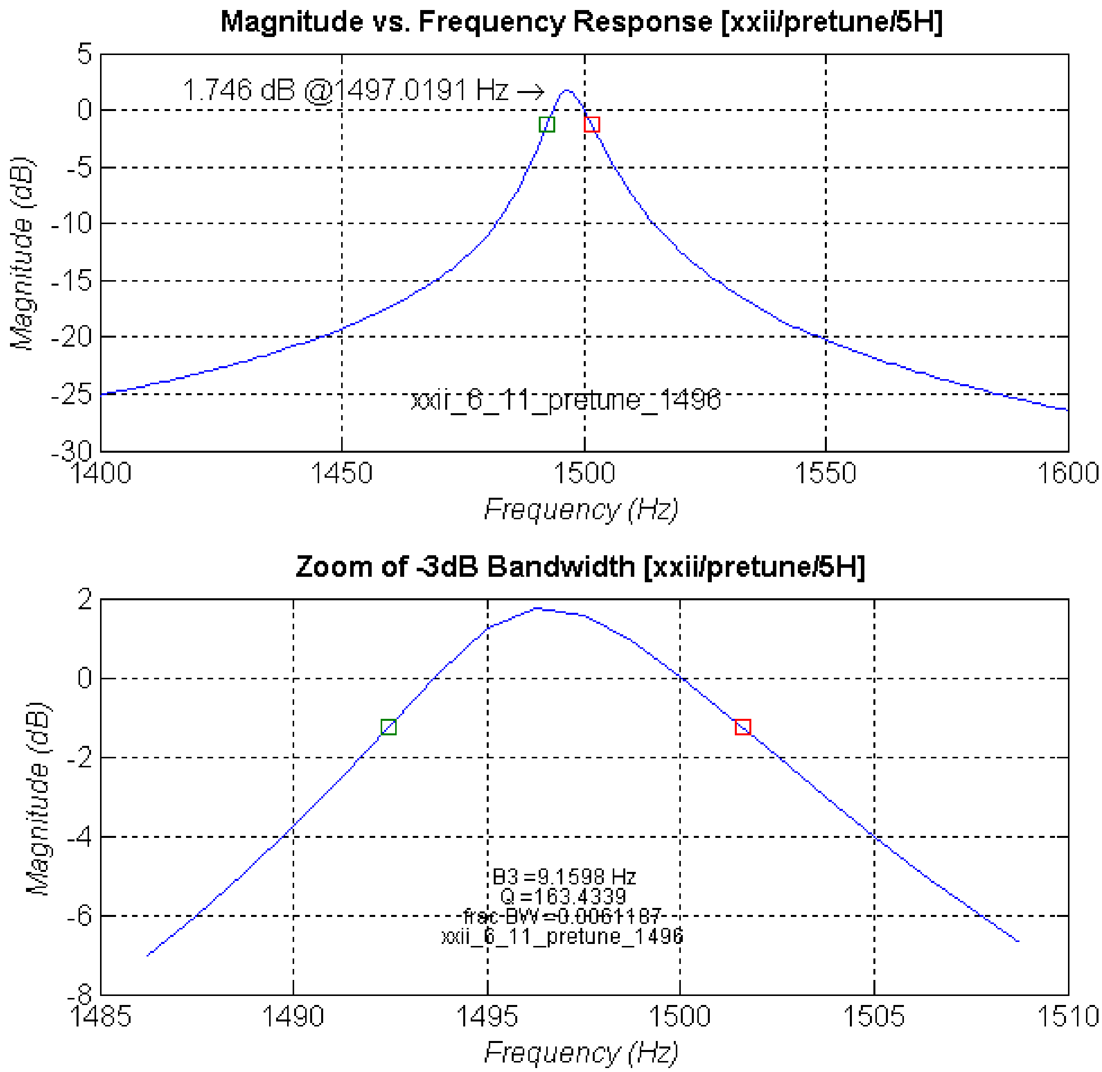

Figure A.18 Frequency response plot of pre-tuned, individual beam 3 of filter 4

BIBLIOGRAPHY

BIBLIOGRAPHY

1. Aatre, Vasudev K. Network Theory and Filter Design. New York: John Wiley & Sons, 1986.

2. Adler, Robert. "Compact Electromechanical Filter." Electronics 20 (Apr 1947): 100-105.

3. Bannon, III, Frank D., John R. Clark, and Clark T.-C. Nguyen. "High-Q HF Microelectromechanical Filters." IEEE Journal of Solid-State Circuits 35.4 (Apr. 2000): 512-26.

4. Belevitch, Vitold. "Tchebyshev Filters and Amplifier Networks." Wireless Engineer (Apr 1952): 106-110.

5. Blinchikoff, Herman J. and Anatol I. Zverev. Filtering in the Time and Frequency Domains. New York: John Wiley & Sons, 1976.

6. Borner, M. "Progress in Electromechanical Filters." Radio and Electronics Engineering (Mar 1965): 173-182.

7. Cohn, Seymour B. "Direct-Coupled-Resonator Filters." Proceedings of the IRE 45 (Feb 1957): 187-196.

8. DeVoe, Don L. "Piezoelectric Thin Film Micromechanical Beam Resonators." Sensors and Actuators A 88 (2001): 263-272.

9. Dishal, Milton. "Design of Dissipative Band-Pass Filters Producing Desired Exact Amplitude-Frequency Characteristics." Proceedings of the IRE - Waves and Electrons Section 37 (Sep 1949): 1050-1069.

10. Dishal, Milton. "Alignment and Adjustment of Synchronously Tuned Multiple-Resonator Circuit Filters." Proceedings of the IRE 39 (Nov 1951): 1448-1455.

11. Dorf, Richard C. Introduction to Electric Circuits. New York: John Wiley & Sons, 1993.

12. Ellis, Michael G. Electronic Filter Analysis and Synthesis. Boston: Artech House, 1994.

13. Ernyei, Herbert H. "Mechanical Bandpass Filter Design with Lumped Element Prototypes." IEEE Transactions on Circuits and Systems CAS-30 (Feb 1983): 89-106.

14. Fedder, Gary K. and Qi Jing. "A Hierarchical Circuit-Level Design Methodology for Microelectromechanical Systems IEEE Transactions on Circuits and Systems – II: Analog and Digital Signal Processing 46-10 (Oct 1999): 1309-1315.

15. Federal Telephone and Radio Corporation and International Telephone and Telegraph Corporation. Reference Data for Radio Engineers. New York: 1949.

16. Fertis, Demeter G. Mechanical and Structural Vibrations. New York: John Wiley & Sons, 1985.

17. Firestone, F.A. "A New Analogy Between Mechanical and Electrical Systems." Journal of Acoustical Society of America 4 (Jan. 1933): 249-267.

18. Fragoulis, D.K. and J.N. Avaritsiotis. "Acoustic Electromechanical Resonance Filters." Sensors and Actuators A 3332 (2002): 1-7.

19. Fujishima, Satoru. "The History of Ceramic Filters." IEEE Transactions on Ultrasonics, Ferroelectrics, and Frequency Control 47-1 (Jan 2000): 1-7.

20. Guenther, Alfhart E. "High-Quality Wide-Band Mechanical Filters Theory and Design." IEEE Transactions on Sonics and Ultrasonics SU-20 (Oct 1973): 294-301.

21. Gunther, A.E., and E. Thiele. "Manufacture Oriented Design of High-Performance Mechanical Filters." IEEE Transactions on Circuits and Systems CAS-27.12 (Dec. 1980): 1241-50.

22. Gunther, Alfhart E., Hans Albsmeier and Karl Traub. "Mechanical Channel Filters Meeting CCITT Specification." Proceedings of the IEEE 67-1 (Jan 1979): 102-108.

23. Gunther, Alfhart E. and Karl Traub. "Precise Equivalent Circuits of Mechanical Filters." IEEE Transactions on Sonics and Ultrasonics SU-27 (Sep 1980): 236-244.

24. Hathaway, J.C. and D.F. Babcock. "Survey of Mechanical Filters and Their Applications." Proceedings of the Institute of Radio Engineers 45 (Jan 1957): 5-16.

25. Havens, D.P. and P. Ysais. "Characteristics of Low Frequency Mechanical Filters." Proceedings of Ultrasonics Symposium (Nov 1974): 599-602.

26. Holland, Richard, and E.P. EerNisse. Design of Resonant Piezoelectric Devices. Cambridge, Massachusetts: M.I.T. Press, 1969.

27. Inman, Daniel J. Engineering Vibration. Upper Saddle River, New Jersey: Prentice-Hall, 2001.

28. Johnson, David E. Introduction to Filter Theory. Englewood Cliffs, New Jersey: Prentice-Hall, 1976.

29. Johnson, R.A. "Mechanical Filters for FM Mobile Applications." IRE Transactions of Vehicular Communications VC-10 (Apr. 1961): 32-37.

30. Johnson, R.A. "A Single-Sideband, Disk-Wire Type Mechanical Filter." IEEE Transactions on Component Parts CP-11 (Dec. 1964): 3-7.

31. Johnson, R.A. and R.J. Teske. "A Mechanical Filter Having General Stopband Characteristics." IEEE Transactions on Sonics and Ultrasonics SU-13 (Jul 1966): 41-48.

32. Johnson, R.A., M. Borner and M. Konno. "Mechanical Filters – A Review of Progress." IEEE Transactions on Sonics and Ultrasonics SU-18 (Jul 1971): 155-170.

33. Johnson, R.A., and A.E. Günther. "Mechanical Filters and Resonators." IEEE Transactions on Sonics and Ultrasonics SU-21.4 (Oct. 1974): 244-56.

34. Johnson, R.A. Mechanical Filters in Electronics. New York: John Wiley & Sons, 1983.

35. Johnson, Robert A. "Electrical Circuit Models of Disk-Wire Mechanical Filters." IEEE Transactions on Sonics and Ultrasonics SU-15 (Jan 1968): 41-50.

36. Johnson, Robert A. "The Design and Manufacture of Mechanical Filters." Proceedings of the IEEE ISCAS (Apr 1976): 750-753.

37. Kamen, Edward W. Introduction to Signals and Systems. New York: Macmillan, 1990.

38. Kinsman, Robert G. Crystal Filters: Design, Manufacture, and Application. New York: John Wiley & Sons, 1987.

39. Kinsman, Robert G. "A History of Crystal Filters." IEEE International Frequency Control Symposium: (1998): 563-570.

40. Konno, Masashi and Hisashi Nakamura. "Equivalent Electrical Network for the Transversely Vibrating Uniform Bar." Journal of the Acoustical Society of America 38 (Oct 1965): 614-622.

41. Konno, Masashi, Chiharu Kusakabe and Yoshiro Tomikawa. "Electromechanical Filter Composed of Transversely Vibrating Resonators for Low Frequencies." Journal of the Acoustical Society of America 41-4 part 2 (Apr 1967): 953-961.

42. Konno, Masashi, Shigeru Oyama and Yoshiro Tomikawa. "Equivalent Electrical Networks for Transversely Vibrating Bars and Their Applications." IEEE Transactions on Sonics and Ultrasonics SU-26 (May 1979): 191-201.

43. Lin, Liwei, Roger T. Howe, and Albert P. Pisano. "Microelectromechanical Filters for Signal Processing." Journal of Microelectromechanical Systems 7.3 (Sep. 1998): 286-294.

44. Logan, Daryl L. A First Course in the Finite Element Method. Australia: Brooks/Cole, 2002.

45. Mason, W.P. and R.N. Thurston. "A Compact Electromechanical Band-Pass Filter for Frequencies Below 20 Kilocycles." IRE Transactions on Ultrasonics Engineering UE-7 (Jun 1960): 59-70.

46. Mitra, Sanjit K. and Carl F. Kurth, eds. Miniaturized and Integrated Filters. New York: John Wiley & Sons, 1989.

47. Natarajan, Sundaram. Theory and Design of Linear Active Networks. New York: Macmillan, 1987.

48. Nguyen, Clark T.-C. "Frequency-Selective MEMS for Miniaturized Communication Devices." Proceedings of 1998 IEEE Space Conference. 1 (1998): 445-460.

49. Nguyen, Clark T.-C. and Roger T. Howe. "An Integrated CMOS Micromechanical Resonator High-Q Oscillator." IEEE Journal of Solid-State Circuits 34-4 (Apr 1999): 440-455.

50. Niewiadomski, Stefan. Filter Handbook: A Practical Design Guide. Boca Raton, Florida: CRC Press, 1989.

51. Orchard, H.J. "Formulae for Ladder Filters." Wireless Engineer (Jan 1953): 3-5.

52. Physik Instrumente. NanoPositioning Catalog. Germany: 1998.

53. Piekarski, Brett, Don DeVoe, Madan Dubey, Roger Kaul, and John Conrad. "Surface Micromachined Piezoelectric Resonant Beam Filters." Sensors and Actuators A 91 (2001): 313-320.

54. Rao, Singiresu S. Mechanical Vibrations. Reading, Massachusetts: Addison-Wesley, 1995.

55. Sawamoto, K. et al. "A Torsional-Mode Pole-Type Mechanical Channel Filter." IEEE Transactions on Sonics and Ultrasonics SU-23 (May 1976): 148-153.

56. Schaumann, Rolf, M.S. Ghausi and Kenneth R. Laker. Design of Analog Filters: Passive, Active RC, and Switched Capacitor. Englewood Cliffs, New Jersey: Prentice-Hall, 1990.

57. Sheahan, Desmond F. and Robert A. Johnson. "Crystal and Mechanical Filters." IEEE Transactions on Circuits and Systems CAS-22 (Feb 1975): 69-89.

58. Su, Kendall L. Analog Filters. London: Chapman & Hall, 1996.

59. Temes, Gabor C. and Sanjit K. Mitra, eds. Modern Filter Theory and Design. New York: John Wiley & Sons, 1973.

60. Tilmans, Harrie A.C. "Equivalent Circuit Representation of Electromechanical Transducers: 1. Lumped-Parameter Systems." Journal of Micromechanical Microengineering 6 (1996): 157-176.

61. VanValkenburg, M.E. Analog Filter Design. New York: Holt, Rinehart, and Winston, 1982.

62. Wang, Kun and Clark T.-C. Nguyen. "High-Order Micromechanical Electronic Filters." IEEE Proceedings of Tenth Annual International Workshop on Micro Electro Mechanical Systems (Jan 1997): 25-30.

63. White Electromagnetics, Inc. Handbook on Electrical Filters; Synthesis, Design and Applications. Rockville, Maryland: White Electromagnetics, 1963.

64. Williams, Arthur Bernard and Fred J. Taylor. Electronic Filter Design Handbook: LC, Active, and Digital Filters. New York: McGraw-Hill, 1988.

65. Wu, Long, Yi-Yeh Lee and Chich-Kwo Liang. "Design of Bandpass Ceramic Filters with Double-Mode Resonator." IEEE Transactions on Components, Hybrids, and Manufacturing Technology 12-3 (Sep 1989): 335-339.

66. Yakuwa, Kazuo. "Characteristics of an Electromechanical Filter Using Piezoelectric Composite Bending Vibrators." Electronics Communications of Japan 48 (Nov 1965): 206-215.

67. Yang, Lung-Jieh, Tsung-Wei Huang, and Pei-Zan Chang. "CMOS Microelectromechanical Bandpass Filters." Sensors and Actuators A 90 (2001): 148-152.

68. Zverev, Anatol I. Handbook of Filter Synthesis. New York: John Wiley & Sons, 1967.